Chemical functionalization of plasma polymer surfaces

Corinne Amy Fail

Chemical Functionalization of Plasma Polymer Surfaces

Ph. D. Thesis

by

Corinne Amy Fail

Department of Chemistry

University of Durham

2001

For my family

STATEMENT OF COPYRIGHT

DECLARATION

The work described in this thesis was carried out in the Chemistry Department of the University of Durham between October 1997 and September 2000. It is the original work of the author, except where previously acknowledged, and has not been submitted previously for a degree at this or any other University.

The original idea for the work in Chapters 2 and 3 were from Simon Evenson. The AFMs in Chapter 3 were obtained by Simon Evenson, and those in Chapter 6 were obtained by Stephen Ebbens. The gas barrier measurements in Chapter 2 were obtained by Luke Ward. TEM images were obatained by Dr Robert Thompson and Mrs Vivian Hewitt of the Biomedical TEM Unit at the Univeristy of Newcastle-upon-Tyne. Film thickness measurements were obtained by Simon Hutton and Wayne Schofield.

PUBLICATIONS

S.A. Evenson, C.A. Fail, J.P.S. Badyal, *Controlled Monomolecular Functionalization of Solid Surfaces*, Chem. Mater., **2000**, *12*, 3038-3043.

C. Fail, S.A. Evenson, L. Ward, W. Schofield, and J.P.S. Badyal, *Controlled Attachment of PAMAM Dendrimers to Solid Surfaces,* Langmuir, **2002**, *18*, 264 - 268.

ACKNOWLEDGEMENTS

I would like to thank my supervisor Professor Jas Pal Badyal for his help, guidance and patience over the last four years. Thanks must also go to everyone in lab 98 past and present, for knowing stuff, general insanity, the ability to go for a pint at a moments notice, and for putting up with me asking for stuff from the other end of the country.

Thanks to George, Kelvin, Barry from the electrical workshop (without whom I would have had no spectra in this thesis), Gordon, Ray, Malcolm and Peter for all their glass-blowing skills, and Jim and Neil in the mechanical workshop.

Finally, thanks to Martin, for making me do my thesis when sometimes I really didn't feel like it, and for being there.

ABSTRACT

The work in this thesis has concentrated upon the chemical functionalization of plasma polymer surfaces. The ability to deposit and then functionalize these surface layers has practical implications for many different areas, such as biomedical uses and heterogeneous catalysis and many different functional groups can be attached to surfaces using the plasma polymer layer as an intermediate. A variety of substrates, from glass to polymer films have been studied.

Two different monomers have been studied in this work. The majority of work was carried out using a maleic anhydride plasma polymer (MAPP), which can be deposited from maleic anhydride under pulsed plasma conditions. The second monomer used was allylamine, whose plasma polymer has previously been studied as a biomedical layer.

For both of these monomers, a variety of functionalization reactions have been studied. In the case of the anhydride group the key reaction is that which occurs between the anhydride group and amines. The reaction of amines with the anhydride is through a ring opening of the anhydride group, leading to the formation of amic acid groups. This part of the thesis allowed an understanding of the mechanism of vapour phase reactions to be acquired. Once this understanding had been achieved, many more amine containing groups were studied, such as poly(amidoamine) (PAMAM) dendrimers, functionalized polystyrene particles, polycations and molecules containing double bonds were reacted with the MAPP surface. These functional molecules can be used for immobilizing metal particles, stabilizing colloids adhering surfaces and Diels-Alder reactions.

In the case of the allylamine, a variety of different functionalization routes we studied. Formation of amide groups at the surface was studied using heptafluorobutryl chloride and carboxylic acid functionalized polystyrene beads. The ability of the allylamine plasma polymer layer to act as a polycationic layer was investigated with an anionic polymeric dye, DNA and gold colloids.

OBJECTIVES

The plasma polymerization of maleic anhydride has been previously studied, and good structural retention of the anhydride ring has been observed. The optimum conditions for the deposition of these plasma polymer layers have previously been determined, and using these optimal conditions a maleic anhydride plasma polymer layer (MAPP) is used as the starting layer to investigate the following:

1. To understand the mechanism by which maleic anhydride plasma polymer (MAPP) reacts with amines in the vapour phase, by using simple amine systems such as trifluoroethylamine. This understanding was then further applied to functionalize MAPP with a variety of amines, in the vapour phase, and in solution.
2. To investigate a variety of different amine containing species could be attached to the plasma polymer surface, and introduce different surface properties.
3. To attach functional groups to the MAPP that could not be deposited from a plasma.
4. To compare the reactions of MAPP with those possible for a plasma polymer of allylamine.

CONTENTS

CHAPTER ONE

An Introduction to Low Pressure Plasmas, Plasma Polymerization, Surface Modification and Characterization

1.1 PLASMAS

1.1.1 The Fundamental Characteristics of a Plasma[1]

The term plasma was first used by Langmuir to describe the fourth state of matter, being at greater energy than solids, liquids or gases.[2] They consist of a quasi-neutral mixture of charged and neutral gaseous particles and radiation characterized by a collective behaviour. Within the plasma, the motions of the particles give rise to localized concentrations of positive and negative charges, which in turn give rise to long-ranging Coulombic effects that can affect the motion of particles within the plasma, even if they are a long way from the charge concentration. The fact that different elements in the plasma can affect each other at large separations give rise to what is known as collective plasma behaviour. A charged particle within the plasma will follow a path through the plasma governed by the average of the electric field. This is in contrast to the random Brownian motion of a neutral gas particle.[1] The processes within the plasma are complex, but by varying the process parameters, such as pressure and power, their characteristics may be controlled.

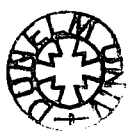

1.1.1.1 Conditions for Creating Plasmas

Non-equilibrium plasmas are created when sufficient energy is applied to a gas causing ionization and the production of electrons. The subsequent recombination of these electrons with ions leads to the formation of neutral atoms and molecules. The energy supplied for excitation can be supplied by various sources, including direct current, alternating current, radio frequency and microwave sources.

1.1.1.2 Plasma Parameters

A plasma contains many different neutral and charged species.[1] It can be broadly characterized by the density of the neutral particles, n_n, the density of the ions, n_i and the density of the electrons, n_e. In a quasi-neutral state, $n_i = n_e = n$, where n is the plasma density. A plasma is also characterized by the energy distributions of the neutral particles, $f_n(W)$, the ions, $f_i(W)$ and the electrons, $f_e(W)$. These plasma characteristics have a direct effect upon the efficiency of the plasma processes and the reaction rates. Within the plasma, it is the electrons that are responsible for the transfer of energy from the external field to the bulk of the gas. Since electrons are the lightest constituent of the plasma, they are most easily accelerated and absorb the largest amount of energy from the applied field. Energy transfer occurs via collisions of electrons with molecules, to give rise to excitation, ionization and dissociation. Increasing the electron density increases the effectiveness of the energy transfer.

Particles within the plasma are in continuous motion, which leads to collisions between particles. There are two types of collisions occurring within the plasma, elastic and inelastic. When electrons collide with a heavy target, but do not excite the target, then the process is known as an elastic collision. If the collision of the electron with the target molecule leaves the target molecule in an excited state, then the collision is inelastic. The fraction of energy transferred to the target in an elastic collision is determined by the mass ratio of the colliding particles;

$$\frac{W_{Tr}}{W} = \frac{M}{M_{in} + M}$$

Equation 1.1[1]

Here W_{Tr} is the energy transfer, W is the energy of the electron, M is the mass of the heavy particle and M_{in} *is* the particle losing energy.

In an inelastic collision between an electron and a heavy particle, an electron can transfer almost all of its energy to the heavy particle, creating energetic plasma species. It is these inelastic collisions, in particular those which cause ionization and create electron-ion pairs which sustain the plasma against energy losses and give it many of its features, with energies in the range 0.1 eV to 30 eV. The density of the charged particles created by this plasma is defined by the degree of ionization, α, where n_i is the ion density and n is the plasma density.

$$\alpha = \frac{n_i}{n}$$

Equation 1.2

This equation specifies the fraction of the particles in the gaseous phase that are ionized. At low pressures, α typically has a value of 10^{-6} - 10^{-3}.

1.1.1.3 Plasma Temperature

One of the physical parameters defining the state of a quasi-neutral gas in thermodynamic equilibrium is the mean translational energy of molecules in the system, represented by T. Although a plasma is a mixture of particles of different charges and masses, it can broadly be considered as two separate systems, at low pressure. The processes undergone by these two sub-systems are characterized by their own specific average temperature: the ion temperature, T_i and the electron temperature, T_e. Electrons gain energy from the electric field, some of this energy is then transferred to heavy particles by collisions. These heavy particles lose heat to the surroundings by radiation or heat transfer.[1]

For a more complete description, other temperatures must also be considered. These are T_g, the translatory energy of the gas, T_{ex}, the energy of the excited particles, T_{ion} and T_d, energy of ionization and dissociation and T_r, the radiation energy. Complete thermodynamic equilibrium is not achieved in such systems because T_r at the envelope of the plasma does not equal the temperature of

the plasma bulk. However, local thermal equilibrium can be achieved in the plasma in volumes of the order of the mean free path length. This is called *Local Thermal Equilibrium Plasma, (LTE plasma).* At low pressures, such as the plasmas produced by DC or RF excitation, *LTE* is not achieved. This gives rise to what is known as a *Non-Local Thermal Equilibrium Plasma (non-LTE plasma).* In a *non-LTE* plasma, the temperature of the heavy particles is usually too small to promote chemical reactions in thermodynamic equilibrium. T_e is therefore the most important factor in *non-LTE* plasmas. The fraction of electrons that will cause different reactions within the plasma, the overall efficiency of the plasma process and the rate of reaction are increased as T_e increases.

1.1.1.4 Electron Temperature[3,4]

The velocity distribution function *f(v)* for a system of particles is defined as the density of particles in the velocity space that satisfies the equation:

$$n(cm^{-3}) = 4\pi \int_0^\infty f(v) v^2 dv$$

Equation 1.3

where *v* is the velocity, *f(v)* is the velocity distribution function and *n* is the density of the particles in the geometrical space. There are several assumptions that can be made in this first approximation:

1. The velocity distribution of electrons within a plasma is isotropic.
2. That inelastic collision effects act only as a perturbation to this isotropy.
3. Electric field effects are negligible.

Following these assumptions, the velocity distribution is Maxwellian. A Maxwellian distribution assumes that the temperature of the electrons, T_e, is equal to the temperature of the gas, T_g. This Maxwellian distribution only gives us a first approximation of the electron energy (velocity) within the plasma. In a low-pressure plasma system, we can use different approximation. These are:[4]

1. The electric field strength is low enough to neglect inelastic collisions, but is large enough for the electron temperature, T_e, to be much higher than the ion temperature, T_i.
2. The electric field is of a frequency, ω, much lower than the frequency of the collisions, ν.
3. The collision frequency is independent of the electron energy.

These assumptions give rise to a Druyvesteyn distribution of electrons within the plasma.[5] This is a better approximation than the Maxwellian one for energy distributions in *non-LTE* plasmas. A Druyvesteyn distribution is characterized by an energy shift to higher electron energies compared to the Maxwellian one. Both distributions have high-energy tails, and this is an important consideration for plasma phase reactions that have a minimum energy threshold. For example, at an average electron energy of 5 eV, there will still be a significant number of electrons with energies of 30 eV and over. The Druyvesteyn distribution in particular predicts a large number of these higher energy electrons. These high-energy electrons can have a significant effect upon reaction rates even though they are present in small concentrations.

The difference between the calculated electron energies using the Maxwellian and Druyvesteyn equations is shown in Figure 1.1, page 6.

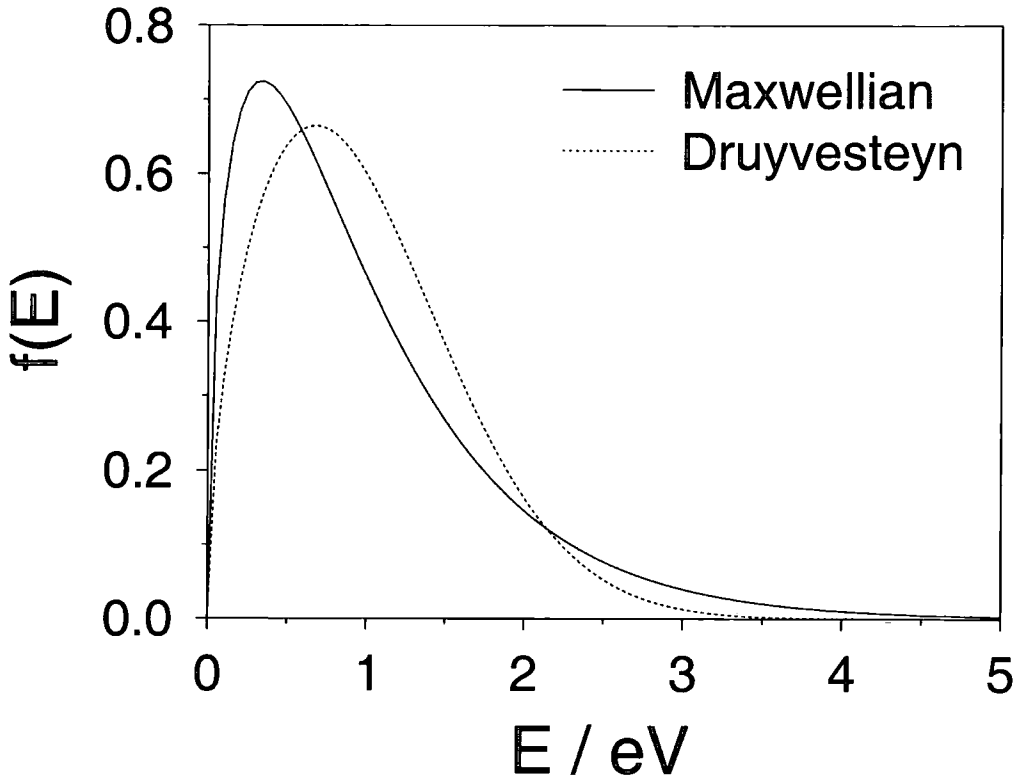

Figure 1.1 The differences on electron distribution as calculated for Maxwellian and Druyvesteyn approximations.

At low pressures, T_e is much greater than T_g. As the pressure increases, the amount of energy transferred from electrons to neutrals increases, causing T_g to rise and T_e to fall. T_e and T_g converge between 10 and 100 torr, and at this point, the plasma becomes arc-like. Within the arc, $T_e = T_g$. At this point, equilibrium relations describe the species within the plasma, where as when T_e is much larger than T_g, the distribution of species is best represented by T_e.

1.1.2 Plasma Types.

Plasmas that occur in nature cover a large range of electron densities and temperatures. The electron density can range from 1 to 10^{20} cm^{-3}, and the electron energy can vary from 10^{-2} to 10^{5} eV.

Table 1.1 Different Plasma Types and Parameters[1]

Plasma Type	*Electron Density / cm^{-3}*	*Electron Energy / eV*
Ionosphere	10^{4}	10^{-2}
Solar corona	10^{4} - 10^{6}	10
Glow discharges	10^{8} - 10^{10}	1 – 10
Low pressure discharges	10^{12} -10^{14}	1 – 10
Thermonuclear fusion	10^{13} - 10^{14}	10^{2} - 10^{3}
Thermonuclear reaction	10^{16} - 10^{18}	10^{4} - 10^{5}

1.1.2.1 Thermal Plasmas

LTE plasmas exist under two circumstances:

1. When the heavy particles are very energetic, at temperatures of 10^{6} - 10^{8} K (10^{2} - 10^{4} eV).
2. When the pressure is atmospheric, even at temperatures as low as 6000 K.

The high temperature of these plasmas renders them highly destructive and unsuitable for most materials. This comparative lack of utility means that no further mention will be made of them, and references to plasmas in this thesis will be referring to non-LTE, or cold plasmas.

1.1.2.2 Cold Plasmas

In low-pressure discharges, thermodynamic equilibrium between the electrons and heavy particles is not reached. These plasmas are of the non-LTE type. In these plasmas the electron temperature, T_e, is much greater than that of the heavy particles, $T_e >> T_i \sim T_g > T_{ex}$, where T_i is the ion temperature, T_g is the gas temperature, and T_{ex} is the excitation temperature that characterizes the energy of the excited particles in the plasma. Electron temperatures can reach 10^{4} - 10^{5} K, (1-10 eV), whilst the temperature of the gas does not exceed room

temperature, hence these plasmas are termed cold plasmas. Cold plasmas are widely used for their non-equilibrium properties and their ability to cause both physical and chemical reactions at low temperatures. Their applications vary from microelectronic fabrication to surface hardening of metals.

1.2 WHY USE PLASMA METHODS?

The use of plasmas for the treatment of solid surfaces has several advantages over conventional solution phase chemistry. Some of these advantages are given below;

1. Plasma polymer film thickness can be easily controlled. Typical thicknesses range from 50nm to 1 micron.
2. Films produced by plasmas are often highly coherent and adhere to a variety of substrates. These include conventional polymers, glass and metal surfaces.
3. The films deposited are pinhole-free and highly crosslinked.
4. Multilayer films or films with grading of chemical and physical properties are easily made.
5. The monomers used can be solid (e.g. maleic anhydride), liquid (e.g. allyl amine), or gas (e.g. hexafluoropropylene oxide).
6. Altering the process parameters can vary the chemical composition of the plasma polymer.
7. Substrate geometry is not a limiting factor, which means that substrates with complex shapes can be treated in the plasma.
8. Very small amounts of precursor are required for plasma formation.
9. Plasma processes are solvent free and energy efficient, rendering them an environmentally friendly and cost effective alternative to traditional methods.

1.2.1 Surface Modification by Plasmas

Plasma techniques for surface modification[6] can be divided up into two general categories. The first of these is the use of non-polymerising gases such as tetrafluoromethane (CF_4), argon (Ar) and helium (He). Generally, plasma treatment with inert gases results in physical ablation and the formation of free

radicals at the surface. Ablation occurs as a result of ion sputtering and collisions of energetic neutral species with the surface. The fragments removed from the surface in this way may be activated by the plasma and reincorporated in the polymer surface, or redeposited as a highly crosslinked layer. The ultraviolet radiation emitted by the plasma causes free radicals to be formed at the polymer surface. This can also enhance the crosslinking, because the free radicals created are able to migrate along the polymer chains. Plasmas of these non-polymerisable gases can be used to activate polymer surfaces as first suggested by Beauchamp and Buttrill,[7] allowing the improvement of surface characteristics without affecting the bulk properties. Surface activation reactions can affect the wetting properties, crosslinking, adhesion, barrier properties and even biocompatibilty.[8-10]

Plasma polymerization is the alternative method of plasma surface modification. It refers to the deposition of polymer films through plasma dissociation and excitation of an organic monomer gas and the subsequent deposition and polymerization of the excited species on the surface of the substrate. This technique can be used to deposit films of thickness from tens to thousands of angstroms.

Plasma polymerization is a strongly system-dependent process. Whereas conventional polymerization processes are based upon molecular processes, polymer formation within a plasma is an atomic process. The polymers formed within the plasma tend to be highly branched and highly crosslinked. Free radicals formed on the polymer surface can be used to initiate graft polymerization.

Plasma polymerization is characterized by several features:

1. Plasma polymers have no obvious repeat units, as in conventional polymers.
2. The monomer used is not necessarily required to have a functional group, such as a double bond for plasma polymerization to occur.

Plasma polymerization occurs in several steps. These are (i) initiation, (ii) propagation, (iii) termination and (iv) reinitiation. In the initiation stage free

radicals and atoms are produced either by collision with energetic electrons and ions with monomer molecules or by ion impact leading to the dissociation of monomers adsorbed onto the surface. During the plasma the substrate surface adsorbs both monomer molecules and free radicals. In the propagation stage of the reaction, the formation of the plasma polymer chains takes place both in the gas phase and at the substrate surface, where the deposited polymer film lies. In the gas phase the propagation process requires the addition of a radical atom to another radical or molecule. At the surface, propagation occurs by interactions between surface free radicals and either gas phase or adsorbed monomers. Termination also occurs in both the gas phase and at the polymer surface in a manner similar to propagation, but ending with either the final product or a closed polymer chain. However, the neutral products formed by this termination step can subsequently undergo re-initiation and propagation reactions. In re-initiation, chain fragments are reconverted to radicals by collision with electrons in the gas phase, the impact of energetic particles or by photon absorption on the surface of the polymer film.

In the case of pulsed plasma polymerisation there have also been studies to determine the deposition mechanism.[11]

Figure 1.2 Diagram of Plasma Polymerization

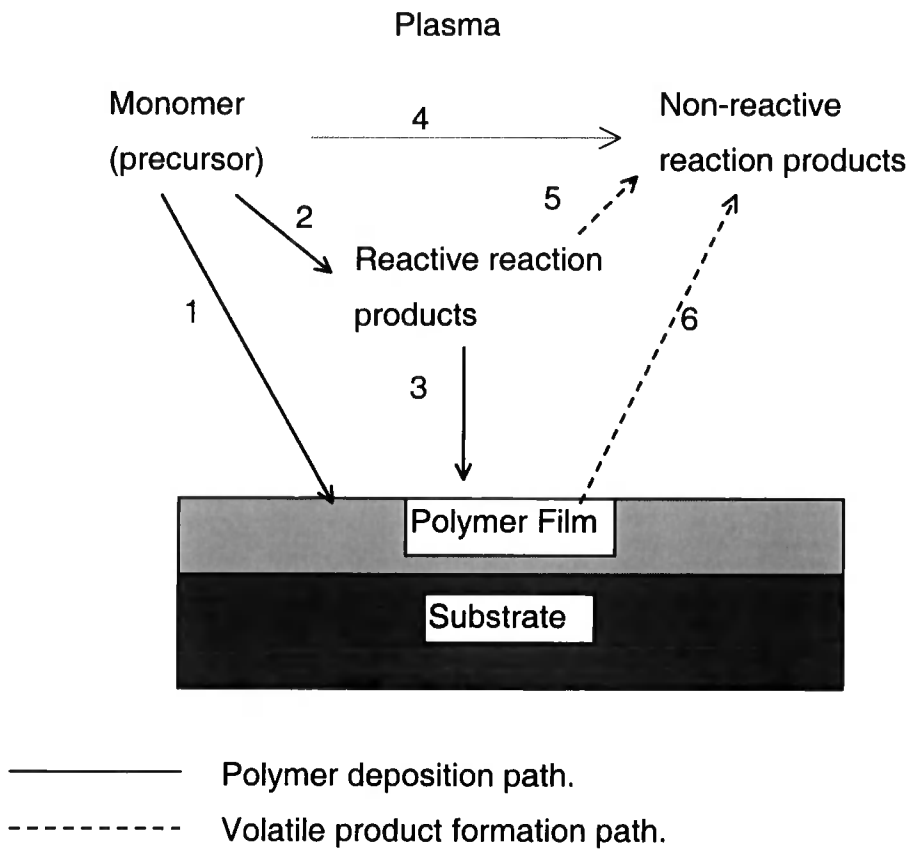

Figure 1.2 summarises the homogeneous polymerization in the plasma phase and the heterogeneous polymerization at the film surface. Path 1 shows that the gaseous monomer can polymerize in the plasma and be deposited as a film. Essentially, it is a conventional molecular polymerization process, resulting in direct polymer formation. This stage occurs only if the starting monomer has polymerisable functional groups. Paths 2 and 3 represent plasma polymerization, a process that does not necessarily require the monomer to possess conventional polymerisable moieties. Path 2 shows that the monomer is also converted into reactive products, or non-reactive products, as shown in path 4. The reactive products can be either converted into polymer film, path 3, or converted to non-reactive products, path 5. Degradation of the polymer film can occur to form non-reactive products, path 6. The intermediate reactive products may be ions, excited molecules and free radicals, not necessarily preserving the original monomer.

The polymers produced in this way are totally amorphous and exceptionally crosslinked. The final structure of a plasma polymer is dependent upon the

monomer that is used and the conditions under which the plasma is produced. Factors that may be varied include the monomer pressure, the power with which the plasma is produced and the duration of the reaction. They differ from conventional or step growth polymers, because there is no obvious repeat unit. Yasuda[10] proposed the following process for plasma polymerization, known as the "rapid step-growth" model, Figure 1.3.

Figure 1.3 Yasuda's rapid-step growth model[10]

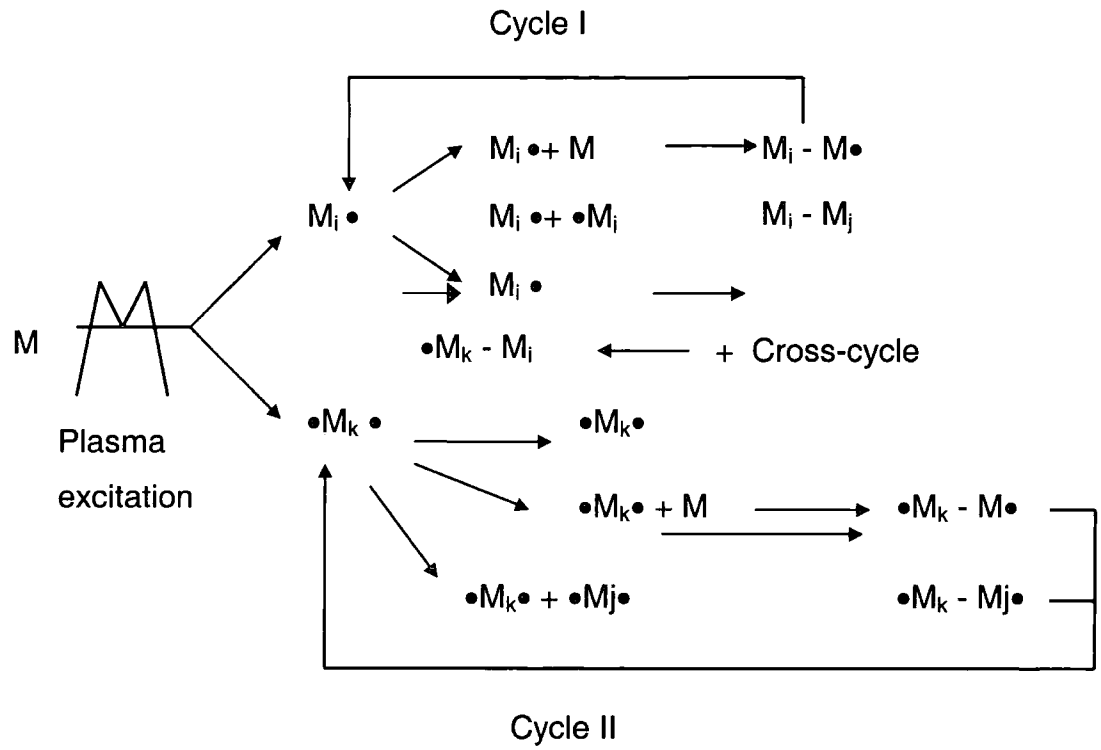

Cycle I represents rapid step-growth by reactivation of reacted products with monofunctional activated species.

Cycle II represents rapid step-growth via multifunctional activated species, such as di-radicals, ion-radicals, etc.

1.2.2 Functionalization of surface groups and plasma polymers

If plasma polymers with functional groups can be deposited, then there is scope for the surface functionalization of these layers. Work has already been carried out to functionalize polymers that have been deposited at surfaces through techniques such as the formation of self-assembled monolayers (SAMs) using conventional solution-based chemistry. The advantage of this type of

functionalization is that the bulk properties of the material under investigation remain unaffected, whilst new functionalities are introduced at the surface.

The most common substrate for the formation of these SAMs is gold, since by using a thiol terminated hydrocarbon chain with a second functional group at the ω end well adhered layers can be produced through the sulphur – gold linkage, with the ω end free to undergo further reactions. The ω groups of these chains are usually carboxylic acids,[12-14] although there has also been work reported with epoxysilane functionalized SAMs[15] and oligo(ethyleneglycol) terminated and amine containing alkanethiolates.[16]

Figure 1.4 SAMS on gold with terminal carboxylic acid groups[13]

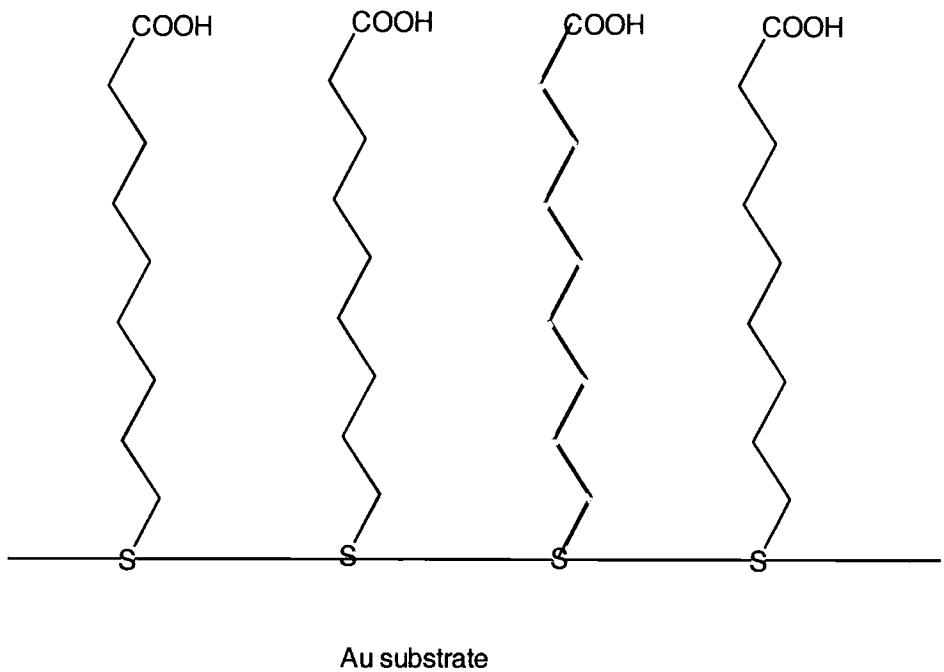

The potential of these SAMs for further functionalization reactions, was exhibited in work by Whitesides,[13] in which the carboxylic acid groups are reacted with trifluoroacetic anhydride and triethylamine to yield surface anhydride groups, Figure 1.4. These groups were then functionalized with poly(ethyleneimine), which was bound to the surface via amide linkages formed through reaction with the anhydride groups, Figure 1.5, page 14. As poly(ethyleneimine) contains many primary and secondary amine functionalities it can be used to attach and stabilize other groups which are reacted with the

surface, such as surfactants and co-polymers such as poly(octadecene-*alt*-maleic anhydride), and poly(styrene-*alt*-maleic anhydride).

Figure 1.5 Reactions of carboxylic acid terminated SAM's to give anydride groups, showing scope for further functionalization.[13]

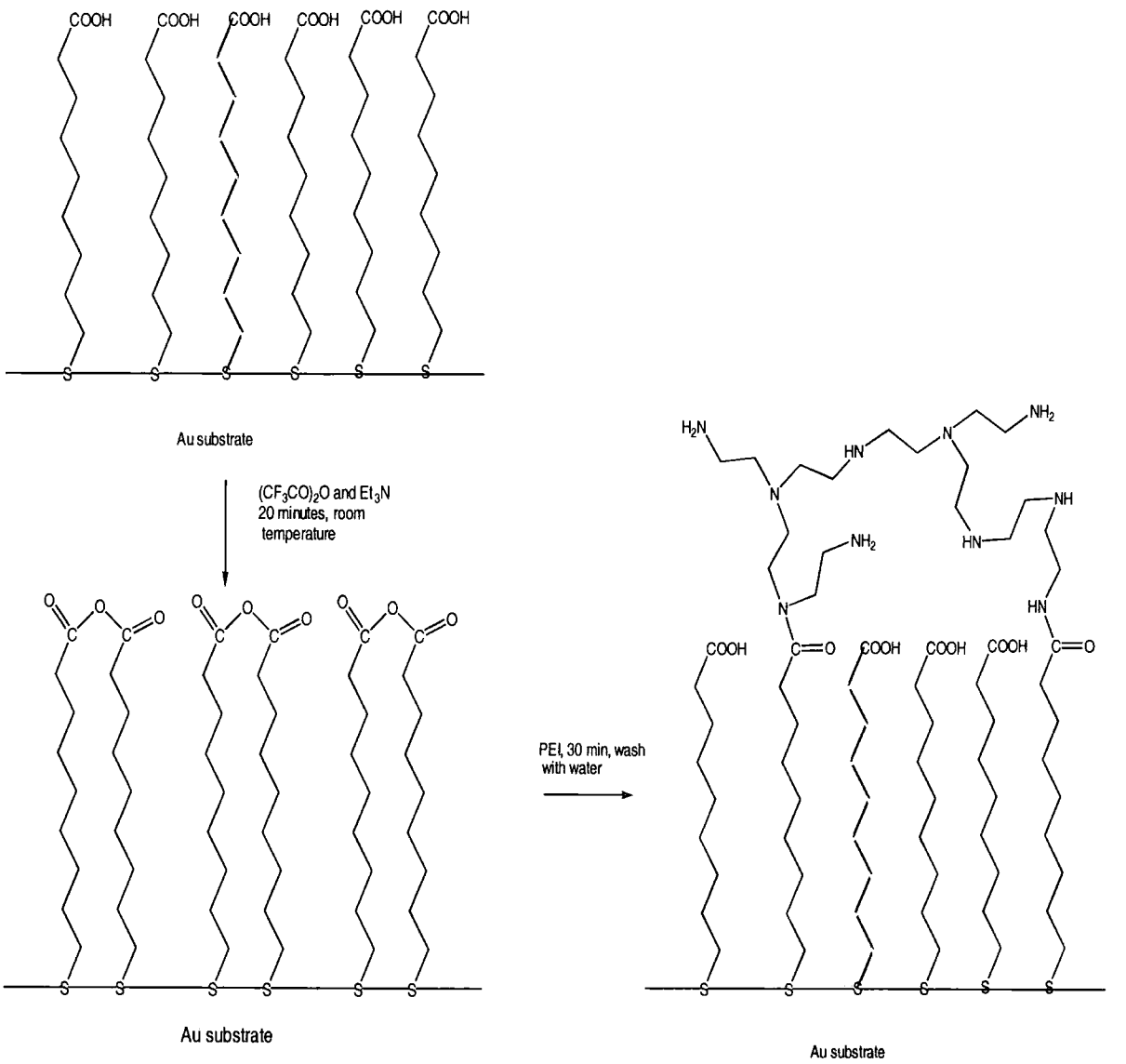

Crooks has also used SAMs on gold to present functional groups at the surface which can then be used to form hyperbranched polymer layers at the surface. Again this requires the use of an alkylthiol terminated functional chain, present carboxylic acid groups at the surface. These carboxylic acid groups are then functionalized with α, ω-diamino-poly(*tert*-butyl acrylate). Hydrolysis of the butyl acrylate groups gives a grafted layer of poly(acrylic acid).[17,18] Since these layers are extremely rich in carboxylic acid groups they have been used for

further reaction with many different functionalized amines and alcohols, in order to introduce groups such as pyrene, ferrocene, poly(ethylene glycol), 15-crown-5, and dyes.[19] This demonstrated the potential for the functionalization of surface reactive groups, in order to control the surface properties. The amount of these groups attaching to the surface can be controlled through using known concentrations of solutions, as demonstrated in the example of pyrene.[19] The advantages of introducing groups at the surface in this way is that it gives rise to a system by which the composition can be easily controlled, and functionalized further. These functionalized alkyl thiols have also been used by Crooks to directly immobilize poly(amidoamine) (PAMAM) dendrimers to gold surfaces, through the formation of multiple amide linkages between the terminal amine groups of the dendrimer and the carboxylic acid groups of the SAM.[20]

In this thesis, the bulk of the work has used a maleic anhydride plasma polymer as a substrate for surface functionalization reactions. The basis for this choice is that the anhydride functionality is more reactive than the corresponding acids, and will readily undergo reactions with amine functionalized molecules, leading to the anchoring of the reactive molecules to the surface via amide linkages. This will be discussed further in Chapter 2.

Pulsed plasma polymerisation is of interest because it allows for greater control of the polymers deposited at the surface. A higher degree of structural retention is possible, since monomer fragmentation is only occurring for a short period of time, in comparison with the longer time intervals between each pulse. It is believed that this improved structural retention is due to the generation of free radicals in the plasma on-time, which allow conventional polymer processes, such as grafting to radical sites in the plasma off-time.[21] Once the free radicals have recombined or disproportionated, activation by another plasma pulse is required. The shorted the plasma on-time with respect to the plasma off-time, the better structure and composition of the plasma polymer layer.

Another method of controlling the structure of the plasma polymer films is through controlling the power of the plasma used to deposit them. By reducing the power, effectively making the plasma less destructive, better retention of the

chemical structure is possible. The average power supplied to the plasma <P>, is given by the equation below:[22]

$$\langle P \rangle = P_{CW} \left\{ \frac{t_{on}}{(t_{on} + t_{off})} \right\}$$

Equation 1.4

P_{CW} is the continuous wave power of the plasma, sometimes called the peak power, t_{on} is the plasma on-time, and t_{off} is the plasma off-time. The plasma duty cycle is give by:

$$\frac{t_{on}}{(t_{on} + t_{off})}$$

Equation 1.5

Plasma duty cycles and power can be varied to give a range of average powers. The general trend is that the lower that power, and the smaller the duty cycle, the better the retention of the chemical structure. A combination of low power, short on-time and long off-time appear to be most effective.

Deposition rates are affected by the changes in the power of the plasma. In the case of acetylene it has been shown that there is a linear relationship between power and deposition rate for the pulsed plasma, but this is not observed for the continuous wave plasma. When referenced against plasma on-time, the deposition rate is considerably larger for a variety of pulsed plasma polymerized monomers than for the continuous wave. This was attributed to better monomer diffusion to the growing surface in the off-time and more complete attachment of fragments, as plasma enhanced desorption only occurs in the off-time.[21]

Another area of work that has looked at controlling and modifying surfaces involves the deposition of alternating layers of polyanions and polycations, an approach which provides scope for the attachment and immobilization of functional molecules at the surface.[23-25] Several active polymers have been used, either as the polyanion or polycation in the construction of these layers.

Examples include DNA,[26-28] other proteins,[29,30] (such as streptavidin), viruses,[31] and metal nanoparticles.[32]

Plasma polymers of allyl amine have been used as the starting point for the attachment of biological molecules to surfaces[33], and studied with a view to providing amine groups for tissue culture studies.[34] Allyl amine plasma polymers can be used as polycations, in a similar way to that described by Lvov and Decher as a starting point to build up electrostatic layers.[23-26,28-32]

1.3 ANALYTICAL TECHNIQUES USED

1.4 X-RAY PHOTOELECTRON SPECTROSCOPY (XPS)

1.4.1 Background

Surface analysis by XPS is achieved by irradiating the sample surface with monoenergetic soft X-rays and analysing the energies of the photoemitted electrons. The two most common X-ray sources are Mg K_α with an energy of 1253.6 eV and a line width of 0.7 eV and Al K_α with an energy of 1486.6 eV and a line width of 0.85 eV. The narrow line widths of these sources avoids limiting the resolution of the technique, whilst their energies are large enough to provide detailed information over a sufficiently large energy range. These soft X-rays have a limited penetrating power in the solid, usually up to 10 micrometers. Their interaction with atoms in the surface region, causes electrons to be emitted in accordance with the photoelectric effect. The emitted electrons have a kinetic energy, KE, given by:

$$KE = h\nu - BE - \phi_s$$

Equation 1.6

where $h\nu$ is the energy of the photon, BE is the binding energy of the atomic orbital from which the electron originates and ϕ_s is the spectrometer work function.

Each element has a unique set of binding energies that XPS can use to identify and determine its concentration at the surface. In addition, binding energies

are sensitive to an element's oxidation state, allowing chemical information to be deduced.[35] The presence of electron withdrawing substituents results in decreased nuclear screening by the valence electrons, and generally increases the binding energy by a few electron volts. Differences arising from the chemical shifts allow identification of different chemical states for the analyzed materials. In the case of carbon (C(1s)), the shifts in binding energy allow the functionality of the carbon atom to be deduced. Typically $\underline{C}H_x$ has a binding energy of 285.0 eV, whereas O=$\underline{C}$-O-$\underline{C}$=O will have a binding energy of 289.4 eV.

Figure 1.6 XPS Processes

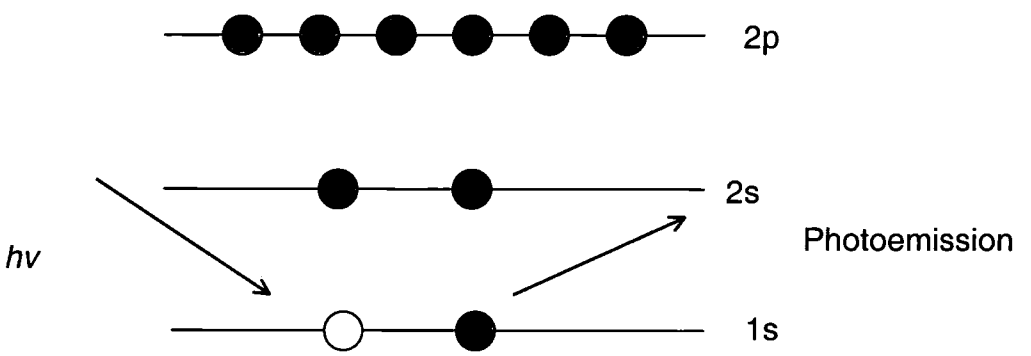

The surface sensitivity of XPS comes from the energy dependence on the escape depth of the photoelectrons. There are three processes of energy loss that can occur in a solid; lattice vibrations (phonons), excitation of collective density fluctuations (plasmons), and excitation of particles. Low kinetic energy (KE) electrons are not able to produce these effects and their escape depth is large. For high KE electrons the cross section for these interactions is again low and so their escape depth is large. However, medium KE electrons have a high cross section for these effects and their escape depth is much smaller. A graph of escape depth against energy is shown in Figure 1.7, page 19.[36]

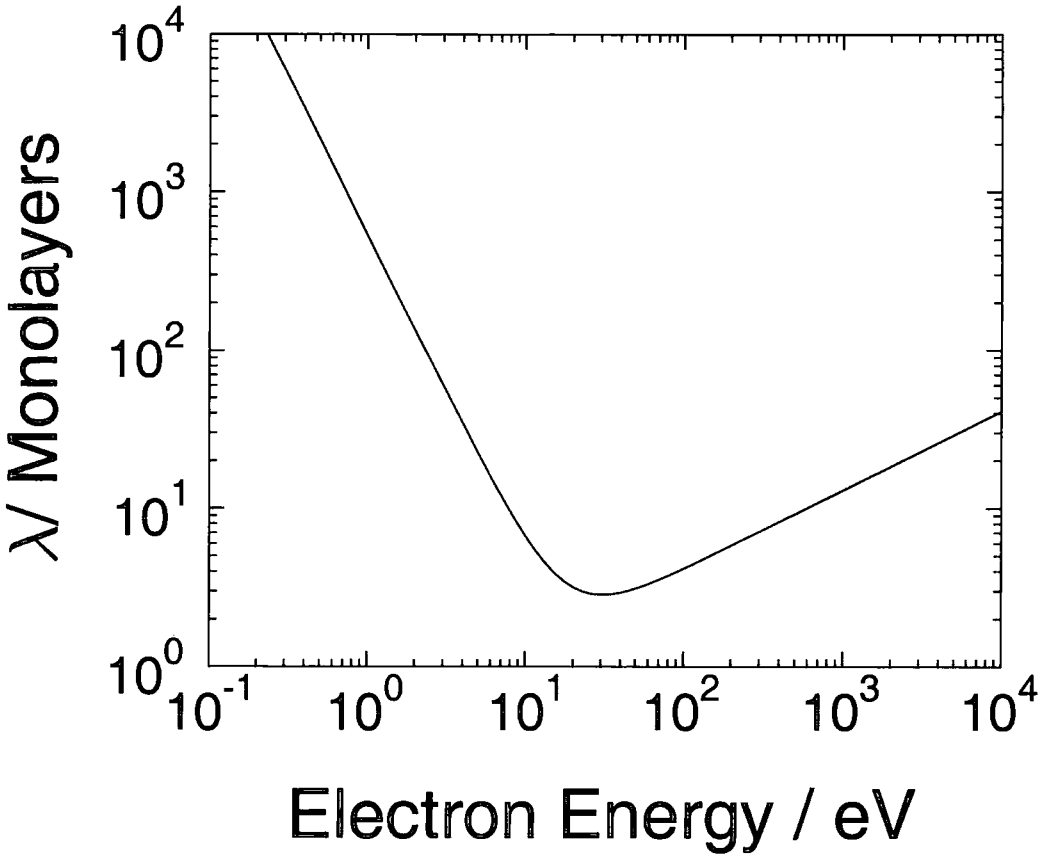

Figure 1.7. Escape depth curve.

The escape depth goes through minimum of 1 nm at an electron KE of approximately 100 eV. The kinetic energies of photoelectrons produced by excitation from an X-ray source are about 100-1000 eV. The corresponding escape depth for these photoelectrons are about 1-5 nm, hence this is a surface sensitive technique.

1.4.2 Instrumentation

All analysis performed in this thesis utilized a VG ESCALAB Mk II surface analysis chamber, all descriptions of instrumentation are made with reference to this piece of equipment.

1.4.2.1 The Analyzer

Electrons are ejected from the sample and are detected by an electron energy analyzer according to their kinetic energy. The analyzer operates as an energy window, and in order to maintain a constant energy resolution, the pass energy is fixed. The electron energy analyzer used in the ESCALAB Mk II is a concentric hemispherical analyzer, (CHA), Figure 1.8. It consists of two hemispheres of radii R_1 (inner) and R_2 (outer), positioned concentrically. Potentials $-V_1$ and $-V_2$ are applied to the inner and outer spheres respectively, such that V_2 has greater magnitude than V_1.[37]

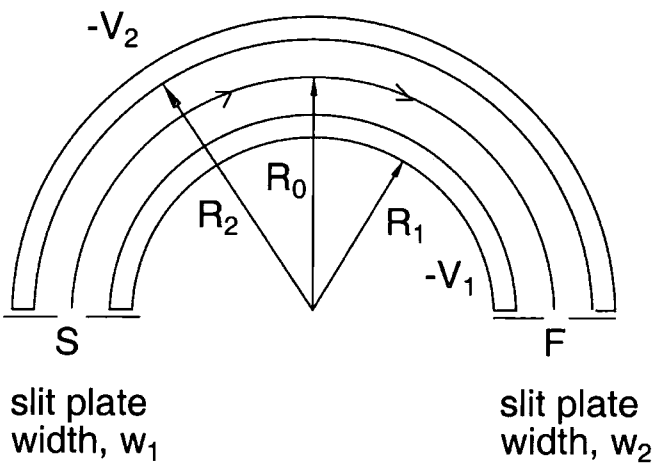

Figure 1.8 Schematic of a Concentric Hemispherical Analyzer

If electrons with energy $E = eV_0$ are injected tangentially to the median surface at radius R_0, they will follow a circular orbit of radius R_0. The potential along the median surface is V_0. Electrons of the correct energy E, injected tangentially at the source, S, are all focused at F for the hemisphere of radius R_0. By changing the voltages between the plates, electrons of specific kinetic energy will pass through the analyser and into a photomultiplier. The signal is

amplified and counts are accumulated on a PC. The output plot displays the binding energies (or kinetic) of the photo-ejected electrons against their intensities.

1.4.2.2 The Use of Vacuum

X-ray photoelectron spectrometry is carried out under vacuum for two main reasons. The first is so that electrons emitted from the sample should meet as few gas molecules as possible so they are not scattered and lost. This means that the mean free path of the emitted electrons must be greater than the dimensions of the spectrometer. The second is that in order to avoid surface contamination by adsorption of gas molecules onto the surface, the pressure in the main chamber of the spectrometer must be less than 10^{-6} torr.[37] XPS is extremely surface sensitive and so is prone to contamination effects.

1.4.2.3 X-ray Source

The X-ray source consists of an earthed filament and an anode at high positive potential. Applying a current to the filament leads to thermionic emission of electrons. These electrons are accelerated towards the anode, and upon collision with the anode, cause photons of a known energy to be emitted. These photons pass out through an aluminium window at the front of the X-ray source and impinge upon the sample under investigation. The aluminium window acts as a barrier, screening the sample from stray electrons, heating effects and contamination arising from the source. In the case of a twin-faced anode each face is coated with a metal film, typically aluminium and magnesium, about 10μm thick. These films are thick enough to exclude Cu $L\alpha$ radiation from the anode, but not thick enough to significantly impair heat transfer.[37]

1.4.2.4 Details of XPS Spectrometer and Spectra

X-ray photoelectron spectroscopy (XPS) analysis was carried out using a VG ESCALAB electron spectrometer equipped with a Mg $K\alpha_{1,2}$ X-ray source (1253.6 eV) and a concentric hemispherical analyzer. Photo-emitted electrons were collected at a take-off angle of 30° from the substrate normal, with

electron detection in the constant analyzer energy mode (CAE, pass energy = 20 eV). Core level XPS spectra were fitted with Gaussian components all having equal full-width-at-half-maximum (FWHM) using Marquardt minimization computer software.[38] Instrumental sensitivity factors determined from chemical standards were found to be in the following ratios:

Table 1.2 Sensitivity factors for the ESCALAB Mk II used in this work

Element (energy level)	Sensitivity factor relative to Carbon (C(1s))
C(1s)	1.0
O(1s)	0.36
F(1s)	0.23
N(1s)	0.72
Au($4f_{7/2}$)	0.09
Cl ($2p_{3/2}$):	0.6
P ($2p_{1/2}$ and $2p_{3/2}$)	0.66

Complete coverage by the plasma polymer layer was checked for by verifying the absence of any signal from the underlying substrate (which in the case of glass was the Si(2p) peak).

1.4.3 Spectral Interpretation

The XPS spectrum is displayed as a plot of counts per second against the electron binding energy. The number of electrons collected for a given atomic core level per unit time is a measure of the elemental abundance. The most intense photoelectron lines are moderately symmetrical and are typically the narrowest lines observed in the spectrum. The full width half maximum (FWHM) of the recorded peaks is a combination of the natural line width of the core level, the width of the photon source (X-ray line) and the analyzer resolution. This is shown in equation 1.7.

$$\Delta E = \left(\Delta E_n^2 + \Delta E_p^2 + \Delta E_a^2\right)^{1/2}$$

Equation 1.7

Here ΔE_n is the natural line width of the core level, ΔE_p is the line width of the photon source and ΔE_a is the analyzer resolution. When comparing XPS lines for the same element in different chemical environments, a change in the chemical shift is observable. This can be explained in terms of the change in binding energy. The attractive potential energy of the nucleus and the repulsive Coulombic interactions with other electrons determines the energy of the electrons bound in the core levels. When the chemical environment changes, a spatial rearrangement of the average charge distribution occurs because of the creation of different potentials by the nuclear and electronic charges of the other atoms present. The magnitude of the shift in binding energy is determined by the type and strength of the bond formed.

1.4.4 XPS Peak Fitting

In this work a Marquardt minimization is used to give a least squares fit. XPS line shapes are often represented by an asymmetric mixed Gaussian-Lorentzian function. The basic shape of the XPS peak is Lorentzian, and this is then modified by instrumental factors, and other effects such as phonon broadening to give the Gaussian contribution.[39,40] The final peak shape is asymmetric because of various loss processes. Both intrinsic and extrinsic loss processes contribute. Intrinsic loss processes include plasmons, satellites and conduction band interaction in conductors. This makes up the primary spectrum, which is considered separately from extrinsic loss processes, such as plasmon peaks and tails to higher binding energy due to inelastically scattered electrons. Intrinsic processes are associated with photoemission and extrinsic processes occur after photoemission.

1.5 ATTENUATED TOTAL REFLECTANCE FOURIER TRANSFORM INFRA-RED SPECTROSCOPY (ATR-FTIR)

Attenuated total reflectance Fourier transform infra-red spectroscopy (ATR FTIR) is used to obtain IR spectra of opaque materials. The sample is placed on top of a crystal (e.g. polished silica, silver chloride, germanium, or diamond) which is transparent in the region of the IR being used. The refractive index of the sample has to be much less than that of the crystal. The differences in

refractive indices between the optically more dense crystal and the sample causes internal reflection to occur at the interface for angles of incidence greater than the critical angle. The critical angle is defined by,

$$\Theta_c = \sin^{-1}\frac{n_2}{n_1} \qquad \textit{Equation 1.8}$$

where Θ_c is the critical angle of incidence, and n_2 and n_1 are the refractive indices of the sample and crystal respectively. The beam is not completely reflected at the interface but propagates a few μm into the surface, Figure 1.9.

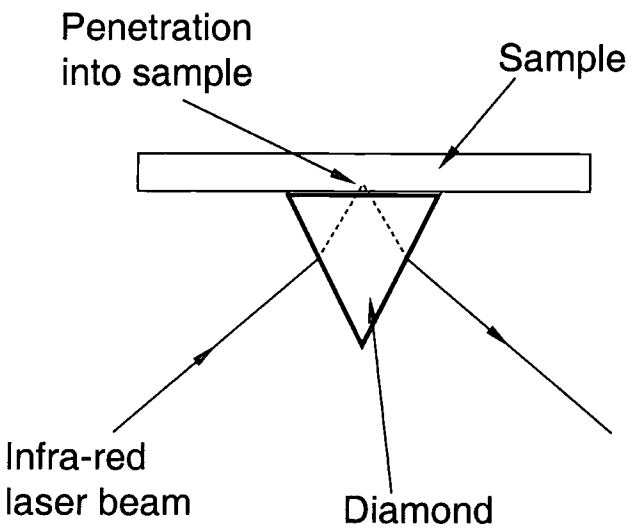

Figure 1.9. Reflection at the interface between the ATR crystal and sample.

The reflected beam can be absorbed by the groups present in this interface region, resulting in an absorption spectra of the surface of the sample. The depth of penetration into the sample is dependent upon the wavelength, and is about 0.1 to 1 μm for infra red radiation,[41] so good contact between sample and the crystal is necessary. The strength of the signal can be improved by allowing multiple passes of the beam through the crystal thereby increasing the effective path length.

ATR-FTIR was performed using a Graseby Specac Golden Gate ATR accessory fitted to a Mattson Polaris instrument. The plasma polymer layers

deposited onto pre-formed NaCl disks were employed for infrared absorption analysis using a. This was operated at 4 cm^{-1} resolution over the 400 - 4000 cm^{-1} range.

1.6 OTHER ANALYTICAL TECHNIQUES

1.6.1 Tapping Mode Atomic Force Microscopy

In Tapping Mode AFM a sharp tip is made to oscillate at or near to its resonance frequency so that it makes intermittent contact with the sample surface.[42] This reduces the lateral forces associated with contact mode AFM, and so allows the examination of soft samples, such as polymers.[43] Height images are recorded by using a feedback circuit to maintain a constant oscillation amplitude. In addition, phase shift images can be simultaneously recorded to allow the mapping of heterogeneous surfaces.[44] This phase contrast has been attributed to adhesion,[45] hydrophobicity[46] and elasticity.[47] In this thesis a Digital Instruments Nanoscope III atomic force microscope was used. The microscope was operated in Tapping Mode, where changes in oscillation amplitude of the cantilever tip provide a feedback signal corresponding to variations in height across the underlying surface.[48]

1.6.2 Transmission Electron Microscopy

In transmission electron microscopy (TEM), a beam of highly focused electrons is directed toward a sample with a thickness of less than 200 nm.[49] Electrons are often more useful than visible photons for generating images because they posses shorter wavelengths.[50] This permits magnification and imaging of a specimen up to 800 times greater than with the best light microscope. These highly energetic incident electrons interact with the atoms in the sample producing characteristic radiation and particles, which can give information for materials characterization. Analysis is possible of both deflected and non-deflected transmitted electrons, backscattered and secondary electrons, and emitted photons. Details about the interior of the specimen may also be obtained, because the electron beam penetrates through the sample. It gives the size, shape, and distribution of the phases that make up the material, as well as the composition of the material, the distribution of the elements, and segregation if present. It shows the crystal structure of the phases and the

character of the crystal defects. In TEM, the areas with the highest concentrations of heavy metal compounds are more dense than surrounding areas. Therefore, less of the electron beam passes through to the detector and the area appears darker in the final image. The signal from the detector is processed and displayed on a fluorescent material for observation, recorded on photographic film as a permanent record, or digitally captured for analysis and/or storage. For biological purposes samples are often stained to improve contrast, although in the case of metallic samples this is not necessary. The TEM's for this work were performed using a Philips CM100 (Compustage) TEM operated at 100kV. For TEM the plasma polymer deposition and functionalization reactions were carried out onto copper grids of 400 mesh. These had been coated with the Pioloform (Agar), and then were carbon coated, prior to plasma treatment.

1.6.3 Optical Microscopy

The optical microscope uses photons of light, rather than electrons, as in the case of TEM. The theoretical limit of magnification for a light microscope is about 1200x whereas a high quality TEM can magnify and resolve a specimen greater than 1,000,000x.[50] Optical microscopy is an easy and useful technique because it can be used to analyze samples in air or water, rather than under vacuum.[51]

1.6.4 Gas Barrier Measurements

Mass spectrometric sampling devices[52] have previously been used to evaluate the permeability of common elastomers[53,54]. Gas permeation measurements for the composite dendrimer layers (Chapter 3, section 3.2.5), were obtained in the manner described below, using a mass spectrometric sampling device.[55] This entailed placing the substrate between two drilled-out stainless steel flanges that were connected to a UHV chamber via a gate valve (base pressure of 5×10^{-10} mbar). One face of the sandwich structure was then exposed to oxygen gas (BOC, 99.998%) at a pressure of 1000 mbar. Gas permeation across the substrate was monitored by a UHV ion gauge (Vacuum Generators, VIG 24) and a quadrupole mass spectrometer (Vacuum Generators SX200).

The quadrupole mass spectrometer's response per unit pressure was calibrated by introducing oxygen gas directly into the UHV chamber and recording the mass spectrum at a predetermined pressure of 4 x 10^{-7} mbar (taking into account ion gauge sensitivity factors). This value was then used to quantify the mean equilibrium permeant partial pressure (MEPPP) of gas permeation through the film in the steady state flow regime.[56] The barrier improvement factor (BIF) was then calculated by referencing to the MEPPP measured for two untreated pieces of polypropylene film loaded into the gas permeability apparatus.

1.6.5 Adhesion Testing

Single lap shear adhesion tests[57,58] were performed using an Instron 5543 tensilometer, operating at a crosshead speed of 10mm min^{-1}. The purpose of these tests was to see if the various diamine containing functionalities were capable of adhering two pieces of substrate treated with the maleic anhydride plasma polymer (MAPP). Adhesion test results are presented in Chapters 2 – 4.

1.6.6 Film Thickness Measurements.

Film thickness measurements were obtained in two ways. The first method is called the Quartz Crystal Microbalance (QCM), and this uses the piezoelectric sensitivity of a quartz crystal to added mass. When a voltage is applied across the faces of a properly shaped crystal, the crystal distorts, and changes shape in proportion to the applied voltage. At certain frequencies of applied voltage, a sharp electro-mechanical resonance is encountered. When mass is added to the face of a resonating crystal, the frequency of the resonance is reduced. This change in resonance frequency was found to be related to the change in mass from the added material.

$$\frac{M_f}{M_q} = \frac{(\Delta F)}{F_q}$$

Equation 1.9

Where M_f is the mass of the added material, M_q is the mass of the uncoated crystal, ΔF is the change in frequency and F_q is the uncoated crystal resonance frequency. Substitution gives rise to the following equation:

$$T_f = \frac{K(\Delta F)}{d_f}$$

Equation 1.10

Where the film thickness T_f, is proportional (through K) to the frequency change (ΔF), and inversely proportional to the density of the film, d_f. Using a quartz crystal sensor (Kronos QM300) assuming a film density of 1.5 gcm^{-3} located adjacent to the substrate in the plasma reactor, and found to be 34±5 nm.

Film thickness' measurements were also obtained using a nkd-6000 spectrophotometer (Aquila Instruments Ltd). The obtained transmission-reflectance curves (over the 350 - 1000 nm wavelength range) were fitted to a Cauchy material model using a modified Levenburg-Marquadt method.

1.7 REFERENCES

1 Grill, A., in Cold Plasma in Materials Technology: From Fundamentals to Applications. Published by IEEE Inc., 1994.

2 Langmuir, I. *Phys. Rev.*, **1929,** *33*, 954.

3 Thornton, J.A., Penfold, A.S., in Thin Film Processes, eds. Vossen, J.L. and Kern, W., p 75. New York, Academic Press, 1978.

4 Chen, F.F., in Introduction to Plasma Physics and Controlled Fusion, 2nd Ed., New York, Plenum Press, 1984.

5 Druvestyn, M.J., Penning, F.M. *Rev. Mod. Phys.*, **1940,** *12*, 88.

6 Inagaki, N., in Plasma Surface Modification and Plasma Polymerization. Published by Technomic, 1996.

7 Beauchamp, J.L., Buttrill, S.E. *J. Chem. Phys.*, **1968,** *48*, 1783.

8 Kramer, P.W., Yeh, Y., Yaasuda, H. *J. Membr. Sci.*,**1989**, *1*, 46.

9 Inagaki, N., Tasaka, S., Ohkubo, J., Chuma, H., Okazaki, S., Saruta, T., Masui, M., Takeuchi, M., in Plasma Polymerization and Plasma Interaction with Polymeric Materials, ed., Yasuda, H.K., p 153, New York, John Wiley and Sons, 1990.

10 Yasuda, H., in Plasma Polymerization, Academic Press, Orlando, Florida, 1985.

11 Shepsis, L.V., Pedrow, P.D., Mahalingam, R., Osman, M.A. *Thin Solid Films*, **2001**, *285*, 11.

12 Huck, W.T.S., Yan, L., Stroock, A., Haag, S., Whitesides, G.M. *Langmuir*, **1999,** *15*, 6862.

13 Yan, L., Marzolin, C., Terfort, A., Whitesides, G.M. *Langmuir*, **1997,** *13*, 6704.

14 Yan, L., Zhao, X., .Whitesides, G.M. *J. Am. Chem. Soc.*, **1998,** *120*, 6179.

15 Tsukruk, V.V., Luzinov, I., Julthongpiput, D. *Langmuir*, **1999,** *15*, 3029.

16 Valiokas, R., Svedhem, S., Svensson, S.C.T., Liedberg, B. *Langmuir*, **1999,** *15*, 3390.

17 Yang, H.C., Dermody, D.L., Xu, C., Ricco, A.J., Crooks, R.M. *Langmuir*, **1996,** *12*, 726.

18 Zhou, Y.F., Bruening, M.L., Liu, Y.L., Crooks, R.M., Bergbreiter, D.E. *Langmuir*, **1996,** *12*, 5519.

19 Bruening, M.L., Zhou, Y.F., Aguilar, G., Agee, R., Bergbreiter, D.E., Crooks, R.M. *Langmuir*, **1997,** *13*, 770.

20 Wells, M., Crooks, R.M. *J. Am. Chem. Soc.*, **1996,** *118*, 3988.

21 Friedrich, J.F., Retzko, I., Kühn, G., Unger, W.E.S., Lippitz, A. *Surf. Coat. Tech.*, **2001**, *142-144*, 460.

22 Nakajima, K., Bell, A.T., Shen, M. *J. Polym. Chem. Polym. Chem. Ed.*, **1979,** *23*, 2627.

23 Decher, G., Hong, J.D. *Makromol. Chem. - Macromol. Symp.*, **1991,** *46*, 321.

24 Decher, G., Hong, J.D. *Ber. Bunsen-Ges. Phys. Chem. Chem. Phys.*, **1991,** *95*, 1430.

25 Decher, G., Hong, J.D., Schmitt, J. *Thin Solid Films*, **1992,** *210*, 831.

26 Lvov, Y., Decher, G., Sukhorukov, G. *Macromolecules*, **1993,** *26*, 5396.

27 Decher, G., Lehr, B., Lowack, K., Lvov, Y., Schmitt, J. *Biosens. Bioelectron.*, **1994,** *9*, 677.

28 Sukhorukov, G.B., Mohwald, H., Decher, G., Lvov, Y.M. *Thin Solid Films*, **1996**, *285*, 220.

29 Cassier, T. Lowack, K., Decher, G. *Supramol. Sci.*, **1998,** *5*, 309.

30 Decher, G. *Science*, **1997,** *277*, 1232.

31 Lvov, Y., Haas, H., Decher, G., Mohwald, H., Mikhailov, A., Mtchedlishvily, B., Morgunova, E., Vainshtein, B. *Langmuir*, **1994**, *10*, 4232.

32 Schrof, W., Rozouvan, S., Van Keuren, E., Horn, D., Schmitt, J., Decher, G. *Adv. Mater.*, **1998,** *10*, 338.

33 France R.M., Short, R.D., Dawson, R.A., MacNeil, S. *J. Mater. Chem.*, **1998,** *8*, 37.

34 Calderon, J.G., Harsch, A., Gross, G.W., Timmons, R.B. *J. Biomed. Mater. Res.*, **1998,** *4*, 597.

35 Briggs, D., Rivière, J.C., in Chapter 3, Practical Surface Analysis, Second Edition, Volume 1 - Auger and X-ray Photoelectron Spectroscopy, Ed. Briggs, D., and Seah, M.P. Published by John Wiley & Sons, 1990.

36 Seah, M.P.,Dench, W.A. *Surf. Interface Anal.* **1979**, *1*, 2.

37 Rivière, J.C., in Chapter 2, Practical Surface Analysis, Second Edition, Volume 1 - Auger and X-ray Photoelectron Spectroscopy, Ed. Briggs, D., and Seah, M.P. Published by John Wiley & Sons, 1990.

38 Evans, J.F., Gibson, J.H., Moulder, J.F., Hammond, J.S., Goretzki, H. *Fresenius Z. Anal. Chemie*, **1984**, *319*, 841.

39 Sherwood, P.M.A., in Practical Surface Analysis, Second Edition, Volume 1 - Auger and X-ray Photoelectron Spectroscopy, Ed. Briggs, D., and Seah, M.P. Published by John Wiley & Sons, 1990.

40 Ansell, R.O., Dickinson, T., Povey, A.F., Sherwood, P.M.A. *J. Electroanal. Chem*, **1979,** *98*, 6875.

41 C. N. Banwell in Fundamentals of Molecular Spectroscopy McGraw-Hill, Great Britian, 3rd Edition, Chapter 3, 1983.

42 Zhong, Q.; Innis, D.; Kjoller, K. K.; Elings, V. B. *Surf. Sci. Lett.*, **1993,** *290*, L688.

43 Digital Instruments Application Notes. http://www.di.com/Appnpte/TapMode/tapmodeMain.html (accessed September 2000).

44 Bar, G., Thomann, Y., Brandsch, R., Cantow, H. J., Whangbo, M. –H. *Langmuir*, **1997,** *13*, 3807.

45 Finot, M.O., Mcdermott, M.T. *J. Am. Chem. Soc.*, **1997**, *119*, 8564.

46 Chen, X., Davies, M.C., Roberts, C.J., Tendlet, S.J.B., Williams, P.M., Davies, J., Dawkes, A.C., Edwards, J.C. *Ultramicroscopy*, **1998,** *75*, 171.

47 Brandsch, R., Bar, G. *Langmuir*, **1997**, *119*, 6349.

48 Babcock, K. L.; Prater, C. B. Phase Imaging: Beyond Topography, Digital Instruments Application Note, California **1995**.

49 http://ntweb.mrl.uiuc.edu/cmm/techniques/tem.html.

50 http://www.bgsu.edu/departments/biology/facilities/MnM/tem.html.

51 http://acept.la.asu.edu/PiN/rdg/elmicr/versus.shtml.

52 Westover, L.B., Tou, J.C., Mark, J.H. *Anal. Chem.*, **1974,** *46*, 568.

53 Laurenson, L., Dennis, N.T.M. *J. Vac. Sci. Technol. A,* **1985**, *3*, 1707.

54 Tou, J.C., Rulf, D.C., DeLassus, P.T. *Anal. Chem.*, **1990**, *62*, 592.

55 Westover, L. B.; Tou, J. C.; Mark, J. H. *Anal. Chem.*, **1974**, *46*, 568.

56 Crank, J., Park, G. S. in Diffusion in Polymers, Academic Press, London, 1968, Ch. 1.

57 Shaw, S.J. in Chemistry and Technology of Epoxy Resins, Ellis, B. Ed.; Blackie Academic and Professionsal: Glasgow, 1993.

58 Anderson, G.P., Bennett, S.J., DeVires, K.L. in Analysis and Testing of Adhesive Bonds; Academic Press: London, 1977.

CHAPTER TWO

Functionalization of Maleic Anhydride Plasma Polymer (MAPP) Layer with Trifluoroethylamine (TFEA) and Jeffamine®

2.1 INTRODUCTION

Well-adhered polymeric surfaces containing anhydride groups are widely sought after for improving interfacial bonding[1], polymer/polymer compatibility,[2] as well as providing anchoring sites for chemical derivatization reactions,[3] (e.g. adhesive coupling reagents). Conventional bulk homopolymerization,[4] copolymerization,[5] and graft polymerization[6] of maleic anhydride have been extensively studied in the past. Forming films from these materials require organic solvents[7-9] or reactive polymer extrusion,[10,11] in conjunction with elevated temperatures and/or pressures. A more straightforward approach has been recently developed comprising of pulsed plasma polymerization of maleic anhydride, where the overall anhydride composition in the film can be controlled by simply programming the electrical discharge parameters (e.g. duty cycle, power, etc.).[12] Pulsing the plasma in this way restricts monomer fragmentation and reduces damage of the growing polymer layer during the duty cycle on-time, as well as encouraging conventional polymerization reaction pathways during the off-period (Scheme 2.1), page 34.[12-14]

Scheme 2.1 Plasma Polymerization of Maleic Anhydride

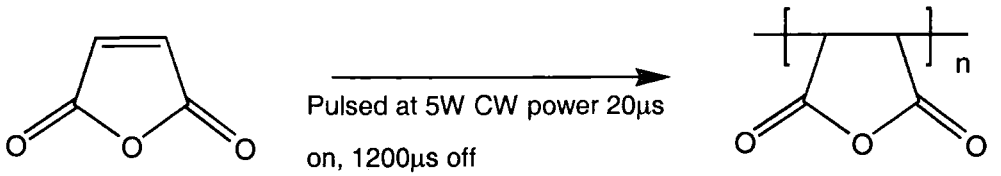

Maleic Anhydride

Maleic Anhydride Plasma Polymer

A major benefit is that the surfaces of complex shaped substrates can be easily functionalized via chemical derivatization chemistry of surface anhydride groups (e.g. nucleophilic attack by amine- or alcohol-terminated moieties to produce amides / imides and ester linkages respectively[15,16]), as demonstrated in Scheme 2.2, page 35.

In this chapter, the functionalization of maleic anhydride pulsed plasma polymer (MAPP) layers with 2,2,2-trifluoroethylamine (TFEA) and Jeffamine®-D230 (poly(propylene glycol) bis(2-aminopropyl ether)) is reported. The former has been chosen as a model nucleophile in order to demonstrate the viability of the proposed derivatization chemistry, whilst surfaces functionalized with the latter reagent (an amine terminated polyether) are of potential interest for adhesion and biomedical purposes (e.g. controlled attachment of heparin),[17,18].

Vapour phase functionalisation reactions have been to modify these MAPP surfaces. Originally, surface functionalisation was carried out in solution used as a "marking" technique in order to make specific functionalities more easily seen by XPS. Trifluoroacetic acid was one of the first labelling reagents used, as a marker for hydroxyl groups and hydrazine for carbonyl groups.[19,20] Subsequently, vapour phase functionalisation reactions have been performed[30,32] and the use of TFEA and Jeffamine in this chapter are an extension of this idea. Vapour phase functionalisation provided a means of labelling surfaces that can not be placed into a liquid, and broadens the applications of these plasma polymer layers.

Scheme 2.2 Reaction of MAPP with amines

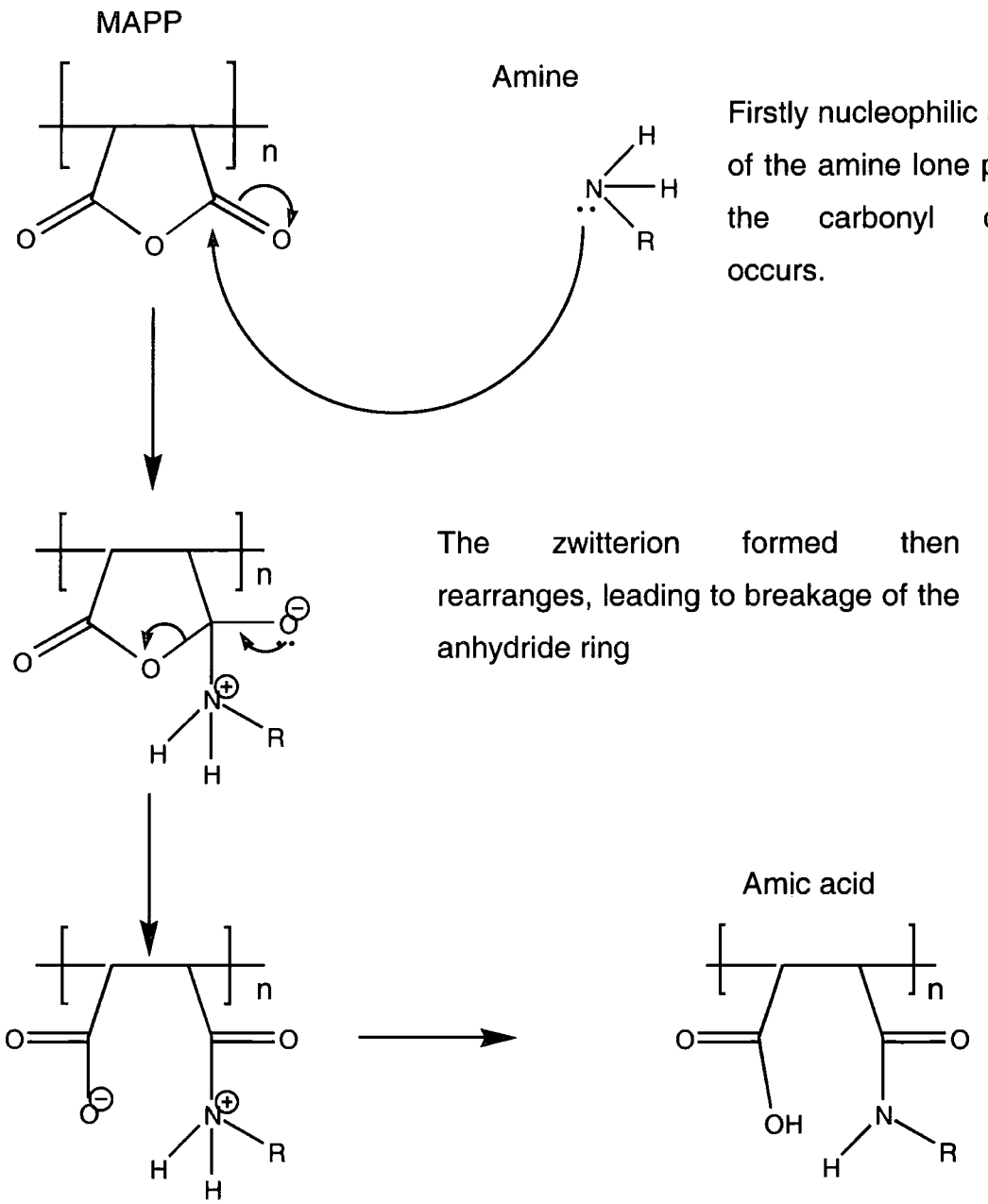

Finally, the ammonium salt loses a proton to the carbonyl anion, giving rise to the amic acid.

The typical reactor set up used is shown below, Figure 2.1.

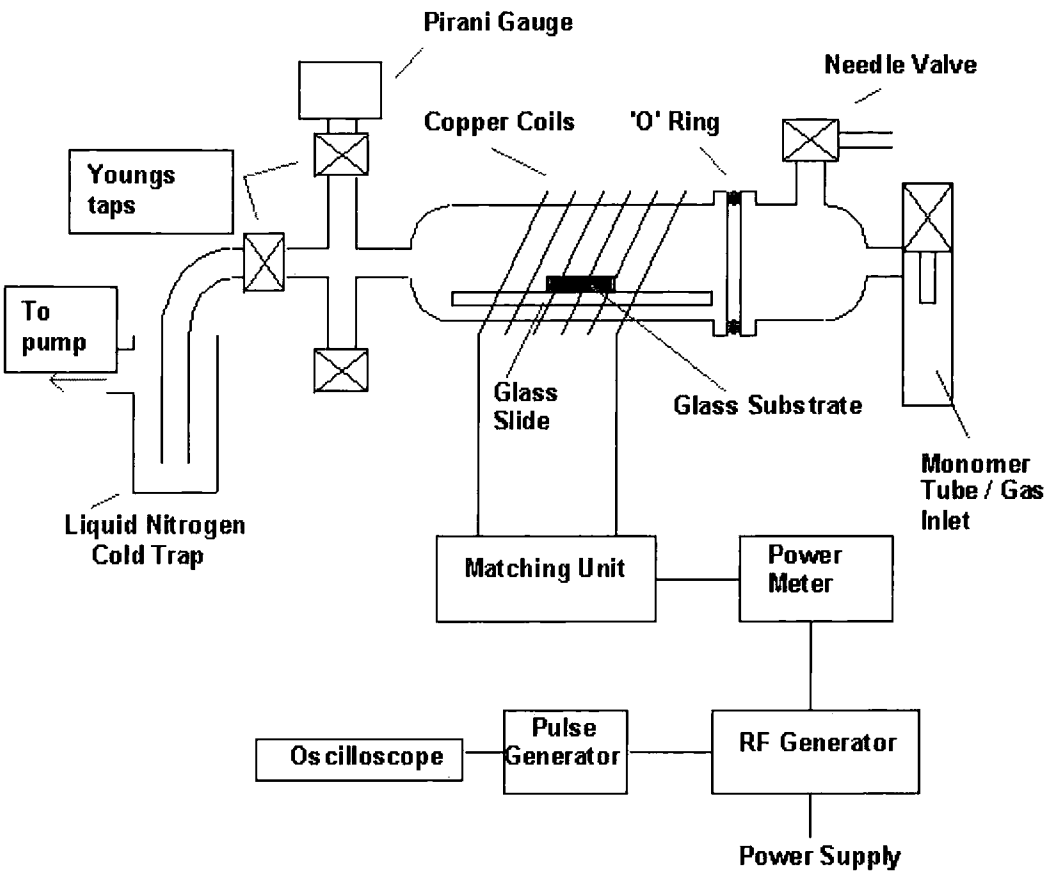

Figure 2.1 Schematic of a typical plasma reactor set-up used in this thesis

2.2.1 Pulsed Plasma Polymerization of Maleic Anhydride

Briquettes of maleic anhydride (Aldrich, 99% purity) were ground into a fine powder and loaded into a monomer tube. Plasma polymerization experiments were carried out in an electrodeless cylindrical glass reactor (4.5 cm diameter, 460 cm^3 volume, base pressure of 5.2×10^{-3} mbar, with a leak rate lower than 1.0×10^{-10} kg s^{-1}) enclosed in a Faraday cage. The reactor was fitted with an externally wound copper coil (4 mm diameter, 9 turns, spanning 8 - 15 cm from the gas inlet), a gas inlet, a thermocouple pressure gauge, and a 30 L min^{-1} two-stage rotary pump attached to a liquid nitrogen cold trap. All joints were grease free. An L-C matching network was used to match the output impedance of the R.F. generator (13.56 MHz) to that of the partially ionized gas load; this was achieved by minimizing the standing wave ratio (SWR) of the

transmitted power. Pulsed plasma polymerization experiments were carried out by using a signal generator to trigger the R.F. power supply. The pulse width and amplitude were monitored with a cathode ray oscilloscope. The average continuous wave power output (P_{cw}) of the R.F. supply spanned 5 - 90 W. Pulse on-times (t_{on}) and off-times (t_{off}) could be varied between 5 - 800 and 5 - 1200 μs respectively. The average power <*P*> delivered to the system during pulsing was calculated using the following expression:

$$\langle P \rangle = P_{CW} \left\{ \frac{t_{on}}{t_{on} + t_{off}} \right\}$$

Equation 2.1

where $t_{on} / (t_{on} + t_{off})$ is defined as the duty cycle.[21]

Prior to each experiment, the reactor was cleaned by scrubbing with detergent, rinsing in isopropyl alcohol, oven dried, followed by a 30 min high-power (50 W) air plasma treatment. The reactor was judged to be clean when the air plasma was a bright pink colour, due to transitions in the nitrogen. Experiments to determine the cleanliness of the reactor were not carried out. Next, the reactor was vented to air and the substrate to be coated (e.g. glass, silicon, polyethylene, etc.) placed at the centre of the chamber, and then evacuated back down to base pressure. The substrate to be coated depended upon the analytical technique being used. For XPS analysis, glass slides were used, for IR analysis either sodium chloride plates or silicon were used. For gas barrier and tensilometer measurements poly(propylene) or poly(ethylene) were used. Subsequently, maleic anhydride vapour was introduced into the reactor at a constant pressure of 2.6×10^{-1} mbar, and a flow rate of approximately 1.6×10^{-9} kg s^{-1}. At this stage, the plasma was ignited and left to run for 10 min. Upon completion of deposition, the R.F. generator was switched off, and the monomer feed allowed to continue to flow through the system for a further 5 min prior to pumping to base pressure. The coating thickness was measured using a quartz crystal sensor (Kronos QM300) assuming a film density of 1.5 gcm^{-1} located adjacent to the substrate in the plasma reactor. Full details are given in Chapter 1, section 1.6.6, page 27.

2.2.2 Reaction of MAPP with Trifluoroethylamine (TFEA)

The deposited MAPP coatings were first reacted with 2,2,2-TFEA (Fluorochem, 99.5%). This was done without exposing the MAPP or the amine to air in order to avoid reaction of amine groups with atmospheric CO_2 and H_2O.[22,23] This was achieved by customising the plasma reactor shown in Figure 2.1, page 36, to have two monomer inlets. This meant that once the MAPP had been deposited, the system could be evacuated down to base pressure and amine vapour fed in without requiring the system to be let up to atmosphere. The vacuum pump was isolated and amine vapour was allowed to fill and equilibrate into the empty chamber (TFEA: 68.5 mbar; Jeffamine: 10.6 mbar) at ambient temperature (~25° C). At this stage, timing of the surface functionalization reaction commenced. Upon termination of exposure, the amine reservoir was isolated, and the whole apparatus was pumped back down to its initial base pressure. Corresponding control experiments examined the reaction of ammonia (Aldrich, +99.99% purity) and diethylamine (Sigma, 98% purity) with the deposited MAPP layers. Also the vapour phase functionalization of poly(acrylic acid) with TFEA, Jeffamine, ammonia and diethylamine was carried out for comparison.

2.2.3 Reaction of MAPP with Jeffamine®

Jeffamine®-D230 (H_2N-$CH(CH_3)$-CH_2-$[OCH_2CH(CH_3)]_n$-NH_2, Aldrich, average molecular weight M_n = 230, which corresponds to 2-3 repeat units). This was done without exposure to air in order to avoid reaction of amine groups with atmospheric CO_2 and H_2O, as explained for the reaction of MAPP with TFEA, section 2.2.2.[22,23] The vacuum pump was isolated and amine vapour was allowed to fill and equilibrate into the empty chamber (Jeffamine: 10.6 mbar) at ambient temperature (~25° C). At this stage, timing of the surface functionalization reaction commenced. Upon termination of exposure, the amine reservoir was isolated, and the whole apparatus was pumped back down to its initial base pressure.

Details of XPS and IR experimental methods can be found in sections *1.4.2.4,* page 21 and *1.5,* page 23 respectively.

2.2.4 Adhesion of the MAPP Layers

For the adhesion measurements, a drop (~ 3 μl) of coupling agent solution (ethylenediamine (Aldrich, 99% purity), 0.5 M in 1,4-dioxane (Aldrich, +99%)) was placed between two MAPP coated strips of polymer film (polyethylene, PE, ICI, 0.08 mm thickness,), and then cured overnight at various temperatures. Details of the experiment are given in Chapter 1, section 1.6.5, page 27.

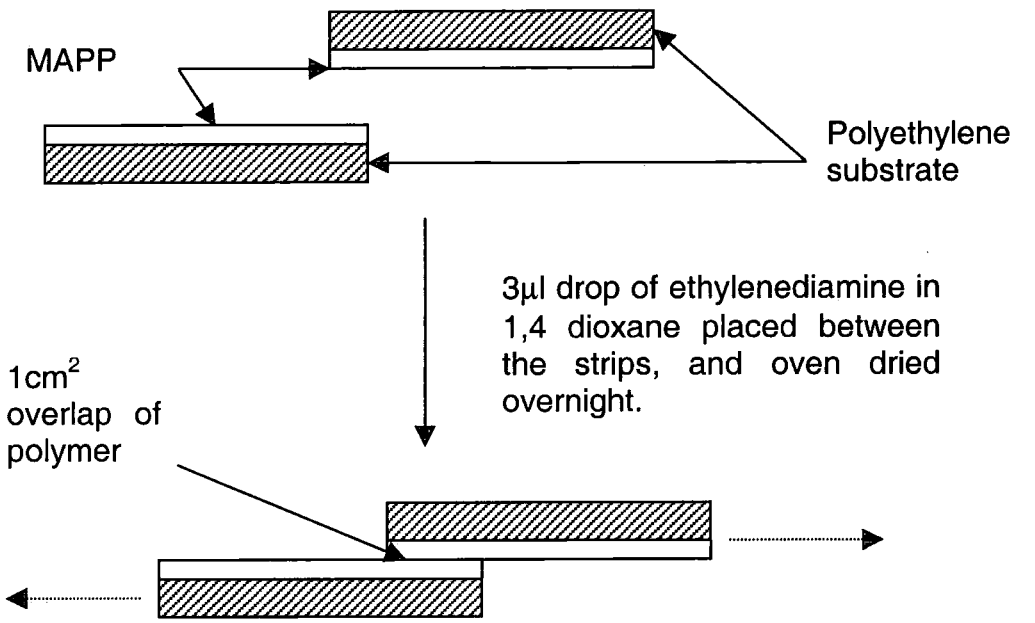

Dotted arrows show direction of tensilometer pull.

Scheme 2.3 Sample preparation for adhesion testing

2.3 RESULTS AND DISCUSSION

2.3.1 Pulsed Plasma Polymerization of Maleic Anhydride

In the past it has been demonstrated that radiation grafting of monomers onto inert polymeric supports can produce materials which combine the desirable surface properties of the graft with the good mechanical properties of the underlying substrate.[24] However the total number of grafting sites can be limited as well as uncontrollable, depending on the nature of the polymer backbone. Continuous wave plasma deposition of reactive monomers has also been utilized in this context with limited success;[25] since the selective incorporation of desired functional groups onto the plasma polymer layer tends to be poor due

to extensive molecular fragmentation processes within the electrical discharge.[25] In the case of pulsed plasma polymerization of maleic anhydride; the large and controllable concentration of surface anhydride groups[12] is ideally suited for subsequent derivatization chemistry (e.g. vapour-phase aminolysis). This approach alleviates many of the drawbacks associated with conventional solution-based and extrusion techniques (e.g. reorientation of surface functional groups and solvent extraction of low molecular weight species).[26] In fact the overall reaction yields measured for 2,2,2-TFEA and Jeffamine-D230 correlate well with previously reported model studies comprising the vapour-phase aminolysis of ethylene maleic anhydride copolymer surfaces.[27]

Previous work carried out at the University of Durham into the pulsed plasma polymerisation of maleic anhydride has studied the optimum pulsing and power conditions to achieve maximum structural retention of the anhydride ring.[12] All of the plasma polymer layers deposited were studied by XPS and IR to determine which set of conditions was most effective. In brief summary, first of all the effect of pulse on-time was studied, whilst the continuous wave power, P_{cw} was kept at 5W, and the off-time was maintained at 1200μs. It was shown that 20 μs was the optimum on-time for structural retention, as longer on-times led to a reduction in the amount of anhydride carbon groups detected. Secondly, the effect of varying the plasma off-time, whilst keeping P_{CW} at 5W, and the on-time at 20μs was looked at. An off-time of 1200μs gave optimum retention of the anhydride ring, and shorter off-times gave poorer retention. Finally P_{CW} whilst the on-time was kept at 20μs and the off time was kept at 1200μs. At high values of P_{CW} there was little retention of the anhydride ring, but as P_{CW} was reduced, the structural retention improved, reaching a maximum at 5W. It was therefore concluded that the use of lower average powers, achieved by a low value of P_{CW}, long off-time and short on-time were the optimal conditions for the deposition and structural retention of maleic anhydride.

High structural retention in the MAPP layers[12,28] was confirmed by infrared analysis, which displayed strong absorbances from the cyclic anhydride group: asymmetric and symmetric C=O stretching, anhydride group stretching, and C-

O stretch vibrations as shown in Figure 2.2, page 44 and Table 2.1, page 42. XPS analysis indicated the presence of five types of C(1s) environment for the MAPP deposited onto glass:[29] hydrocarbon ($\underline{C}H_x$ ~ 285.0 eV), carbon singly bonded to an anhydride group ($\underline{C}$-C(O)-O- ~ 285.7 eV), carbon singly bonded to oxygen (-$\underline{C}$-O ~ 286.6 eV), carbon doubly bonded to oxygen (O-$\underline{C}$-O / -$\underline{C}$=O ~ 287.9 eV), and anhydride groups (O=$\underline{C}$-O-$\underline{C}$=O ~ 289.4 eV), Figure 2.3(a), page 45. Complete coverage was confirmed by the absence of any Si(2p) signal showing through from the underlying glass substrate. Pulsing the electrical discharge on the μs - ms timescale allowed the coating composition to be controlled (i.e. the concentration of anhydride functionalities)[12]. Optimum anhydride group retention (t_{off} = 1200 μs, t_{on} = 20 μs, P_{CW} = 5 W)[12] corresponds to 58% of the surface carbon atoms belonging to cyclic anhydride repeat units. Both ellipsometry and quartz crystal sensor found the MAPP film to be 34 ± 5nm thick, Chapter 1, section 1.6.6, page 27.

Table 2.1 Infrared assignments of MAPP, nucleophilic reagents, and corresponding derivatized plasma polymer.

Peak Position/ cm^{-1}	*Assignment*	*MA*	*TFEA*	*MA+TFEA*	*Jeffamine*	*MA+Jeffamine*
1849	C=O anhydride stretch	*		*		*
1780	C=O anhydride stretch	*		*		*
1725-1700	Carboxylic acid stretch			*		*
1772, 1710	Imide bands					*(after heating)
1660 – 1563 (Broad band)	Amide I (C=O stretching)and Amide II (N-H bending)			*		*
1627-1590	NH_2 bands		*		*	
1625 – 1560, and 1550 - 1505	NH_3^+, antisymmetric and symmetric deformations					*
1490-1400	C-NH stretch of monosubstituted amide			*		*
1400-1000	CF_3 stretches		*	*		
1288-1240	Cyclic anhydride stretch	*				
1180-1000	C-N stretch		*	*	*	
1150	Imide stretch					*(after heating)
1150-1060	C-O-C stretch				*	*
958-935	Cyclic unconjugated anhydride	*				
950-780	C-C skeletal bands				*	*
850	NH_2 wag		*		*	*

2.3.2 Functionalization Reactions with TFEA

A key reaction between anhydride groups and primary amines is aminolysis.[30] The deposited MAPP layer was exposed to TFEA vapour, with the aim of producing amide linkages at the surface, as depicted in Scheme 2.2, page 35. In this ring opening reaction, nucleophilic attack occurs at one of the carbonyl carbons. The resulting structure rearranges, giving rise to a carbanion and an ammonium ion. The ammonium ion loses a hydrogen atom to the carbanion, giving rise to what is termed an amic acid, containing an amide group and an acid group. Infrared spectroscopy confirmed that ring opening of the cyclic anhydride centres had occurred to yield amide and carboxylic acid groups, as seen by the appearance of the following new absorbances superimposed on the background MAPP spectrum: overlapping amide I and amide II bands (1660 – 1563 cm^{-1}), carboxylic acid stretching (1725 – 1700 cm^{-1}), and C-NH monosubstituted amide stretching (1490 – 1400 cm^{-1}), Figure 2.2, page 44 and Table 2.1, page 42. Furthermore, infrared spectroscopy indicated that heating at 120 °C gave rise to ring closure and the formation of cyclic imides, Scheme 2.4, page 47. The presence of background spectral features from the underlying MAPP layer was consistent with functionalization occurring at just the surface (ATR-FTIR sampling depth is approximately 100 nm[31]). The use of angle resolved XPS spectroscopy here might have provided information about the depth of functionalisation occurring,

The reaction efficiency within the outermost 5nm of the surface was investigated by XPS. Details of the peak fitting parameters can be found in chapter 1, section 1.3.4, page 21. The C(1s) spectra following exposure to TFEA vapour could be fitted to six different types of carbon functionality:[29] hydrocarbon ($\underline{C}H_x$ ~ 285.0 eV), carbon singly bonded to an amide / carboxylic acid groups ($\underline{C}H_2C(O)NHR$ / $\underline{C}H_2C(O)OH$) ~ 285.7 eV), carbon singly bonded to both nitrogen and a trifluoromethyl carbon (N-$\underline{C}$-CF_3 ~ 287.0 eV), amide group (RHN-$\underline{C}$=O ~ 287.9 eV), anhydride / carboxylic acid groups (O=$\underline{C}$-O-$\underline{C}$=O / $\underline{C}$(O)OH ~ 289.4 eV), and trifluoromethyl carbon (-$\underline{C}F_3$ ~ 292.5 eV), with a corresponding Mg$K\alpha_{3,4}$ satellite ~ 283.7 eV), Figure 2.3(b). The unambiguous assignment of the trifluoromethyl C(1s) peak, as well as the contribution from

the three trifluoromethyl fluorine atoms (-C<u>F</u>$_3$ ~ 687.7 eV)[29] to the F(1s) region, confirmed that surface functionalization had indeed taken place. The N(1s) peak was assigned to amide groups (RH<u>N</u>-C=O ~ 399.8 eV)[29], and the peak areas were used to calculate the overall aminolysis efficiency,[30,32] Figure 2.4(b), page 46. Nitrogen incorporation at the surface reached a limiting value after approximately 30 min exposure to TFEA vapour, which corresponds to an overall conversion factor of 0.93 ± 0.01 in the outermost 2-3 nm region (the XPS sampling depth[29]). Heating at 120 °C gave rise to no change in the N(1s) XPS spectrum. This was to be expected since the N(1s) binding energy values of amide and imide linkages are very similar (≈ 400 eV)[29], Scheme 2.4, page 47.

Figure 2.2 IR spectra of (a) TFEA liquid; (b) untreated MAPP; (c) plasma polymer functionalized with TFEA; and (d) heating of (c) to 120°C. (A similar spectra appeared in the Ph.D. thesis of S.A. Evenson, University of Durham, 1997).

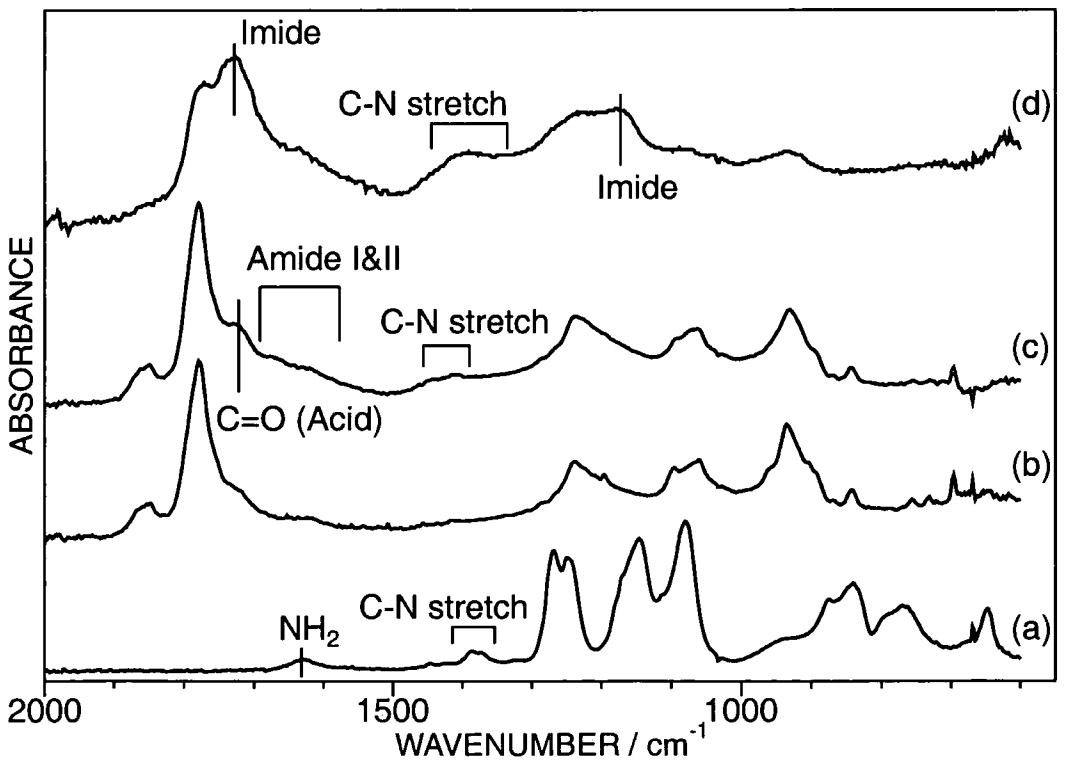

Figure 2.3 C(1s) spectra of (a) untreated MAPP; (b) the plasma polymer functionalized with TFEA; and (c) the plasma polymer functionalized with Jeffamine®. (i) Indicates the position of the $\underline{C}F_3$ peak, (ii) indicates the position of the $\underline{C}(O)$-O peak. (A similar spectra appears in the thesis of S.A. Evenson, University of Durham, 1997).

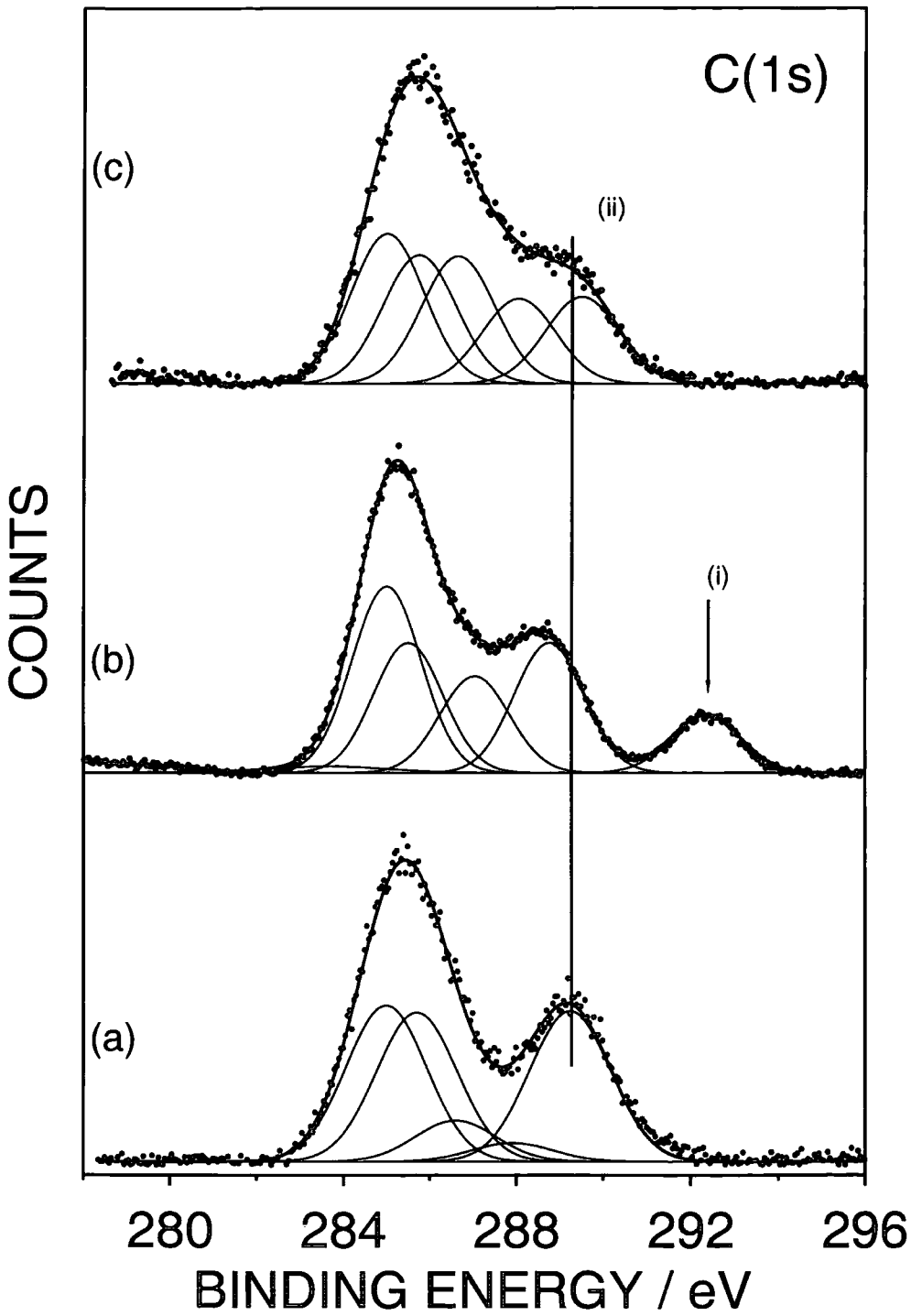

Figure 2.4 N(1s) spectra of (a) untreated MAPP; (b) the plasma polymer functionalized with TFEA; (c) the plasma polymer functionalized with Jeffamine® and (d) MAPP functionalized with Jeffamine® and oven heated to 120°C. (A similar spectra appears in the thesis of S.A. Evenson, University of Durham, 1997).

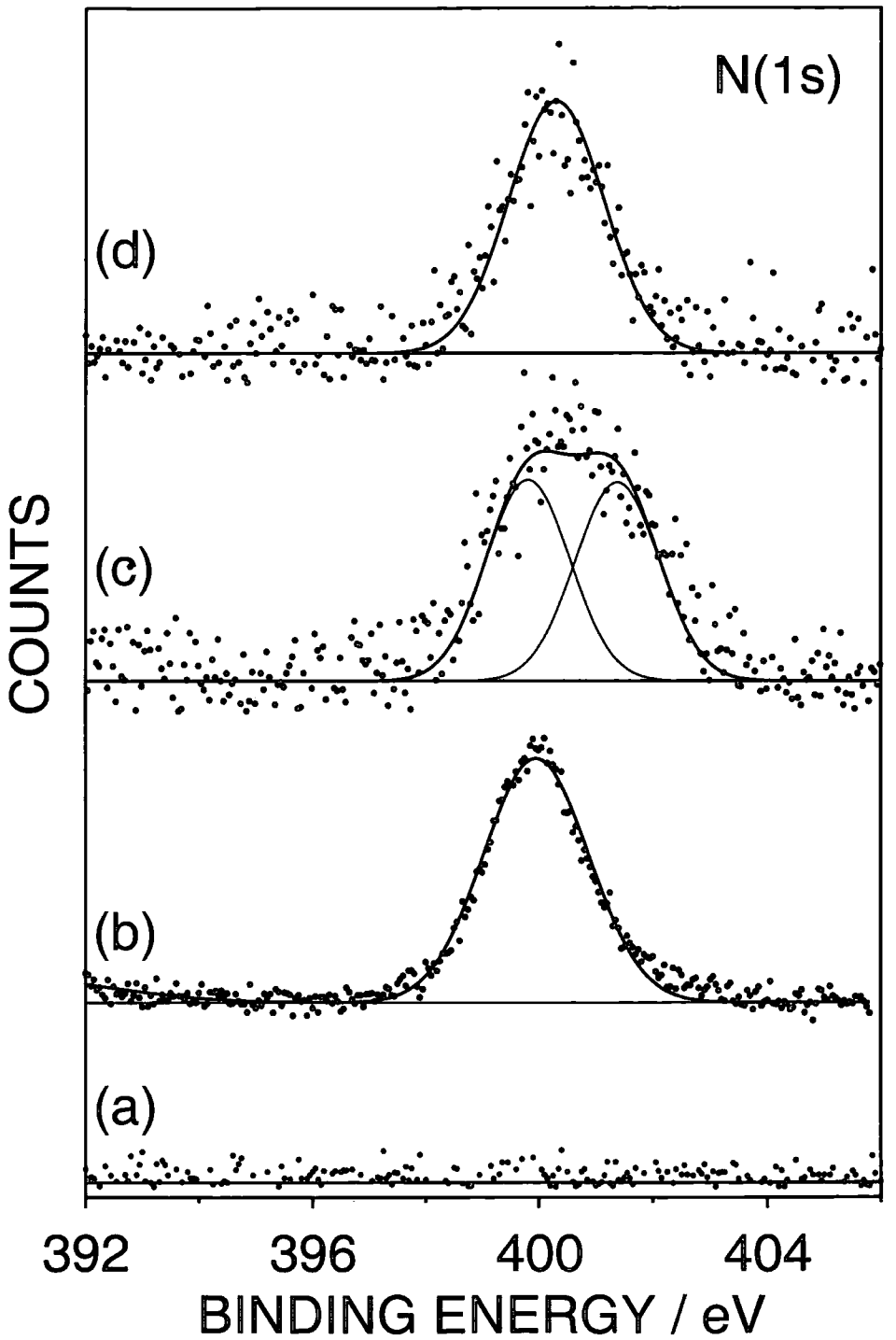

Scheme 2.4 Imide formation upon heating of the functionalized MAPP.

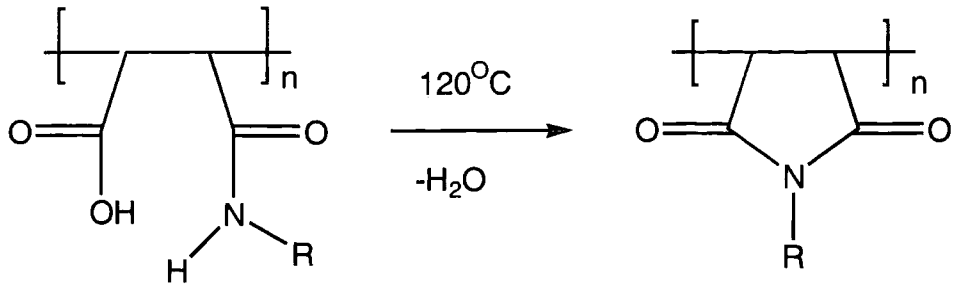

It is interesting to note that in contrast to the other amines TFEA does not yield the additional ammonium salt during amide formation at each cyclic anhydride centre, Table 2.2, page 49. This can be accounted for on the basis of acid dissociation constants (K_a). TFEA has a K_a value of 2.5×10^{-6}, whereas ammonia and diethylamine have values of 5.6×10^{-10} and 1×10^{-11} respectively[33,34]. Hence ammonia and diethylamine are much more basic compared to TFEA, and therefore far more likely to accept a proton from the carboxylic acid group formed adjacent to the amide linkage during cyclic anhydride ring opening, Scheme 2.2, page 35. Furthermore, the second dissociation constant for maleic acid is 8.57×10^{-7},[34] this can be attributed to the proximity of the carboxyl groups in the *cis* configuration giving energetically unfavourable electrostatic effects[35]; whereas poly(acrylic acid) is a stronger acid[34] ($K_a = 5.6 \times 10^{-4}$) compared to the carboxylic acid group formed adjacent to the amide linkage, and therefore poly(acrylic acid) is more capable of donating a proton to a weaker acid such as TFEA (K_a value of 2.5×10^{-6}), Table 2.2, page 49.

2.3.3 Functionalization Reaction with Jeffamine

Jeffamine was also found to readily undergo reaction with the MAPP layer, Scheme 2.5, page 50. This was confirmed by infrared spectroscopy: overlapping amide I and amide II bands, carboxylic acid stretch, and C-NH monosubstituted amide stretching, Figure 2.5, page 51 and Table 2.1, page 42. Once again, heating at 120 °C indicated ring closure and the formation of cyclic imides.

On this basis, the following carbon functionalities were fitted to the C(1s) XPS envelope of Jeffamine functionalized MAPP:[29] hydrocarbon ($\underline{C}H_x$ ~ 285.0 eV), carbon singly bonded to amide / carboxylic acid groups ($\underline{C}H_2C(O)NHR$ / $\underline{C}H_2C(O)OH$) ~ 285.7 eV), amine groups ($\underline{C}$-NH_2 ~ 286.0 eV), carbon singly bonded to oxygen ($\underline{C}$-O ~ 286.4 eV), carbon singly bonded to nitrogen in the Jeffamine end groups ($\underline{C}$-NH-C(O)CH_2- ~ 286.5 eV), amide groups ($\underline{C}$(O)NHR ~ 287.9 eV), and anhydride / carboxylic acid groups (O=$\underline{C}$-O-$\underline{C}$=O / $\underline{C}$(O)OH ~ 289.4 eV)), Figure 2.3(c). Interestingly, the N(1s) XPS region indicated the presence of two different types of nitrogen environment in approximately equal concentrations, Figure 2.4(c), page 46 and Table 2.2, page 49. The higher binding energy peak (402 eV) can be assigned to ammonium salt formation following protonation of terminal amine groups on the Jeffamine chain by surface carboxylic acid centres generated during aminolysis of the cyclic anhydride groups. This was confirmed by reacting a series of amines with poly(acrylic acid), Table 2.2, page 49. The other N(1s) feature at approximately 400 eV can be attributed to either amine (a free end of Jeffamine) or amide linkages[29]. Since the N(1s) peak area ratio of amide/amine to ammonium salt is approximately 1:1, then each Jeffamine chain must be bonded via an amide linkage at one end and looped around to form an ammonium salt complex at its other end (if additional Jeffamine chains from the vapour phase had reacted with the carboxylic acid centres generated during aminolysis of the cyclic anhydride groups, then the ratio of amide/amine to ammonium salt N(1s) environments should have been greater than 1:1, i.e. much closer to 3:1). This assignment was confirmed by heating at 120 °C, this gave rise to the disappearance of the ammonium salt feature at 402 eV to produce the cyclic imide linkage (~400 eV), Figure 2.4(d), page 46, in conjunction with detachment of the other end of the Jeffamine chain, Scheme 2.5, page 50. Corresponding heating experiments conducted with ammonium salts of poly(acrylic acid) confirmed that amide formation via dehydration of the ammonium salt was not a possibility at 120 °C, Table 2.2, page 49.

Table 2.2 Influence of heating at 120 °C upon amide/amine (400 eV) versus ammonium salt (402 eV) N(1s) peak area ratios for MAPP and poly(acrylic acid) surfaces.

Nucleophile	*MAPP*		*Poly (acrylic acid)*	
	Unheated	*Heated*	*Unheated*	*Heated*
TFEA	1 peak at 400 eV	1 peak at 400 eV	1 peak at 402 eV	1 peak at 402 eV
Jeffamine	≈1:1	1 peak at 400 eV	1 peak at 402 eV	1 peak at 402 eV
Ammonia	≈2.9:1	1 peak at 400 eV	1 peak at 402 eV	1 peak at 402 eV
Diethylamine	≈3.6:1	≈3.6:1	-	-

Furthermore, the inability of a secondary amine (diethylamine) to undergo the imide cyclization reaction to form the maleimide (i.e. ammonium salt was retained) is consistent with this explanation (secondary amines are prevented from reacting beyond the amide because of the lack any additional N-H bonds), Scheme 2.5, page 50 and Table 2.2, page 49. On this basis, the extent of Jeffamine attachment was calculated to be 0.95 ± 0.02 from the N(1s) peak areas after 30 min reaction time.

Scheme 2.5 Reaction between the MAPP and Jeffamine (Looping around of the Polypropylene Glycol (PPG) need not necessarily occur at the adjacent acid site).

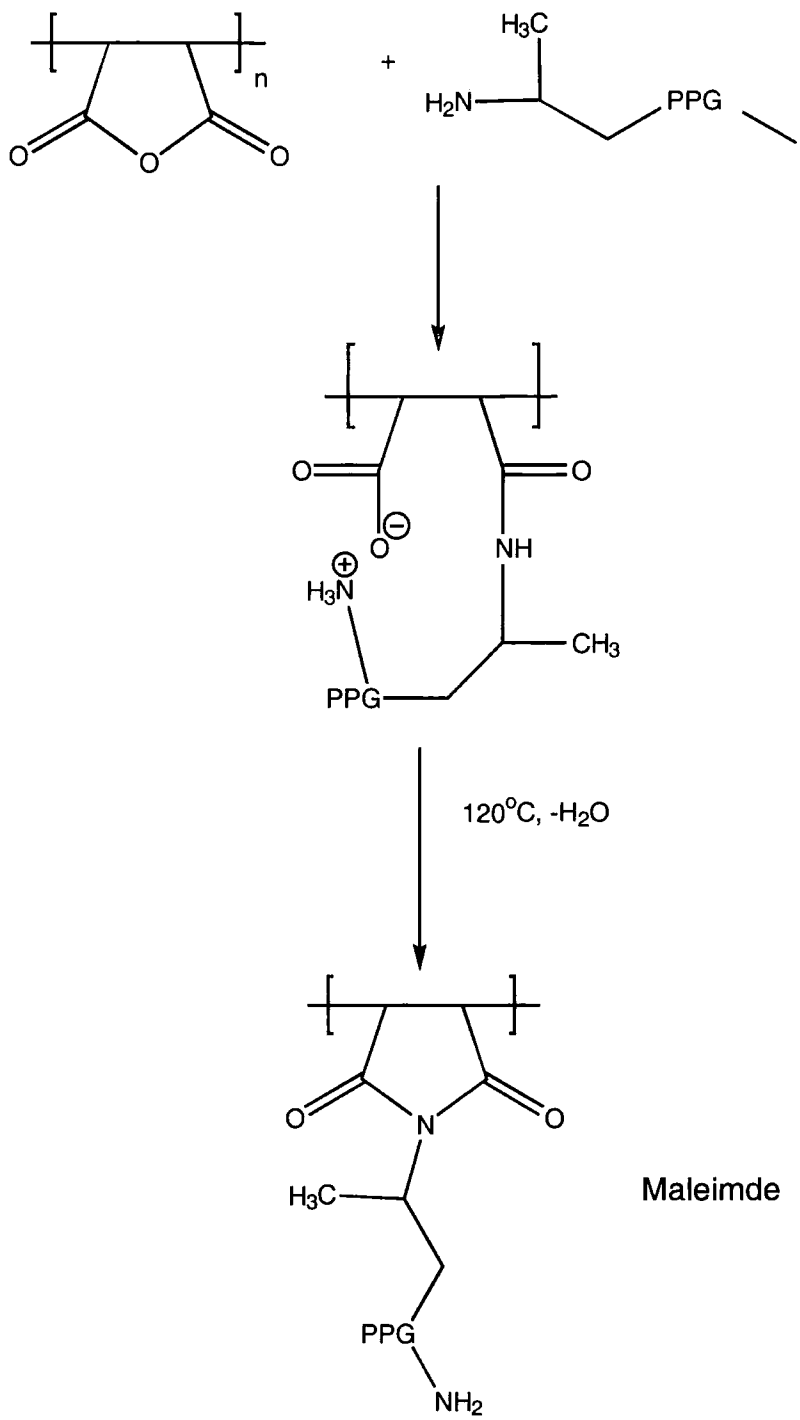

Maleimde

Figure 2.5 IR spectra of (a) Jeffamine® liquid; (b) untreated MAPP; (c) plasma polymer functionalized with Jeffamine®; and (d) heating of (c) to 120°C.

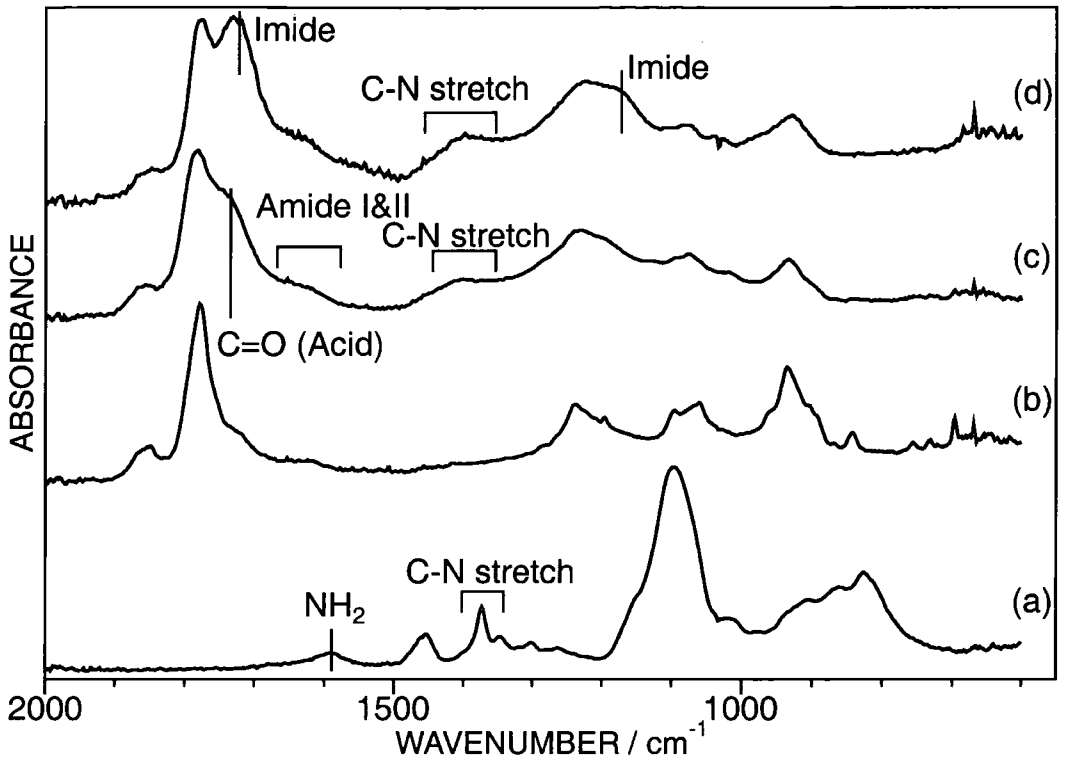

2.3.4 Adhesion

Jeffamine and ethylenediamine, (EDAM), (a shorter chain analogue of Jeffamine) were used as coupling agents for adhering two pieces of poly(ethylene) together (each of which had been coated with MAPP and then exposed to the diamine). It was found that heating (imide formation) gave rise to good adhesion, Table 2.3.

Table 2.3 Lap joint adhesion test measurements.

Substrate	*Maximum Recorded Load / N cm^{-2}*
Polyethylene (PE)	15.7
PE, MA deposited	Did not adhere
PE, MA deposited, Jeffamine labelled in vapour phase, no heating	Did not adhere
PE, MA deposited, Jeffamine labelled in solution phase, no heating	2.78
PE, MA deposited, Jeffamine labelled in vapour phase, heated to 120°C	7.10*
PE, MA deposited, Jeffamine labelled in solution phase, heated to 120°C	10.27
PE, labelled with EDAM, unheated	Did not adhere
PE, labelled with EDAM, heated to 60°C	12.4
PE, labelled with EDAM, heated to 80°C	13.9
PE, labelled with EDAM, heated to 120°C	13.9

The breaking load of the polyethylene substrate is approximately 15.7 Ncm^2. In the absence of a curing agent, such as Jeffamine or EDAM, no adhesion is observed between the samples. Similarly, if a curing agent is used, and forming amic acid groups at the two MAPP surfaces, but is not heated, no adhesion strength is recorded. When the curing agent it used, and the sample is heated to 120°C, then it has been shown that the amic acid groups will undergo a ring closure reaction, as shown in Scheme 2.4, page 47. This

results in a strengthening of the adhesive layer, and explains the increase in the measured adhesion of the layers.

2.4 CONCLUSIONS

Amine terminated nucleophiles can be chemically fixed onto any shaped solid substrate via reaction with a well-adhered MAPP layer. The intermolecular spacing and concentration of amine containing moieties attached to the surface can be finely tuned by controlling the level of anhydride group incorporation during pulsed plasma deposition.

Once the MAPP has been deposited on the substrate, either glass, sodium chloride or polyethylene, a variety of reactions can be carried out to derivatize the surface, and introduce new functional groups. This has been demonstrated with TFEA and Jeffamine, used as two model nucleophiles in order to try and understand the reactions occurring at the surface. It has been shown that the TFEA, being more acidic than hydrocarbon amines will not form ammonium salts at the MAPP surface, whereas the more basic Jeffamine will do so.

Furthermore, it has been demonstrates that the amic acid groups will form surface imide groups when heated. This was most readily observed in the case of the Jeffamine functionalized MAPP, through the loss of the peak in the N(1s) spectrum attributable to the ammonium salt. The imide groups formed were found to be effective in adhering polyethylene substrates that had been coated with MAPP.

2.5 REFERENCES

1 Hindryckx, F., Dubois, P., Patin, M., Jerome, R., Teyssie, P. *J. Appl. Polym. Sci.* **1995**, *56*, 1093.

2 Oostenbrink, A. J., Gaymans, R. J. *Polymer*, **1992**, *31*, 3086.

3 Gaboury, S. R., Urban, M. W. *Langmuir*, **1994**, *10*, 2289.

4 Tsiourvas, D., Paleos, C. M, P. Dais *J. Appl. Polym. Sci.* **1989**, 38, 257.

5 Kuo, P. -L., Ni, S. - C., Lai, C. -C. *J. Appl. Polym. Sci.* **1992**, *45*, 611.

6 Samay, G., Nagy, T., White, J. L. *J. Appl. Polym. Sci.* **1995**, 56, 1423.

7 Harris, R. F., Lopez, K. M *J. Appl. Polym. Sci.* **1993**, *50*, 559.

8 Harris, R. F., DePorter, C. D., Potter, R. B. *Macromolecules* **1991**, *24*, 2973.

9 Felix, J. M., Gatenholm, P. *J. Appl. Polym. Sci.* **1991**, *42*, 609.

10 Vermeesch, I., Groeninckx, G. *J. Appl. Polym. Sci.* **1994**, *53*, 1365.

11 Koning, C., Ikker, A., Borggreve, R., Leemans, L., Moller, M. *Polymer* **1993**, 34, 4410.

12 Ryan, M. E., Hynes, A. M., Badyal, J. P. S. *Chem. Mater.* **1996**, *8*, 37.

13 Rinsch, C. L., Chen, X., Panchalingham, V., Everhart, R. C., Wang, J., Timmons, R. B. *Langmuir* **1996**, *12*, 2995.

14 Hynes, A. M., Badyal, J. P. S. *Chem. Mater.* **1998**, *10*, 2177..

15 Trivedi, B. C., Culbertson, B. M. *Maleic Anhydride*, Plenum: New York, **1982**.

16 McMurry, J. *Organic Chemistry,* Brooks/Cole: Pacific Grove, CA, 1992, 813.

17 Vulic, I., Okano, T., Kim, S. W. *J. Polym. Sci. Part A Polym. Chem.* **1988**, 26, 381.

18 Dérand, H., Wesslén, B. *J. Polym. Sci. Part A Polym. Chem.* **1995**, *33*, 571.

19 Chilkoti, A., Ratner, B.D., Briggs, D. *Chem. Mater.*, **1991**, *3*, 51.

20 Ameen, A.P., Ward, R.J., Short, R.D., Beamson, G., Briggs, D. *Polymer*, **1993**, *34*, 1795.

21 Savage, C. R., Timmons, R. B. *Chem. Mater.* **1991**, *3*, 575.

22 A.K. Chakraborty, K.B. Bischoff, G. Astarita, J.R. Damewood Jr. *J. Am. Chem. Soc.*, **1988**, *110*, 6947.

23 D.E. Penny, T.J. Ritter, *J. Chem. Soc., Faraday Trans. 1.*, **1983** *79*, 2103.

24 Cohn, D., Hoffman, A. S., Ratner, B. D. *J. Appl. Polym. Sci.* **1984**, *29*, 2645.

25 Chilkoti, A., Ratner, B. D., Briggs, D. *Chem. Mater.* **1991**, *3*, 51.

26 Nakayama, Y., Takahagi, T., Soeda, F., Hatada, K., Nagaoka, S., Suzuki, J., Ishitani, A. *J. Polym. Sci.* **1988**, 26, 559.

27 Evenson, S. A., Badyal, J. P. S. *J. Phys. Chem. B* **1998**, *102*, 5500.

28 Silverstein, R. M., Bassler, G. C., Morril, T. C. *Spectrometric Identification of Organic Compounds*, Wiley: Singapore, **1991**.

29 Beamson, G., Briggs, D. *High Resolution XPS of Organic Polymers*, Wiley: Chichester, **1992**.

30 Sutherland, I., Sheng, E.-S., Brewis, M., Heath, R.J. *J. Mater. Chem.* **1994**, 4, 683.

31 Sampling depth of golden gate ATR-FTIR

32 Popat, R.P., Sutherland, I., Sheng, E.-S. *J. Mater. Chem.* **1995**, 5, 713.

33 Feiser, M., Feiser, L.F. *Reagents for Organic Synthesis,* 8, Wiley, New York, **1967.**

34 Lide, D.R., Editor-in-Chief. *CRC Handbook of Chemistry and Physics, 72nd Edition*, Chemical Rubber Publishing Company. **1991-1992.**

35 Ka values .....v*cis* configuration giving energetical unfavourable electrostatic effects

CHAPTER THREE

Functionalization of Maleic Anhydride plasma polymer (MAPP) with poly(amidoamine) (PAMAM) dendrimers

3.1 INTRODUCTION

Dendrimers are highly ordered, three-dimensional, tree-like, functional polymers comprising branched repeat units emanating from a central core.[1] Their high density of terminal groups provides a large number of reactive sites.[2] Potential applications include:[3-6] nanoscale catalysts, micelle mimics, drug delivery agents, chemical sensors, high performance polymers, and adhesives. A number of studies have been reported in the literature describing the immobilization of poly(amidoamine) (PAMAM) dendrimers onto solid surfaces (predominantly multi-step wet chemical strategies), these include silica[7-13], gold[14-17], and mica[18] substrates. In the case of covalent attachment of dendrimers to solid surfaces, an intermediate coupling layer is normally required[18-21]. However, the substrate-specific nature of such reactions prohibits their more widescale applicability.

Here an alternative methodology based on the aminolysis reaction[22,23] between

amine terminated dendrimers and maleic anhydride pulsed plasma polymer (MAPP) surfaces. In this case, the concentration of anhydride functional groups present at the surface (and hence aminolysis with amine terminated dendrimers) can be controlled by programming the electrical discharge parameters (e.g. duty cycle, peak power, etc.), Scheme 3.1, page 63. Furthermore, the reactivity of such surface immobilized PAMAM dendrimer structures towards trifluoroacetic acid and gold (III) chloride are demonstrated. Adhesive and gas barrier performances have also been investigated.

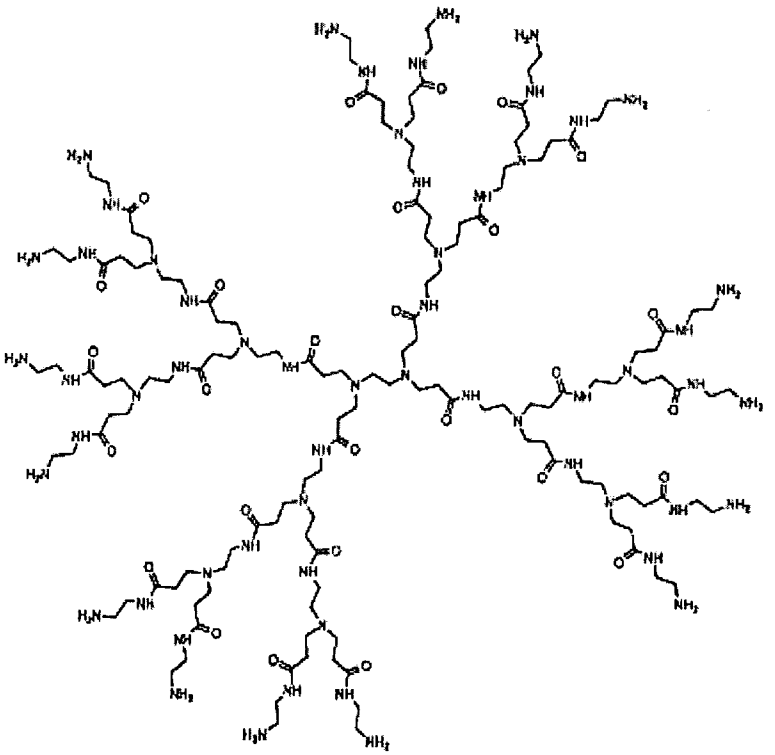

Figure 3.1 A second generation PAMAM dendrimer

PAMAM dendrimers have an ethylenediamine (EDA) core, and the structure is built out from both ends of the starting molecule, Figure 3.1, page 58. With each generation the number of terminal amine groups doubles, Table 3.1, page 59. It is the primary amines on the outside of the PAMAM dendrimers and the secondary amines within the molecule that enable many different reactions to occur, some of which are detailed in this chapter.

3.2 EXPERIMENTAL

Experimental details on the plasma polymerization of maleic anhydride can be fond in Chapter 2, section 2.2, page 36.

3.2.1 Attachment of Dendrimers to the MAPP

Drops of poly(amidoamine) (PAMAM) Starburst™ dendrimer solution (Aldrich, supplied as 10% wt. / vol. in methanol) were pipetted onto the plasma polymer surfaces under a nitrogen atmosphere. Any remaining unreacted dendrimers were removed by subsequent rinsing with methanol. Solutions containing different dendrimer generations and concentrations were employed in order to study the changes in dendrimer packing density at the surface. Details of the different dendrimer generations available are given in Table 3.1.

Table 3.1 Details of different dendrimer generations

Dendrimer Generation	*Molecular Weight*	*Measured Molecular Diameter / nm* *	*Calculated Molecular Volume / nm^3* ⊗	*Number of Surface Groups* *
0	517	1.5	1.8	4
1	1430	2.2	5.6	8
2	3256	2.9	12.8	16
3	6909	3.6	24.4	32
4	14215	4.5	47.7	64

* Values taken from Dendritech Inc. product literature; ⊗ - Calculated using $V = \frac{4}{3}\pi r^3$.

A Digital Instruments Nanoscope III atomic force microscope (AFM) was used to identify individual dendrimers at the MAPP surfaces. Further details about the AFM can be found in Chapter 1, section 1.6.1, page 25. XPS was also used, and details can be found in Chapter 1, section 1.4.2.4, page 21.

3.2.2 Functionalization of dendrimers with Trifluoroacetic Acid (TFAAcid)

4th generation PAMAM dendrimers immobilized onto MAPP surfaces were chemically functionalized by placing the dendrimer coated substrate into a glass vacuum apparatus and evacuating to a pressure of 5 x 10^{-3} mbar. The rotary pump was then isolated from the system and the dendrimer layer exposed to TFA Acid vapour for 30 mins. The whole apparatus was then evacuated back down to its initial base pressure. Samples were analysed by XPS and ATR-FTIR, details of which can be found in Chapter 1, sections 1.4.2.4, page 21 and 1.5, page 23 respectively.

3.2.3 Functionalization of dendrimers with Gold (III) Chloride

The PAMAM dendrimer layers were functionalized with gold (III) chloride (20% w/v in methanol). The gold (III) chloride was dropped onto the dendrimer functionalized MAPP films and left for 10 minutes and were then rinsed with methanol and allowed to dry in air. The gold (III) chloride functionalized layers were then subjected to a hydrogen plasma (20 watts, 5 minutes, 0.4 torr), to reduce the gold (III) chloride to gold. Samples were analysed by XPS, ATR-FTIR, TEM, and AFM. Details of these techniques can be found in Chapter 1, sections 1.4.2.4, page 21, 1.5, page 23, 1.6.1, page 25 and 1.6.2, page 25.

3.2.4 Adhesion studies.

Adhesion performance was explored by placing a 0.01 ml drop of 10% wt. / vol. 4th generation PAMAM dendrimer solution between two MAPP coated strips of polypropylene film (ICI, 50mm x 10mm, 0.80μm thickness) to make a 1 cm^2 overlap joint. This was then cured overnight at 120°C. Subsequently, single lap adhesion tests were performed on these laminates using an Instron 5543 tensilometer operating at a crosshead speed of 10 mm min^{-1}. The schematic diagram for producing samples for adhesion testing is given in Chapter 2, scheme 2.3, page 38.

3.2.5 Gas barrier studies.

Finally, the gas permeation characteristics of immobilized 4th generation PAMAM dendrimer layers was evaluated by reacting one piece of MAPP coated polypropylene film with dendrimer solution followed by rinsing in methanol to remove any excess, Scheme 3.2, page 63. Next, a second piece of MAPP coated polypropylene was placed face down on top, in order to sandwich the PAMAM dendrimer layer between anhydride functionalities. This composite structure was then clamped between two pieces of glass and placed in an oven to cure at 120 °C for 12 hours. Details of how gas permeation measurements are obtained can be found in Chapter 1, section 1.6.4, page 26.

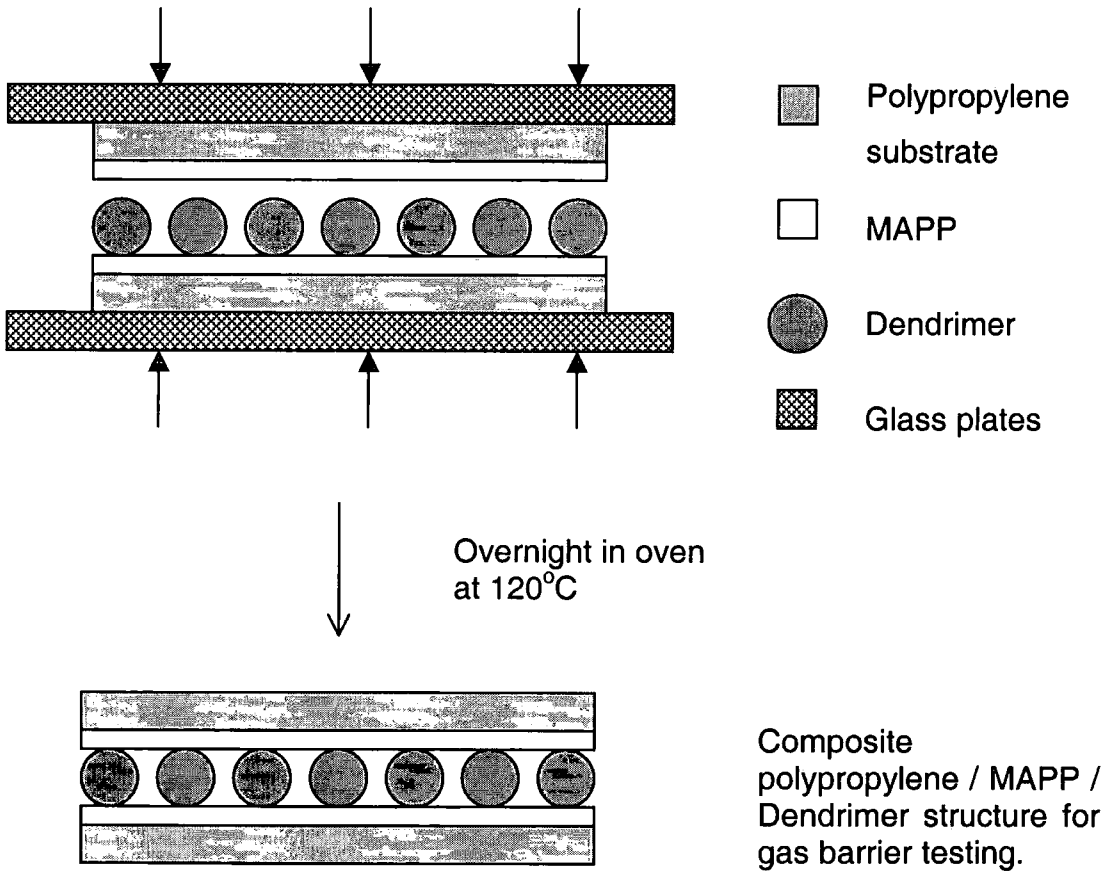

Scheme 3.1 Schematic of sample preparation for gas barrier testing

3.3 RESULTS AND DISCUSSION

3.3.1 Pulsed Plasma Polymerization of Maleic Anhydride

Details of XPS and ATR-FTIR characterization can be found in Chapter 2, section 2.3.1. The flat topography of the underlying glass substrate, Figure 3.1 (a) as seen by AFM was retained at the surface of the deposited pulsed plasma polymer layer, Figure 3.1 (b). As discussed in Chapter 2 2.2.1, page 37, the MAPP layers are 34 ± 5 nm thick.

3.3.2 Functionalization of MAPP with PAMAM Dendrimers

Exposure of the MAPP film to dendrimer solution followed by rinsing in methanol gave rise to the stable attachment of dendrimers to the surface. The morphology, size and intermolecular spacing of the immobilized dendrimer moieties were examined by atomic force microscopy, Figure 3.2(c), page 64. AFM micrographs of 4^{th} generation PAMAM dendrimers bonded to the MAPP layer appear as small dots (height = 2.5 ± 0.03nm; width = 5.3 ± 0.04nm, measurements obtained from Figure 3.2, page 64, from work done by S.A. Evenson), these represent individual dendrimers immobilized onto the underlying (darker shading) plasma polymer surface. Assuming a spherical shape, the dendrimers should be 4.5 nm wide[24,25]. Therefore it appears that the dendrimers have slightly flattened out on the MAPP surface (in order to maximize amide bond formation). This is consistent with previous computer simulation and AFM studies which have reported a flattening and spreading out of PAMAM dendrimer molecules upon attachment to a surface[13-15,26]. Scheme 3.1 shows the deposition of the dendrimers at the MAPP surface.

Scheme 3.2 Immobilization of PAMAM dendrimers onto maleic anhydride pulsed plasma polymer surfaces.

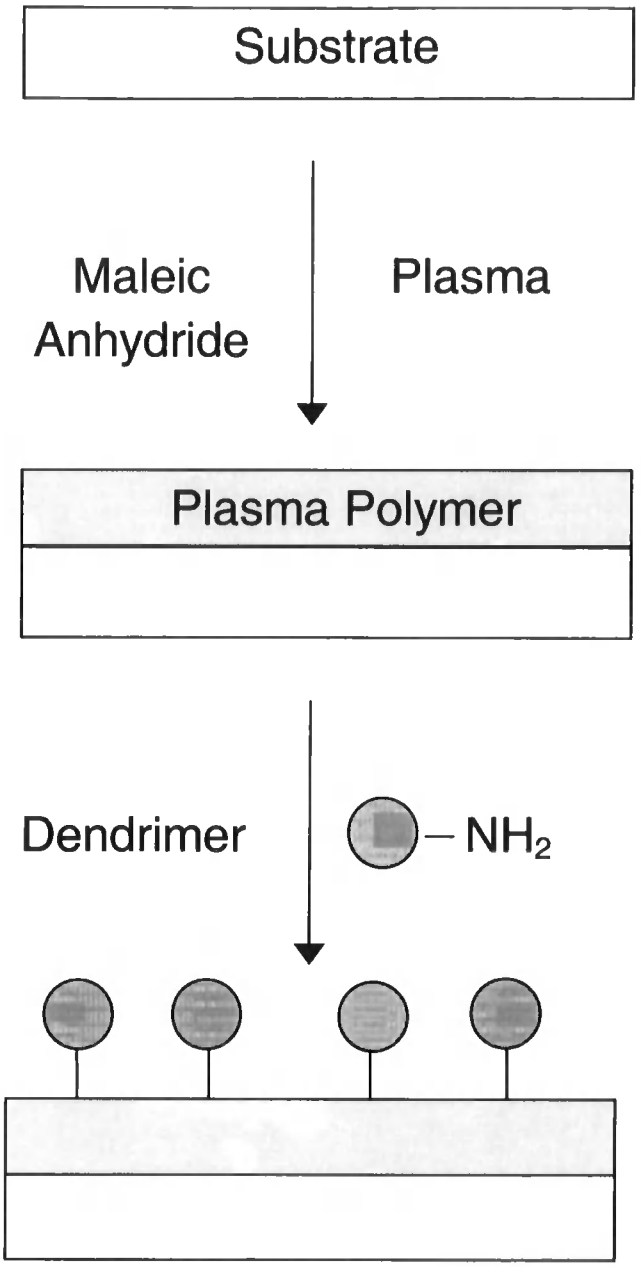

Figure 3.2 Tapping mode AFM images of (a) the glass substrate; (b) maleic anhydride pulsed plasma polymer deposited onto glass (P_p = 5W; t_{on} = 20 μs; t_{off} = 1200 μs; 10 mins); and (c) 4th generation PAMAM dendrimers (white spots) attached to the maleic anhydride pulsed plasma polymer layer (darker background). These images were obtained by S. A. Evenson, and included in his thesis (University of Durham 1997)

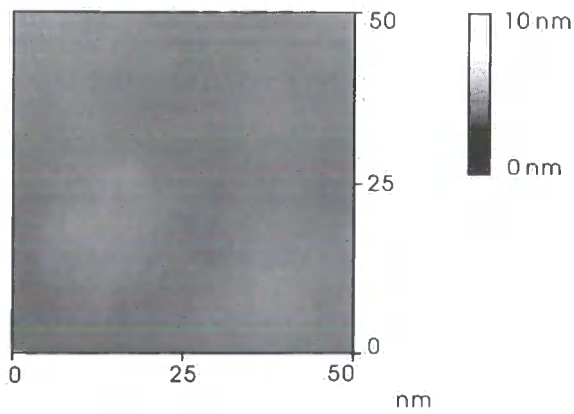

(a)

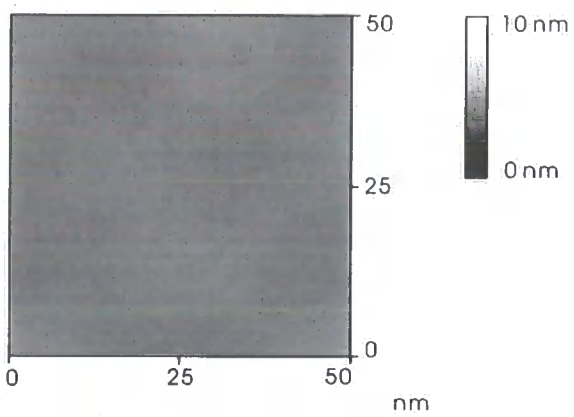

(b)

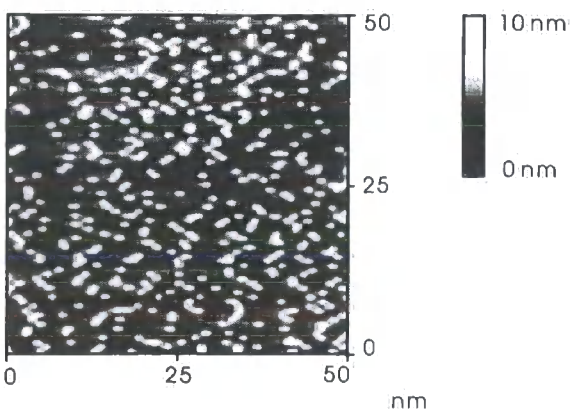

(c)

XPS analysis verified that reaction had taken place at the surface Figure 3.2. The dendrimer species contribute three types of carbon functionality to the C(1s) spectra:[27] carbon singly bonded to an amide carbon / amine nitrogen (C-C-NHR(=O) / C-N ~ 285.7 eV), carbon singly bonded to an amide nitrogen (-CH_2-NH-C=O ~ 286.6 eV), and an amide group (RHN-C=O ~ 287.9 eV), Figure 3.3. These give rise to an attenuation of the anhydride group C(1s) signal (O=C-O-C=O ~ 289.4 eV) as the surface coverage of PAMAM dendrimers increased. A corresponding rise in the N(1s) peak at ~ 400 eV was seen and can be taken to be indicative of dendrimer attachment to the MAPP surface via amide linkages[16] (a weak N(1s) component at 401.9 eV was attributed to reaction of dendrimer amine groups with atmospheric CO_2[28,29]), Figure 3.4, page 67. The percentage of nitrogen present at the surface was determined by XPS analysis, and the use of the experimentally determine sensitivity factor for the N(1s) level. The packing density of dendrimers at the surface could be varied by diluting the solution with methanol, Figure 3.4. For all three dendrimer generations under investigation, the surface concentration of nitrogen (% N) was found to correlate to the degree of dilution. Submonolayer coverage corresponds to dilutions below 0.01% wt. / vol., this ties in with the reappearance of the anhydride group peak (O=C-O-C=O ~ 289.4 eV) in the C(1s) XPS envelope, Figure 3.3, page 66. An alternate way of varying the number of dendrimers attached to the surface would be to change the concentration of anhydride groups (i.e. alter the pulsed plasma deposition conditions.[30]

Figure 3.3 C(1s) XPS spectra of: (a) maleic anhydride pulsed plasma polymer layer; (b) the plasma polymer functionalized with a 0.00125% wt. / vol. solution of 4th generation PAMAM dendrimers; (c) the plasma polymer functionalized with a 10% wt. / vol. solution of 4th generation PAMAM dendrimers; and (d) following reaction of (c) with trifluoroacetic acid vapour.

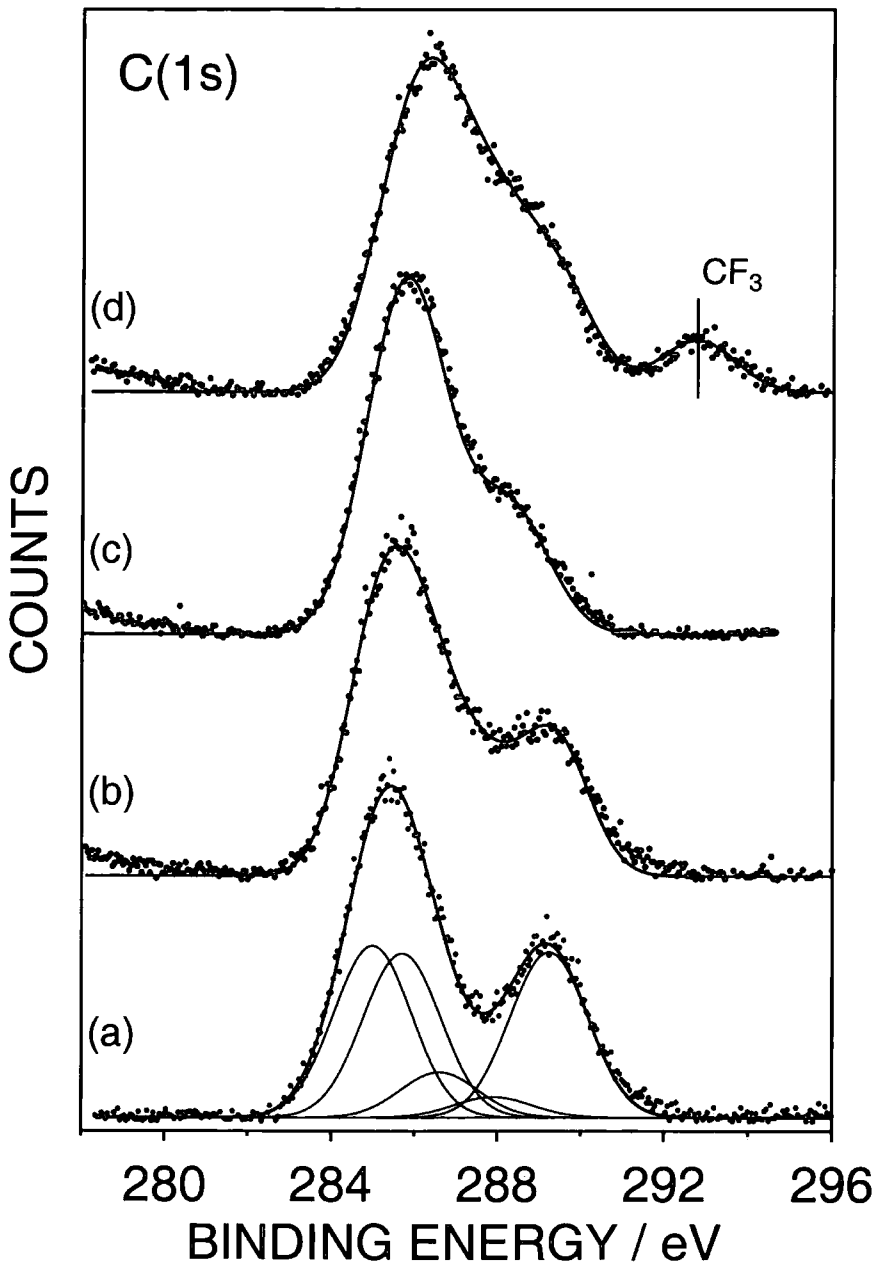

Figure 3.4 Nitrogen concentration (% N) at the surface of the plasma polymer layer after functionalization versus the dilution of dendrimer molecules (% wt. / vol.).

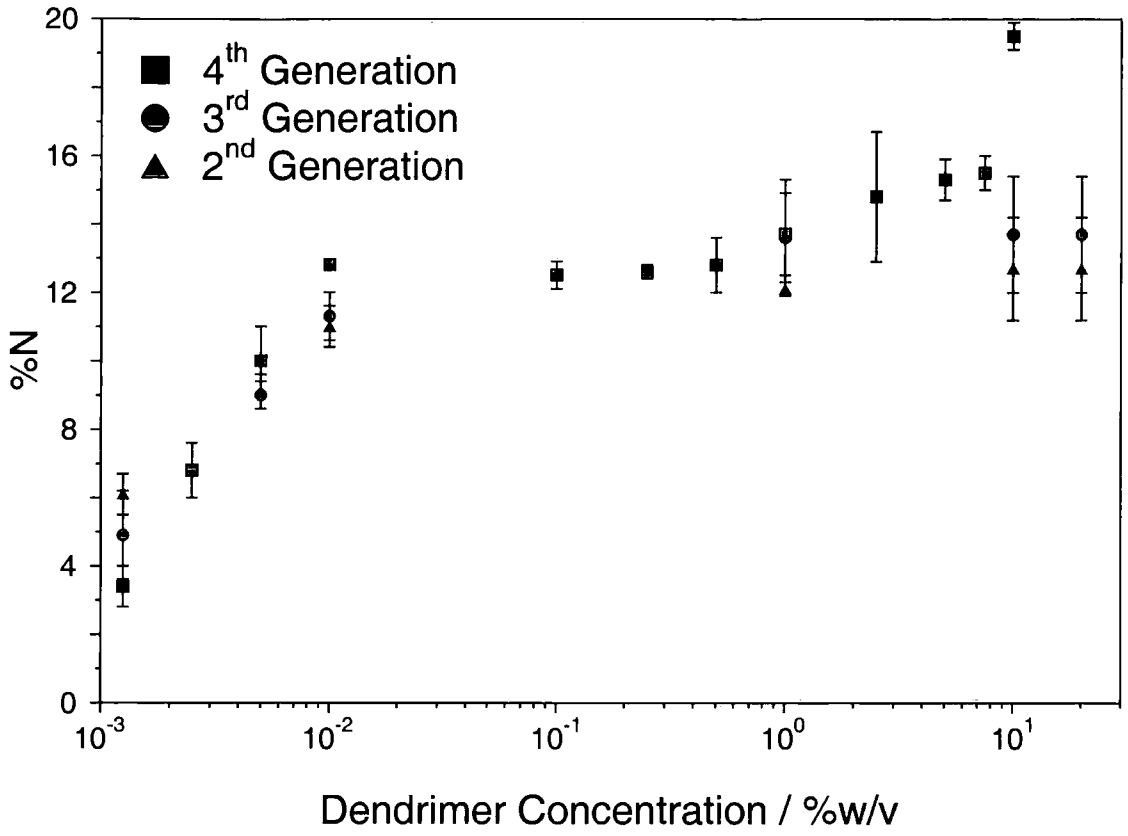

Infrared spectroscopy showed the appearance of amide absorption bands[31] (1650 cm^{-1} and 1580 cm^{-1}) characteristic of the dendrimer molecules (internal amide bonds and amic acid groups formed between terminal dendrimer amine groups and the MAPP surface), Figure 3.5, page 69. The absorbance at approximately 1450 cm^{-1} can be attributed to CH_2 groups present in the dendrimer molecules. Heating at 120 °C caused a decrease in the amide band intensities relative to the peak at 1450 cm^{-1}. This occurs as a consequence of the internal amide groups in the PAMAM dendrimer molecules undergoing a retro Michael reaction to form imide linkages (1710 cm^{-1});[32] there should also be imide bond formation at the dendrimer binding sites on the maleic anhydride pulsed plasma polymer surface. The described approach for attaching PAMAM dendrimers onto solid surfaces is applicable to a whole variety of substrates and therefore offers a distinct advantage compared to alternate methods (e.g. poly(maleic anhydride)-*c*-poly(methyl vinyl ether) layers fixed onto aminosilane functionalized silicon surfaces[21]).

Figure 3.5 Infrared spectra of: (a) maleic anhydride pulsed plasma polymer layer (P_p = 5 W; t_{on} = 20 μs; t_{off} = 1200 μs; 10 mins); (b) 10% wt. / vol. solution of 4th generation PAMAM dendrimer solution; (c) 4th generation PAMAM dendrimers deposited from 0.01% wt. / vol. solution onto maleic anhydride pulsed plasma polymer surface; and (d) following annealing of (c) to 120 ^{O}C.

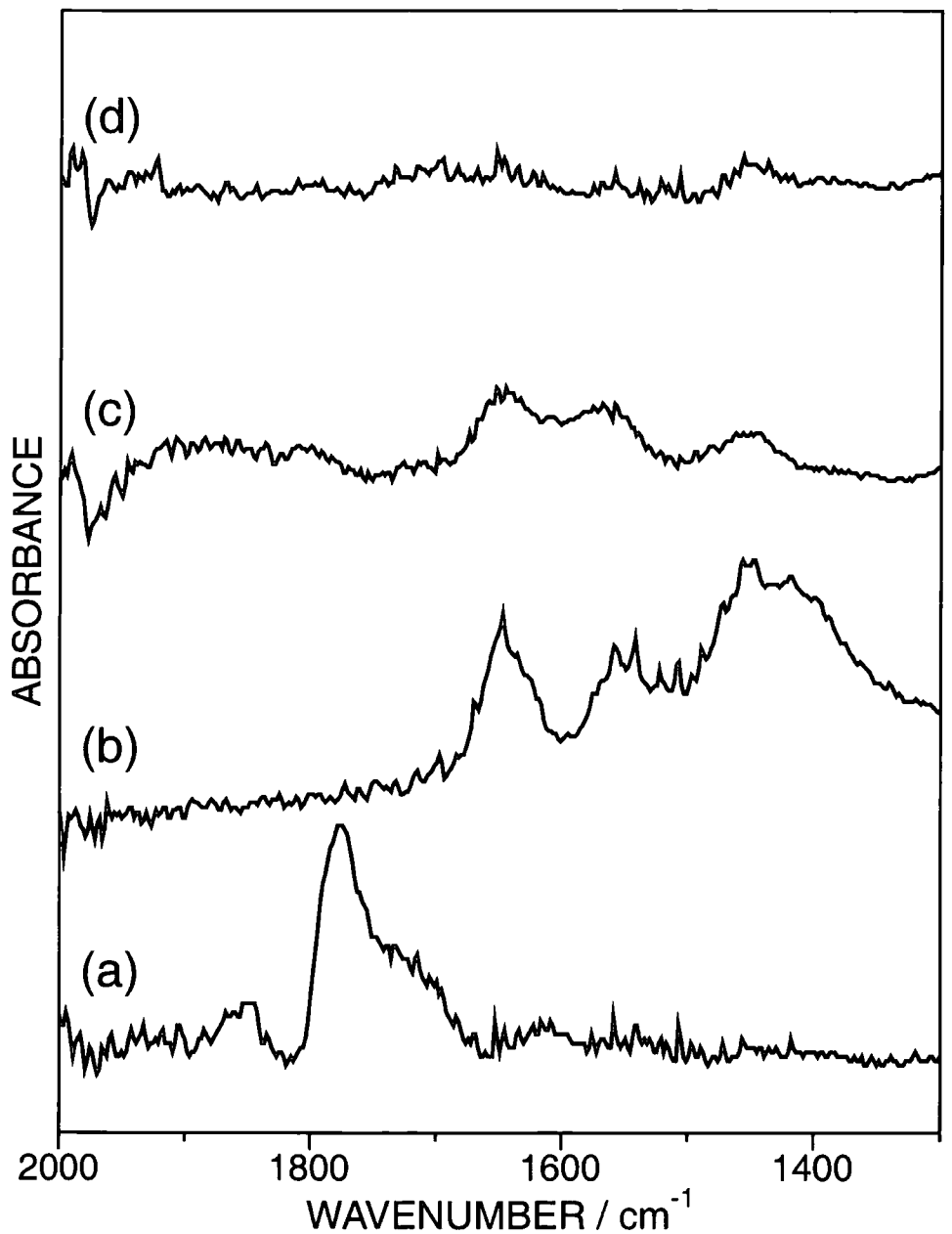

3.3.3 Reaction of PAMAM dendrimers with Trifluoroacetic acid

Further verification of the immobilization of PAMAM dendrimers onto maleic anhydride pulsed plasma polymer surfaces was obtained by reacting the remaining terminal PAMAM dendrimer amine groups with trifluoroacetic acid vapour to produce amide linkages. In this case, the $\underline{C}F_3$ functionality in the C(1s) XPS spectrum at 293 eV served as a marker, Figure 3.3(d), page 66. A good correlation was found between the amount of nitrogen measured at the surface, (i.e. dendrimer density) and the F(1s) signal detected by XPS following exposure to trifluoroacetic acid, Figure 3.5. These results are consistent with previous studies where 4-(trifluoromethyl)benzoyl chloride was used to functionalize a PAMAM dendrimer monolayer adsorbed onto a flat gold substrate[17].

Figure 3.6 XPS correlation between the amount of nitrogen present at the surface and fluorine detected following exposure to trifluoroacetic acid vapour, in the case of 4th generation PAMAM dendrimers immobilized onto maleic anhydride pulsed plasma polymer layers.

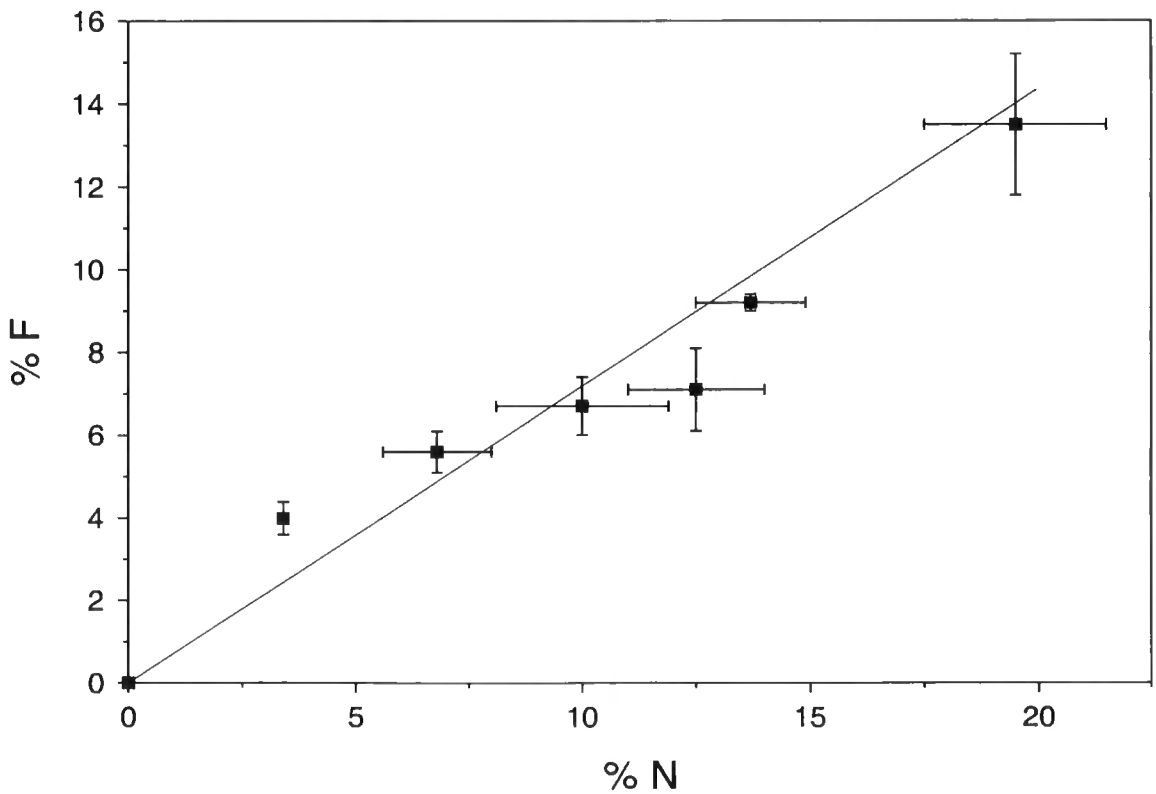

3.3.4 Reaction of PAMAM dendrimers with gold (III) chloride

Gold (III) Chloride was used because it has previously been shown to interact with amide linkages to form complexes which are stable under reducing conditions, leaving elemental gold at the surface.[33]

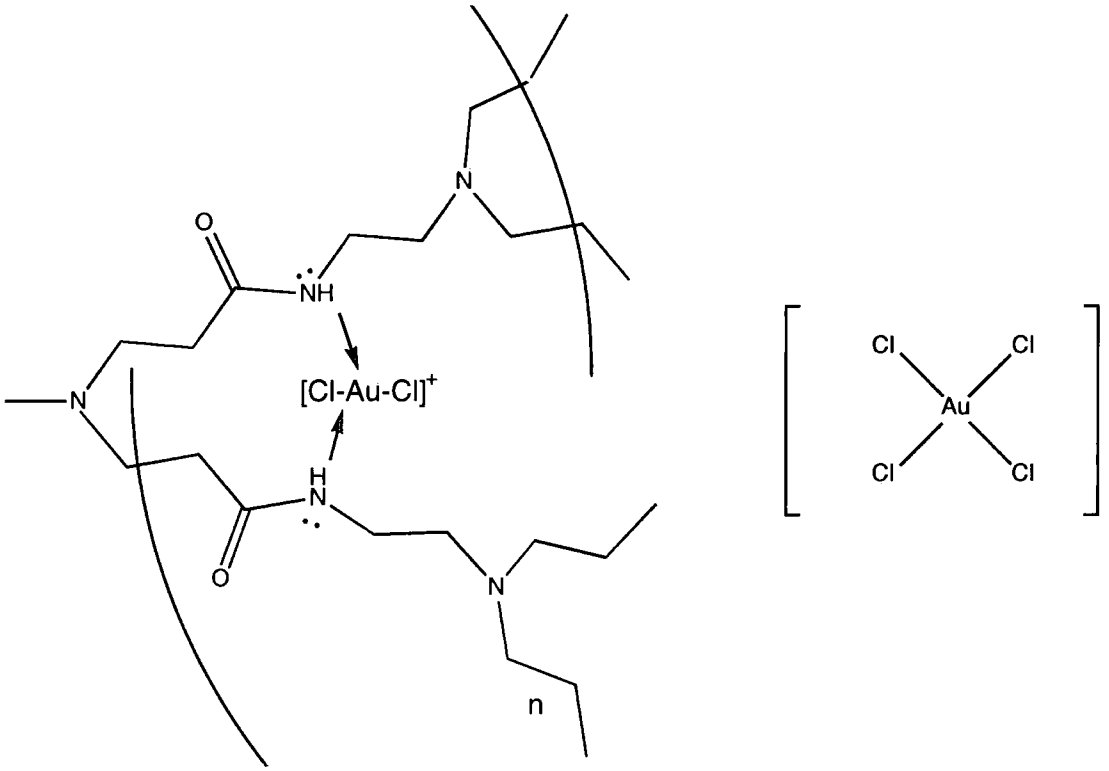

Scheme 3.3 The interaction of gold (III) chloride with PAMAM dendrimer.

Amide groups are capable of bonding to gold (III) chloride, due to the affinity of gold in the +3 oxidation state towards nitrogen-based ligands,[34] which promoting the co-ordination of the gold (III) chloride to the dendrimer. This Lewis acid-base interaction between metal chlorides and polyamides in solution has been observed before[35,36] and generally leads to the formation of ionic species of the type $[L_xMCl_{y-2}]^+[MCl_y]^-$, where L is the dendrimer and M is the metal.

It has also been observed that varying the dendrimer concentration at the plasma polymer surface allows the amount of gold attached to the surface to be controlled. The greater the number of dendrimers attached to the surface

the more gold detected in the Au(4f 7/2) spectra. This can be seen in Figure 3.6, which shows the relationship between the percentage nitrogen at the surface, which corresponds to the number of dendrimers, and the percentage of gold detected at the surface after functionalization.

Figure 3.7 The correlation between dendrimer concentration, percentage nitrogen detected by XPS and percentage gold detected by XPS.

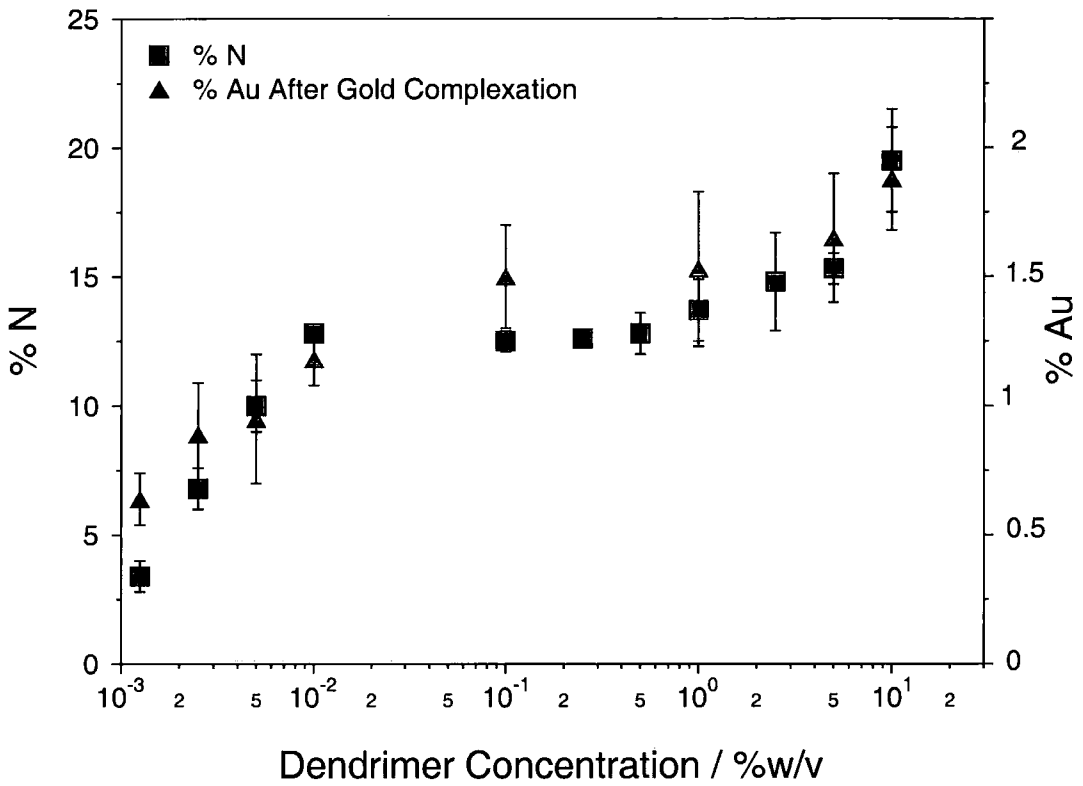

Table 3.2 Average particle sizes of gold (III) chloride functionalized dendrimers, as determined by TEM.

Dendrimer Concentration	*Average Particle size, as measured by TEM / nm*
0.0025	6.884 ± 1.2
0.01	7.313 ± 1.4
0.25	9.774 ± 1
10	9.089 ± 1.46

Table 3.2 shows the changing size of the gold functionalized dendrimer particles as measured by TEM. All of these samples have been hydrogen plasma reduced as explained in section 3.2.3, page 60. Previous studies have suggested that the 4th generation PAMAM dendrimers are smaller when immobilized on surfaces than the measured dendrimer particle size.[37-39] However, there are explanations given in the literature for this type of effect. The first possible reason is that different ratios of dendrimer to gold chloride produce particles of differing size.[37] At metal to dendrimer ratios of 1:1, the largest particles are observed by TEM. The particles have been recorded in the range 7.3 ± 1.5nm. As the metal to dendrimer ratio reduces (0.1:1 and 0.01:1), the sizes of the measured particles reduce. Final measurements for these particles are in the range 3.2 ± 0.7nm. The second possible reason is that the dendrimers can aggregate.[39] Fourth generation PAMAM dendrimers form a well defined aggregate with a size of 7nm. The formation of aggregates for low generation dendrimers could be due to the fact that a small dendrimer has insufficient material to stabilize one the surface of one gold colloid. Aggregation of these 4th generation PAMAM dendrimers on the MAPP surface would explain the greater than expected sizes recorded at the surface.

3.3.5 Adhesion using PAMAM dendrimers

Adhesion studies were undertaken by placing a 0.1 ml drop of 4th generation PAMAM dendrimer solution between two pieces of polypropylene coated with MAPP followed by heating to 120 °C. A maximum force per unit area of 20 N cm^{-2} was recorded for this sandwich structure, Figure 3.8. This compared favourably with the substrate failure value for the parent polypropylene film of approximately 26 N. No adhesion was observed in the absence of dendrimer. It was found that the heating step (imide formation) was a prerequisite for achieving good adhesion.

Figure 3.8 Lap-shear adhesion test: (a) bulk failure of polypropylene substrate; and (b) polypropylene / plasma polymer / 4th generation PAMAM dendrimer / plasma polymer / polypropylene joint (heated to 120 C).

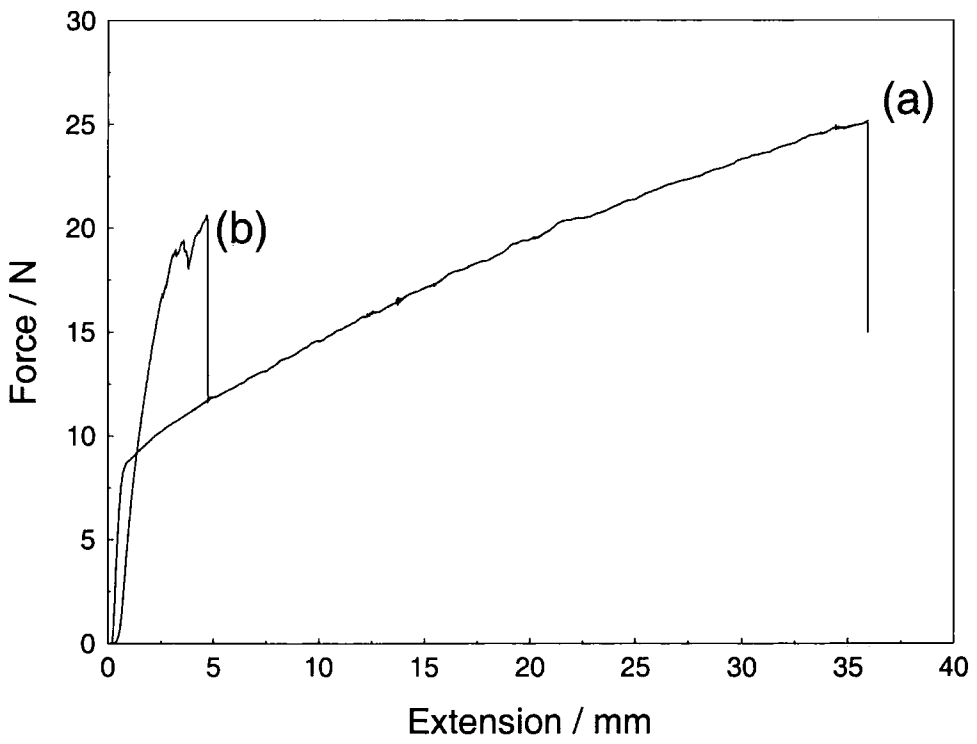

3.3.6 Gas Barrier

Oxygen gas permeation measurements were also carried out for dendrimer layers sandwiched between MAPP coated polypropylene film. Thermal curing at 120 °C gave rise to a significant improvement in gas barrier, Table 3.3. This can also be attributed to imidization and retro-Michael chemistry giving rise to a highly crosslinked impermeable structure[32]. Thermally induced retro-Michael reactions at the β-aminocarboxamide sites within the PAMAM dendrimer give rise to primary amines in place of tertiary amines, and it is the primary amines which further crosslink through conventional Michael chemistry to give the impermeable structure. As explained in section 1.6.4, page 26, the gas barrier improvement factor (GBIF) measured was referenced against two pieces of polypropylene film placed on top of each other (i.e. no MAPP coating or dendrimer molecules). The GBIF is therefore unit-less, since it is a relative improvement factor, compared against the control.

Table 3.3 Gas barrier measurements for dendrimer molecules sandwiched between polypropylene film and then cured at 120 °C

Plasma Polymer	Gas Barrier
Yes	34.9
No	2.1

In the table given above, the difference between a layer using the MAPP as an adhesive layer for the PAMAM dendrimers and not using such a layer is clearly seen. It shows that the MAPP acts an effective binding layer to adhere the PAMAM dendrimers to the surface, since in it's absence of the chance in GBIF is much smaller, which can be attributed to considerably fewer PAMAM dendrimers attaching to the surface.

3.4 CONCLUSIONS

Starburst PAMAM dendrimers can be chemically fixed onto solid substrates by pre-depositing a well-adhered maleic anhydride pulsed plasma polymer layer. The MAPP layer is believed to be well-adhered as XPS analysis of the deposited layers shows no evidence of the underlying substrate, normally glass, even after washing in a variety of solvents, predominately methanol in this chapter. It has been shown that the intermolecular spacing and concentration of dendrimer molecules attached to the surface can be controlled by either varying the level of anhydride group incorporation into the plasma polymer film or by changing the dilution of the dendrimer solution.

The external amine groups associated with the fixed dendrimers can undergo further chemical reaction, in this case fluorination, metal attachment, adhesion and gas barrier). The amount of fluorine incorporated at the MAPP / PAMAM dendrimer surface was found to be proportional to the concentration of the dendrimers attached. The ability of the PAMAM dendrimers to undergo further chemical modification was further demonstrated by using gold (III) chloride, which binds to the amine groups and is then capable of undergoing a reduction to give rise to elemental gold. This ability to immobilize metals on surfaces could have use in heterogeneous catalysis. The adhesion obtained between two MAPP layers through use of dendrimers is also interesting, as potentially gives a means using very thin layers to achieve large improvements in adhesion. Finally, the improvement in the gas barrier properties of these layers could have uses in packaging and other systems that require protection from the atmosphere for a period of time.

3.5 REFERENCES

1 Tomalia, D. A.; Naylor, A. M.; Goddard III, W. A. *Angew. Chem. Int. Ed. Engl.* **1990**, *29*, 138.

2 Tomalia, D. A. *Macromol. Symp.* **1996**, *101*, 243.

3 Dagani, R. *Chem. & Eng. News* **1996**, *June 3*, 30.

4 Yoon, H. C., Hong, M. Y., Kim, H. S. *Langmuir*, **2001**, *17*, 1234.

5 Service, R. F. *Science* **1995**, *267*, 458.

6 Bosman, A. W., Janssen, H. M., Meijer, E. W. *Chem. Rev.* **1999**, *99*, 1665.

7 Fujiki, K., Sakamoto, M., Sato, T., Tsubokawa, N. *J. Macromol. Sci. – Pure Appl. Chem*, **2000**, *37*, 357.

8 Baker, L.A., Zamborini, F.P., Sun, L., Crooks, R.M. *Anal. Chem.* **1999**, *71*, 4403.

9 Rubin, S., Bar, G., Taylor, T. N., Cutts, R. W., Zawodzinski Jr., T. A. *J. Vac. Sci. Technol. A.* **1996**, *14*, 1870.

10 Bar, G., Rubin, S., Cutts, R. W., Taylor, T. N., Zawodzinski, T. A. *Langmuir* **1996**, *12*, 1172.

11 Evenson, S. A., Badyal, J. P. S. *Adv. Mater.* **1997**, *9*, 1097.

12 Tsukruk, V. V., Rinderspacher, F., Bliznyuk, V. N. *Langmuir*, **1997**, *13*, 2171.

13 Bliznyuk, V. N., Rinderspacher, F., Tsukruk, V. V. *Polymer*, **1998**, *21*, 5249 .

14 Hierlemann, A., Campbell, J.K., Baker, L.A., Crooks, R.M., Ricco, A.J. *J. Am. Chem. Soc.*, **1998**, *120*, 5323.

15 Li, J., Piehler, L.T., Qin, D., Baker, J.R., Tomalia, D.A., Meier, D.J. *Langmuir*, **2000**, *16*, 5613.

16 Yoon, H.C., Kim, H.S. *Anal. Chem.*, **2000**, *72*, 922.

17 Tokuhisa, H., Zhao, M., Baker, L. A., Phan, V. T., Dermody, D. L., Garcia, M. E., Peez, R. F., Crooks, R. M., Mayer, T. M. *J. Am. Chem. Soc.* **1998**, *120*, 4492.

18 Wells, M., Crooks, R. M. *J. Am. Chem. Soc.* **1996**, *118*, 3988.

19 Tokuhisa, H., Crooks, R.M. *Langmuir*, **1997,** 13, 5608.

20 Liu, Y., Zhao, M., Bergbreiter, D.E., Crooks, R.M. *J. Am Chem. Soc.*, **1997,** *119*, 8720.

21 Liu, Y., Bruening, M. L., Bergbreiter, D. E., Crooks, R.M. *Angew. Chem. Int. Ed. Engl.* **1997**, *36*, 2114.

22 Evenson, S. A., Badyal, J. P. S. *J. Phys. Chem. B* **1998**, *102*, 5500.

23 Evenson, S. A., Fail, C. A., Badyal, J. P. S. *Chem. Mater.* **2000**, *12*, 3038.

24 Prosa, T. J., Bauer, B. J., Amis, E. J., Tomalia, D. A., Scherrenberg, R. *J. Polym. Sci.* **1997**, *35*, 2913.

25 Grohn, F., Bauer, B. J., Akpalu, Y. A., Jackson, C. L., Amis, E. J. *Macromolecules*, **2000**, *33*, 6042.

26 Mansfield, M. L. *Polymer* **1996**, *37*, 3835.

27 Beamson, G., Briggs, D. *High Resolution XPS of Organic Polymers*; Wiley: Chichester, **1992**.

28 Yan, L., Marzolin, C., Terford, A., Whitesides, G. M. *Langmuir*, **1997**, *13*, 6704.

29 Sprik, M., Delamarche, E., Michel, B., Rothlisberger, U., Klein, M. L., Wolf, H., Ringsdorf, H. *Langmuir*, **1994**, *10*, 4116.

30 Ryan, M. E., Hynes, A. M., Badyal, J. P. S. *Chem. Mater.* **1996**, *8*, 37.

31 Williams, D. H., Fleming, I. *Spectroscopic Methods in Organic Chemistry*, 4th ed.; McGraw-Hill Ltd, London, 1989.

32 Zhao, M. Q., Liv, Y. L., Crooks, R. M., Bergbreiter, D. E. *J. Am. Chem. Soc.* **1999,** *121,* 923.

33 Crowther, J.M., Badyal, J.P.S. *Adv. Mater.*, **1998**, *10*, 407.

34 Puddephat, R.J. in *The Chemistry of Gold,* Elsevier, Amsterdam, **1978**, Ch. 5.

35 Lassègues, J.C., Grondin, J., Hernandez, M., Rey, I., Servant, L., Wen, S.-J. *New. J. Chem.*, **1996**, *20,* 317.

36 Yen, C.-C., Huang, C.-J., Chang, T.-C. *J. Appl. Polym. Sci.*, **1991**, *42,* 439.

37 Manna, A., Imae, T., Aoi, K., Okada, M., Yogo, T. *Chem. Mater.,* **2001**, *12*, 1681.

38 Esumi, K., Suzuki, A., Yamahira, A., Torigoe, K. *Langmuir,* **2000**, *16*, 2604.

39 Gröhn, F., Bauer, B.J., Akpalu, Y.A., Jackson, C.L., Amis, E.J. *Macromolecules*, **2000,** *33,* 6042.

CHAPTER FOUR

Further applications of amine reactions at the Maleic Anhydride Plasma Polymer (MAPP) surface

4.1 INTRODUCTION

It has been shown previously that the maleic anhydride, and its plasma polymer layer can easily derivatized through processes such as nucleophilic attack of an amine or alcohol at the anhydride centre to form amides, which can form imides upon heating, and ester linkages.[1-3] Details of the reaction of MAPP with 2,2,2 trifluoroethylamine, and Jeffamine (a poly(propylene glycol) bis (2-aminopropyl ether), have already been discussed in Chapter 2 (and references there in).[3] In this chapter the scope for further reaction and the introduction of new functional groups at the surface is demonstrated.

The MAPP layer has been functionalized with aminopropyl terminated polydimethyl siloxane (PDMS), to study another means of adhering surfaces together. Amine and carboxylic acid functionalized polystyrene spheres, were used to introduce new functional groups and to bring about a surface roughening effect and

polyethyleneimine was used as a means of immobilizing gold colloid particles on to the plasma polymer surface.[4]

4.2 EXPERIMENTAL

4.2.1 Plasma Polymerization of Maleic Anhydride

Experimental details for the deposition of the MAPP can be found in Chapter 2, section 2.2.1, page 36.

4.2.2 Reaction of the MAPP layer with Aminopropyl terminated Polydimethylsiloxane (NH_2-PDMS).

The deposited MAPP coatings were reacted with aminopropyl terminated PDMS, (Fluorochem, viscosity = 50, SG = 0.95, M_w = 2,500). This was done by applying 0.1mL of aminopropyl terminated PDMS to the MAPP layer. After 30 minutes the surfaces were rinsed with methanol to remove excess NH_2-PDMS, and allowed to dry in air. Analysis of the samples was carried out immediately using XPS. For adhesion experiments two pieces of MAPP coated poly(propylene), (ICI, 0.8μm x 1cm x 5cm) were used. One piece of the functionalized substrate was treated with the NH_2-PDMS and rinsed, before a second piece of functionalized substrate was placed treated side down on the NH_2-PDMS layer, and the whole system was cured in an oven at 120°C overnight. Details of the adhesion experiment are given in Chapter 1, section 1.6.5, page 27.

4.2.3 Reaction of the MAPP layer with amine and carboxylic acid functionalized Polystyrene beads.

Functionalized polystyrene beads are supplied a solution in water (Bangs Labs. Inc., PS-NH_2 beads are 0.66 μm mean diameter, PS-COOH beads are approximately 0.6μm mean diameter). These beads are diluted by ten times to give a bead concentration of 6.327 x 10^{10} beads per ml. For surface modification reactions 0.2ml of the bead solution was placed on the plasma polymer surface and left for between 10 minutes and 60 minutes. Samples were then rinsed with high purity water and left to dry in air before analysis.

4.2.4 Reaction of the MAPP layer with Polyethyleneimine (PEI).

Polyethyleneimine (PEI) was made up into a 1% weight by volume solution with isopropyl alcohol, and stored under a nitrogen atmosphere in a glove box. Samples were placed in the PEI solution and left for 1 hour, before being rinsed with isopropyl alcohol and allowed to dry in air. These PEI layers were used to stabilize gold colloids. (The gold colloids were supplied as a solution in water (average diameter = 250 nm, concentration = 1.2×10^8 n /ml, Agar Ltd.)). TEM and XPS were used to characterize these layers.

4.3 RESULTS AND DISCUSSION

4.3.1 Pulsed Plasma Polymerization of Maleic Anhydride

Maleic anhydride plasma polymer (MAPP) surfaces discussed in previous chapters were used.

The C(1s) spectra of the functionalized MAPP layers is shown in Figure 4.1, page 84. Elemental abundances can be found in Table 4.1.

Table 4.1 Elemental XPS analysis.

Substrate	*Atomic percentage*					
	C	*O*	*Si*	*N*	*Au*	*Cl*
1) MAPP	67.6 ± 0.8	32.5 ± 0.8				
2) MAPP exposed to aminopropyl terminated PDMS	57.5 ± 0.1	22.9 ± 1.6	15.2 ± 1.6	4.2 ± 0.1		
3) MAPP exposed to amine functionalized polystyrene beads	71.3 ± 0.8	26.3 ± 0.7		2.4 ± 0.2		
4) MAPP exposed to polyethyleneimine	63.5 ± 2.4	21.4 ± 2.3		14.4 ± 0.5		
5) Exposure of 4) to gold colloid solution	68.3 ± 4.1	19.4 ± 1.7		12.2 ± 5.8	0.15 ± 0.04	
6) MAPP exposed to gold colloids	65.9 ± 0.4	34.1 ±0.4				

Figure 4.1 C(1s) spectra of (a) pulsed plasma polymerized maleic anhydride; (b) following reaction with aminopropyl terminated PDMS; (c) following reaction with amine functionalized polystyrene beads; (d) following reaction with 1-pyrenemethylamine hydrochloride and (e) following reaction with poly (ethyleneimine).

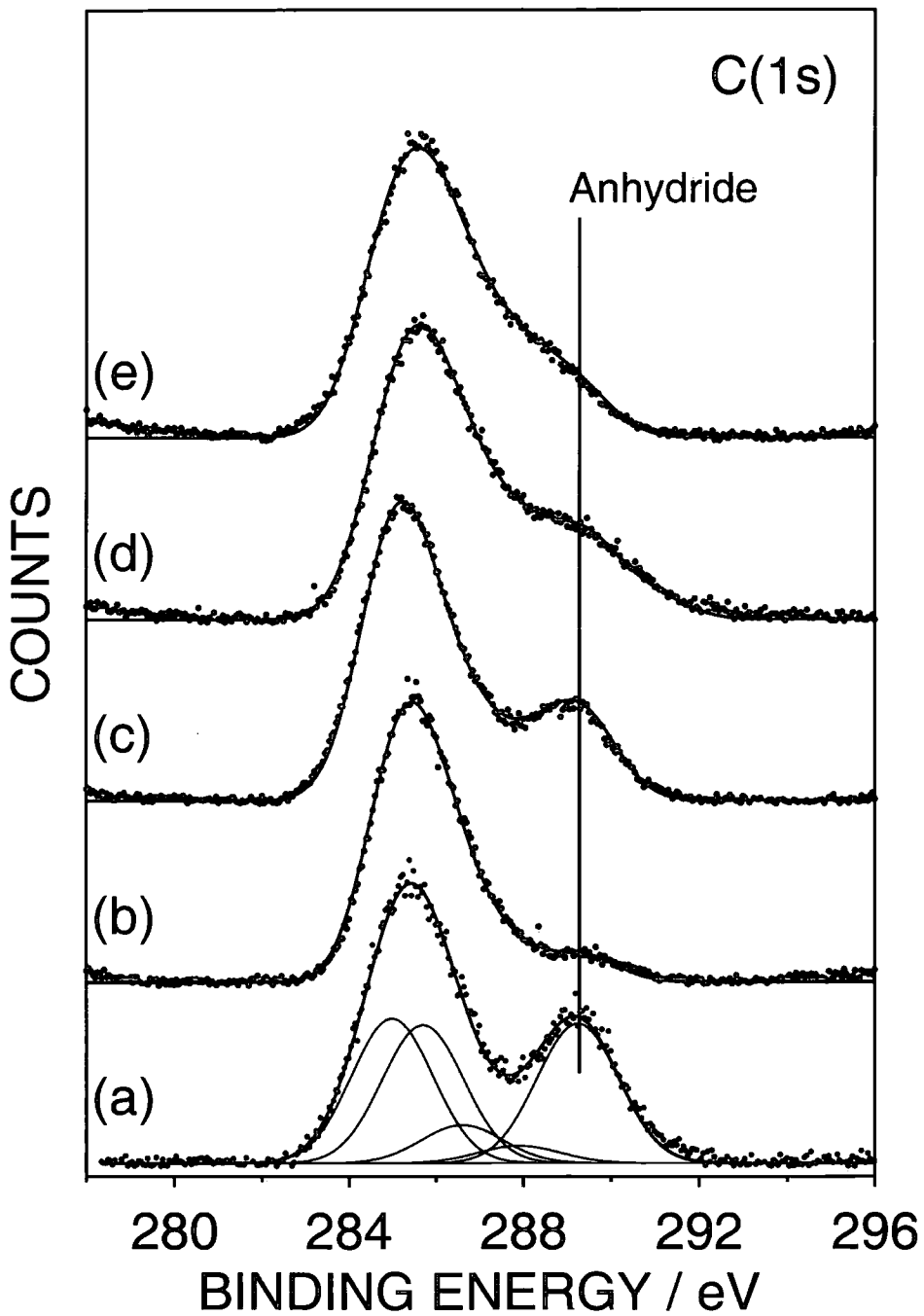

4.3.2 Functionalization of the MAPP layer with Aminopropyl terminated PDMS.

Functionalization of the MAPP layers with aminopropyl terminated PDMS gave rise to the attachment of PDMS chains at the surface, as demonstrated in Scheme 4.1. XPS studies of the sample showed two peaks in the N(1s) region at 400 eV and 402 eV, corresponding to amine groups and ammonium groups respectively, and a peak due to Si(2p) from the PDMS backbone at 102 eV. The peak in the C(1s) spectrum at 289.4 eV, attributed to the anhydride group was reduced considerably, Figure 4.1 (b). In order to demonstrate that only one end of the PDMS chain had reacted with the anhydride group, which was indicated by the fact that the two N(1s) peaks were of equal intensity, adhesion studies were carried out. This was done in order to promote ring closure and hence imide formation. An improvement in the adhesion was observed, as seen in Table 4.2, page 86.

Scheme 4.1 Functionalization of MAPP wirh aminopropyl terminated PDMS.

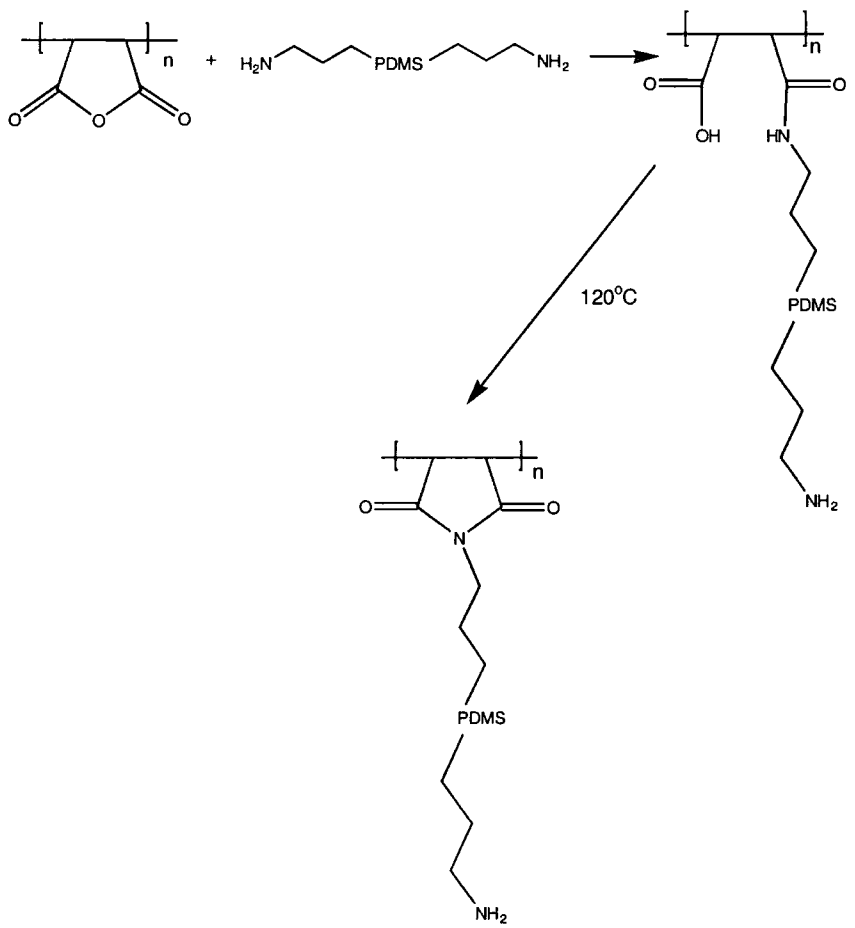

Table 4.2 Adhesion between MAPP functionalized polypropylene surfaces with aminopropyl terminated PDMS

Plasma Polymer	*Aminopropyl terminated PDMS*	*Heat*	*Maximum Force N cm^{-2}*
No	No	No	Did not adhere
No	No	120 °C	Did not adhere
Yes	On one piece	No	Did not adhere
Yes	On one piece	120 °C	10 ± 3

Polypropylene substrate failure occurs at 25 N.

Adhesion levels similar to those obtained for Jeffamine ® were observed when aminopropyl terminated PDMS was used to adhere the polypropylene layers together. The mechanism for this reaction is identical to that occurring in the case of the Jeffamine ®, as shown in Scheme 4.1.

4.3.3 Functionalization of the MAPP layer with amine and carboxylic acid functionalized Polystyrene beads.

The relative reactivity of the MAPP films towards amine versus carboxylic acid functionalized polystyrene spheres was investigated, Scheme 4.2, page 87. Optical microscopy confirmed that aminolysis was the preferred reaction pathway, Figure 4.2(a), whereas carboxylic acid terminated beads did not adhere to the surface, Figure 4.2(b), page 88. For the amine functionalized polystyrene, the XPS C(1s) envelope changes its appearance in accordance with the presence of the following functionalities: CH_x at 285.0 eV, C-C-NHR(=O) / C-N at 285.7 eV, CH_2-NH-C=O at 286.6 eV, RHN-C=O at 287.9 eV and C(O)-O / COOH at 289.4 eV, Figure 4.1 (c), page 84. There is also a signal due to the N(1s), as shown in Table 4.2. AFM imaging of these surfaces may be useful to show changes in the surface topography, but to date this has not been carried out.

Scheme 4.2 Reaction of amine functionalized polystyrene spheres with the MAPP.

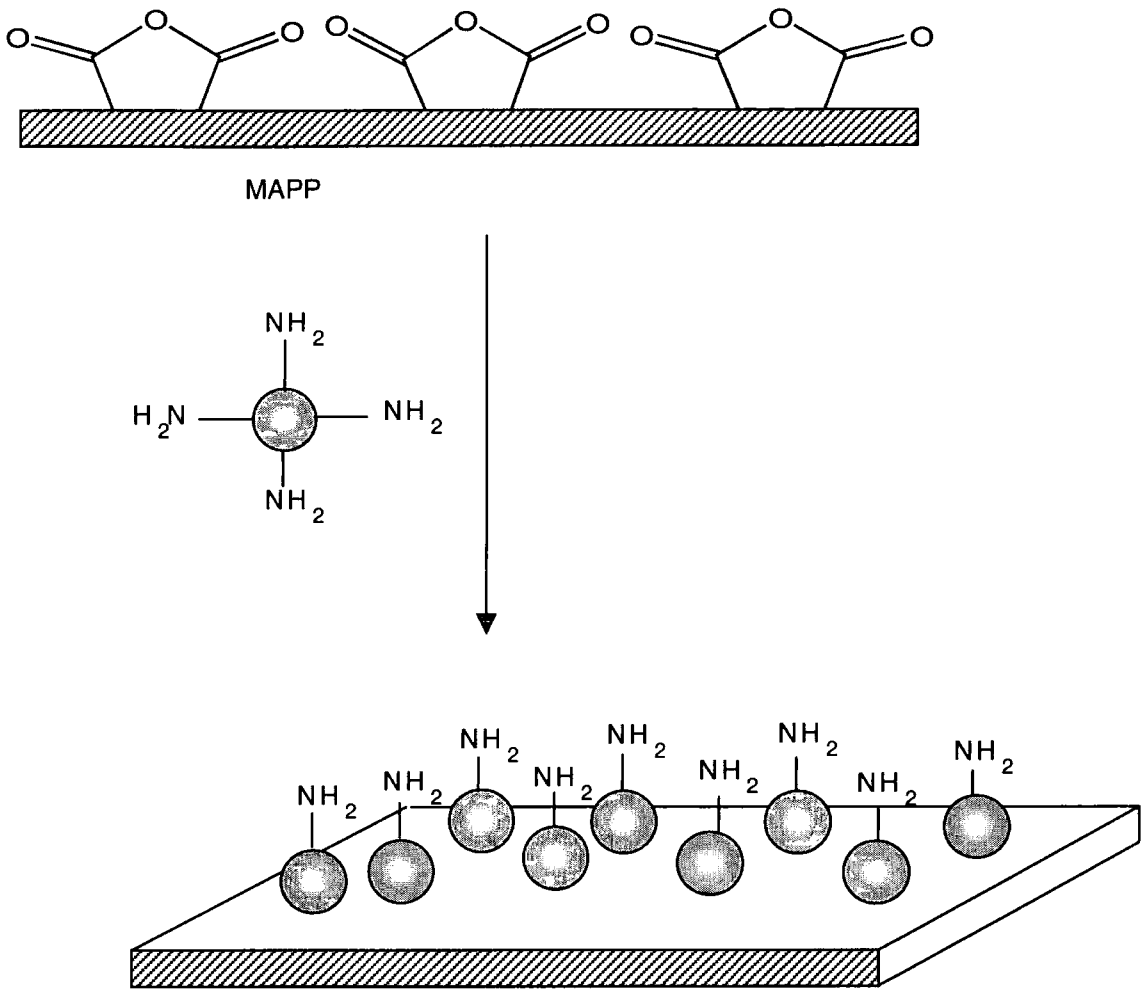

Figure 4.2 (a) Amine functionalized polystyrene beads on MAPP.

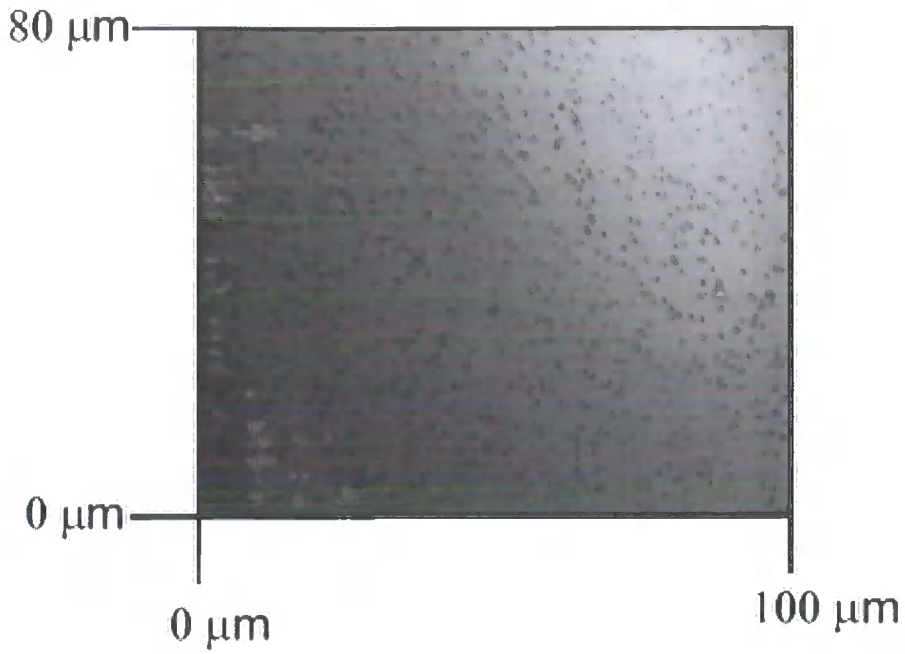

Figure 4.2 (b) Carboxylic acid functionalized polystyrene beads on MAPP.

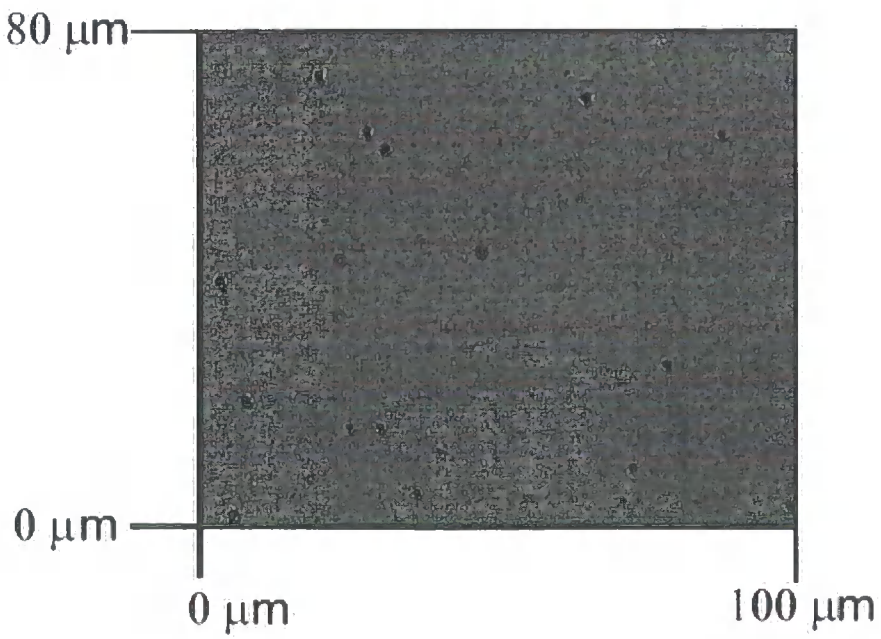

In this example it can be seen that the amine-functionalized beads react preferentially with the MAPP surface. This was predicted before the experiment, as amine groups have previously been shown to react with anhydride groups, Chapter 2 and references therein. Carboxylic acid groups do not react with anhydride groups, and the few visible on the surface are probably not chemically bonded.

4.3.4 Functionalization of the MAPP layer with Polyethyleneimine.

The deposited maleic anhydride layers were exposed to a 1% w/v solution of polyethyleneimine in isopropyl alcohol for 1 hour inside a sealed beaker. The extent of functionalization was studied by XPS, which revealed a change in the C(1s) spectra, and nitrogen was also detected. The peaks present after reaction are attributed to $\underline{C}H_x$ at 285.0 eV, $\underline{C}$-C-NHR(=O) / C-N at 285.7 eV, $\underline{C}H_2$-NH-C=O at 286.6 eV, RHN-$\underline{C}$=O at 287.9 eV and C(O)-O / COOH at 289.4 eV, Figure 4.1 (d). The mechanism by which the PEI reacts with the MAPP surface will be the same as that detailed in Chapter 2, giving rise to amide linkages between the MAPP and the PEI, and leaving some free acid groups at the surface.

These layers were further functionalized with a gold colloid suspension in water for 1 hour. XPS of these samples revealed that the surfaces contained approximately 0.15 % $\pm$ 0.07 gold, which is comparable with a low concentration of PAMAM dendrimers adhered to the surface, Table 4.1, Scheme 4.3. The gold colloid particles are stabilized at the surface by the presence of the amine groups in the PEI.[5,6] The gold is therefore not covalently bound to the surface, and it is possible that leaching of the gold particles could occur over a period of time.

Scheme 4.3 MAPP functionalized by polyethyleneimine and then gold colloids.

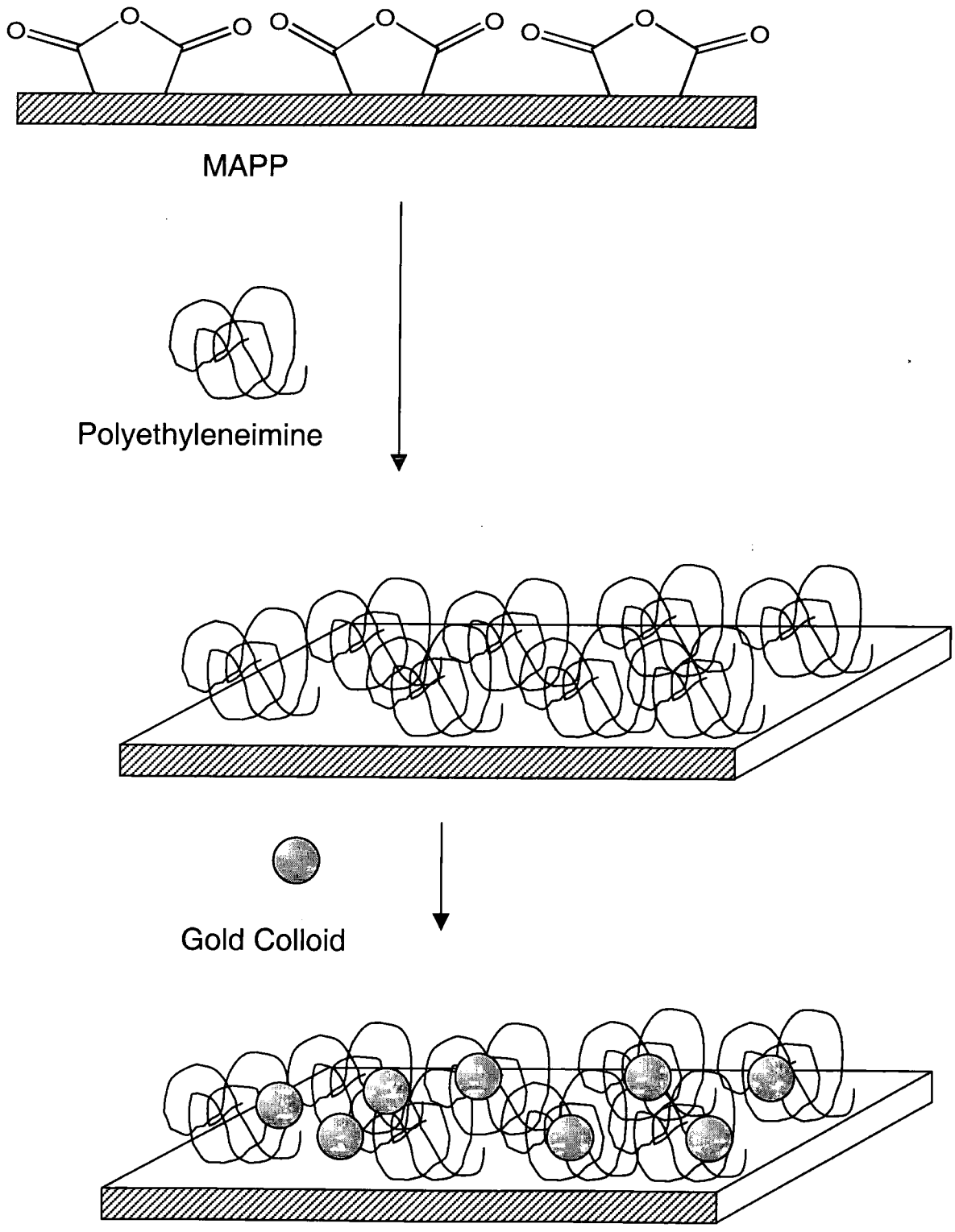

4.4 CONCLUSIONS

This chapter has been intended to demonstrate the further suitability of the MAPP surface for reaction with amine containing functionalities. By using a variety of functional groups attached to the amines, it has been shown that it is possible to attach many different moeities to the solid surface. This could have many applications, especially from a biological persepctive, where functionalized surfaces are of considerable interest for implant modification, to prevent adverse reactions with in the body. Reactive surfaces could also have application in sensor technology, as there will be preferential reactions occurring between the surface, and other species.

4.5 REFERENCES

1 Trivedi, B. C.; Culbertson, B. M. Maleic Anhydride; Plenum: New York, 1982.

2 McMurry, J. Organic Chemistry; Brooks/Cole: Pacific Grove, CA, 1992; 813.

3 Evenson, S.A., Fail, C.A., Badyal, J.P.S. *Chem. Mater.*, **2000**, *12*, 3038.

4 Yonezawa, T., Onoue, S.Y., Kunitake, T. *Adv. Mater.*, **1998**, *10,* 414.

5 Grabar, K.C., Freeman, R.G., Hommer, M.B., Natan, M.J. *Anal. Chem.*, **1995**, *67*, 735.

6 Jin, Y.D., Kang, X.F., Song, Y.H., Zhang, B.L., Cheng, G.J., Dong, S.J. *Anal Chem*, **2001,** *73,* 2843.

CHAPTER FIVE

Surface Diels-Alder Reactions

5.1 INTRODUCTION

5.1.1 Diels-Alder Reactions

A Diels-Alder cycloaddition reaction forms two carbon–carbon bonds in a single step, and gives rise to cyclic molecules. It is named after Otto Diels and Kurt Alder who won the 1950 Nobel Prize for Chemistry for this discovery.[1] It is a pericylic reaction, which means that the reaction takes place in a single step. It also involves the cyclic redistribution of bonding electrons. Simply, a Diels-Alder reaction can be represented as shown below, Scheme 5.1.

Scheme 5.1 Schematic of a Diels-Alder reaction.

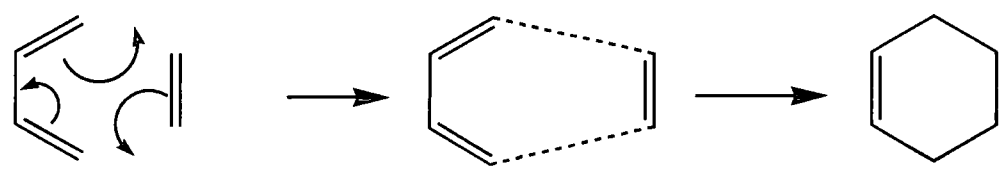

Diene Dienophile Cyclic Transition State Product

A Diels-Alder reaction requires two components, a dienophile and a diene. The dienophile will be more reactive if it has electron-withdrawing groups attached, so by this analogy ethyl acrylate will be a better dienophile than ethene. The diene must be able to adopt a cis like configuration around the single bond in

order to bring carbons 1 and 4 sufficiently close together to react through a cyclic transition state to form the cyclic product, Scheme 5.2.

Scheme 5.2 Bond rotation between cis and trans configurations

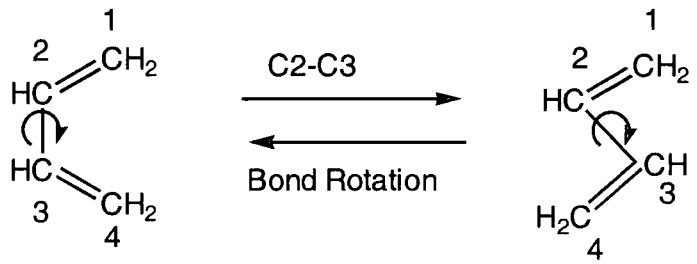

The reaction is also stereospecific, so a cis dienophile will only yield a cis product, and similarly the trans dienophile will only yield a trans product. A reaction is only observed if the reactant molecular orbitals are of the same symmetry as product molecular orbital. If they are the same, then the reaction is symmetry-allowed. Symmetry allowed reactions may occur under mild conditions, i.e. room temp or mild heat. To decide if a reaction will occur, the frontier orbitals need to be considered. The orbitals are called the Highest Occupied Molecular Orbital (HOMO) and the Lowest Unoccupied Molecular Orbital (LUMO). A reaction occurs when the HOMO of one reactant overlaps with the LUMO of a second reactant in a bonding manner. The symmetry of the orbitals is such that bonding overlap of terminal lobes can occur in suprafacial geometry. In the example given in Scheme 5.3, page 95, the diene is the LUMO and the dienophile is the HOMO.

Scheme 5.3 Molecular Orbital representation of a Diels-Alder reaction

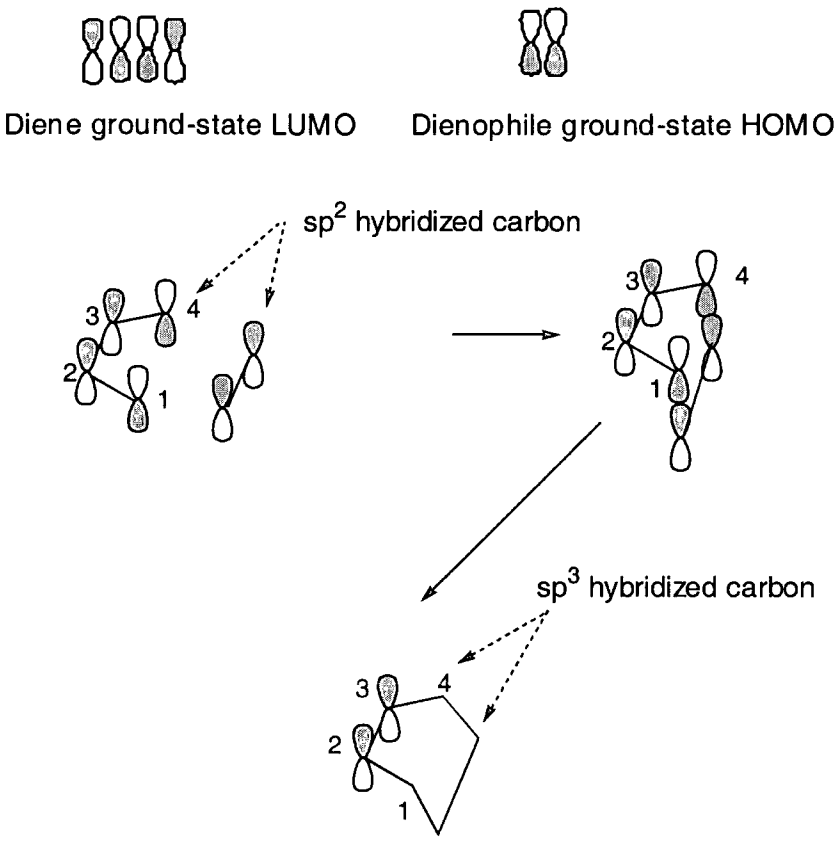

5.1.2 Diels-Alder reactions at surfaces

Work has recently been carried out looking at Diels-Alder reactions occurring at surfaces. Theoretical studies have looked at the likelihood of such reactions[2,3]. In the first of these examples,[2] a dimer on the reconstructed Si (100)-2x1 surface acts as the dienophile, as it has two dangling bonds that are weakly coupled. This is because the (100) surface undergoes a 2 x 1 reconstruction, in which pairs of atoms are bonded by a strong sigma (σ) bond and a partial pi (π) bond[4]. These surface dimers can undergo reaction with dienes, in a manner analogous to the Diels-Alder reaction to form six-membered rings at the surface, Scheme 5.4, page 96.

Scheme 5.4 Diels-Alder reaction at the Si (100)-2x1 surface[3]

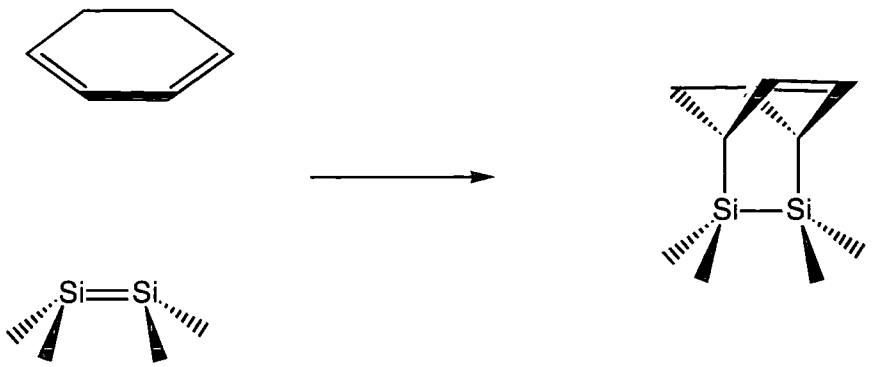

This work showed that it was possible to passivate the dangling bonds at the surface, at the same time giving a product that contains a C-C double bond. Later work[3] further demonstrated the potential for this type of reaction, suggesting that providing that the diene molecule has a 1,3 dipole, the silicon (100)-2x1 surface can act as a dienophile and attach molecules such as ozone, nitro compounds (R-NO_2), azides (R-NNN), diazo compounds (R,R'CNN), and nitrile oxides (RCNO). The schemes proposed from the theoretical results are similar to the reaction given above, but lead to the formation three and five membered rings.

The majority of the work to date on surface Diels-Alder reactions has been carried out assuming that specific surfaces of elements such as carbon[4,5], silicon[6] and germanium[7,8] have bonds at the surface are capable of acting as the dienophile). These results largely refer to the [4 + 2] reaction between a diene and a dienophile. There is also evidence that the [2 + 2] reaction can occur, and this has been found to be facile.[5]

SAMs that present surface double bonds for Diels-Alder reactions have also been examined.[9] The reduction of hydroquinone to quinone was studied using the Diels-Alder reaction as a marker to measure the attachment of biological molecules to the surface of the SAM, through the changes in the cyclic voltammograms measured as the reaction progressed.[9] In this case the Diels-Alder reaction occurring at the surface was shown to be an effective method for bio-immobilization, as well as providing a quantitative measure of the extent of the reaction through the reactions previously well characterized kinetics. This is demonstrated in Scheme 5.5, page 97.

Scheme 5.5 Surface reduction of hydroquinone to quinone[9]

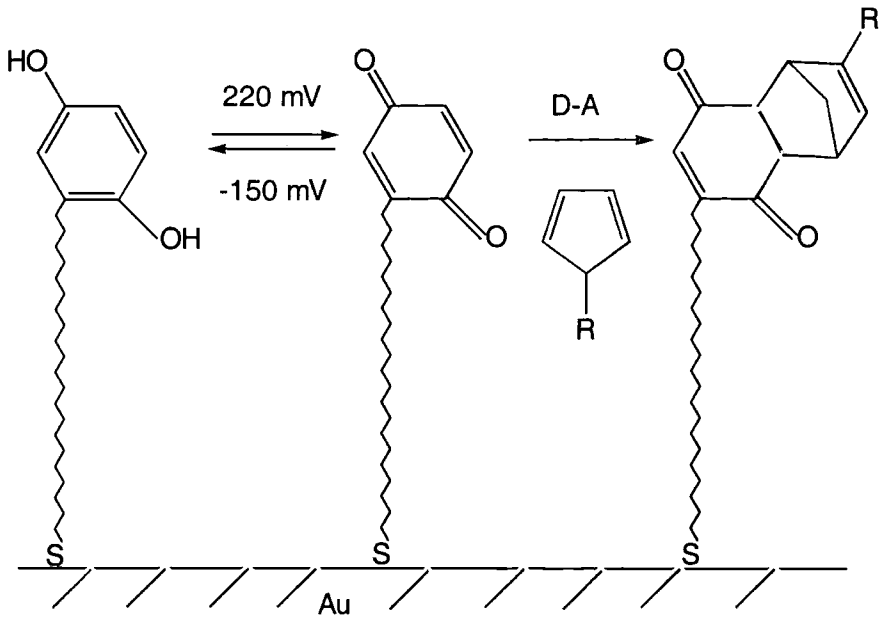

In this chapter the maleic anhydride plasma polymer (MAPP) has been functionalized with allyl amine to leave a free double bond at the surface. This has been reacted with ozone, butadiene and cyclohexadiene, and the surfaces produced characterized by XPS and ATR-FTIR, details of which can be found in Chapter 1, sections 1.4.2.4, page 21 and 1.5, page 23 respectively.

5.2 EXPERIMENTAL

5.2.1 Plasma Polymerization of Maleic Anhydride.

Details of the plasma polymerization of maleic anhydride can be found in Chapter 2, section 2.2, page 36.

5.2.2 Reaction with Allylamine

The deposited MAPP coatings were reacted with Allylamine (Aldrich, 99+%). This was carried out according to the method given in Chapter 2, section 2.2.1, page 36 and 2.2.2, page 38. The reaction of amines with the MAPP has previously been studied, and the mechanism shown here has been proved.[10]

5.2.3 Functionalistion with Ozone

In order to expose the allylamine treated MAPP to ozone, the treated samples were placed in a dielectric barrier discharge, out of sight of the discharge itself, but close enough to react with the ozone produced by the reaction.

5.2.4 Functionalization with Cyclohexadiene

In order to expose the allylamine treated MAPP to cyclohexadiene, the treated samples were placed in a vacuum chamber, isolated from the pump and exposed to the cyclohexadiene vapour for 30 minutes. After the reaction was complete the vacuum chamber was evacuated back top base pressure.

5.2.5 Functionalization with Butadiene

In order to expose the allylamine treated MAPP to butadiene, the treated samples were placed in a vacuum chamber, isolated from the pump and exposed to the butadiene vapour for 30 minutes. After the reaction was complete the vacuum chamber was evacuated back top base pressure.

All samples were analysed immediately after the completion of treatment. XPS and ATR-FTIR were used to characterize these layers. Experimental details can be found in Chapter 1, sections 1.4.2.4, page 21 and 1.5, page 23 respectively.

5.3 RESULTS AND DISCUSSION

5.3.1 Pulsed Plasma Polymerization of Maleic Anhydride

The results of the plasma polymersiation of maleic anhydride can be found in Chapter 2, section 2.3.1, page 39.

5.3.2 Functionalization of the MAPP Layer with Allylamine

The mechanism by which amines react with MAPP has been discussed extensively in previous chapters. Evidence for the reaction between allylamine vapour and deposited MAPP layers was obtained by XPS analysis. The characteristic anhydride group feature in the C(1s) spectrum at 289.4 eV disappeared with the concurrent appearance of an amide shoulder at 287.9 eV, RHN-C=O, Figure 5.1, page 100. In addition, a doublet was seen in the N(1s) spectrum, Figure 5.2, page 101, at 400 eV and 402 eV corresponding to amide (76 %) and ammonium salt (24 %) linkages respectively at the ring opened maleic anhydride centres.[10] Subsequent annealing at 120° C produced a much narrower N(1s) envelope at 400 eV, which can be taken as evidence for ring closure to yield imide linkages, Scheme 5.6, page 99.[10]

Scheme 5.6 Reaction of Allylamine with MAPP

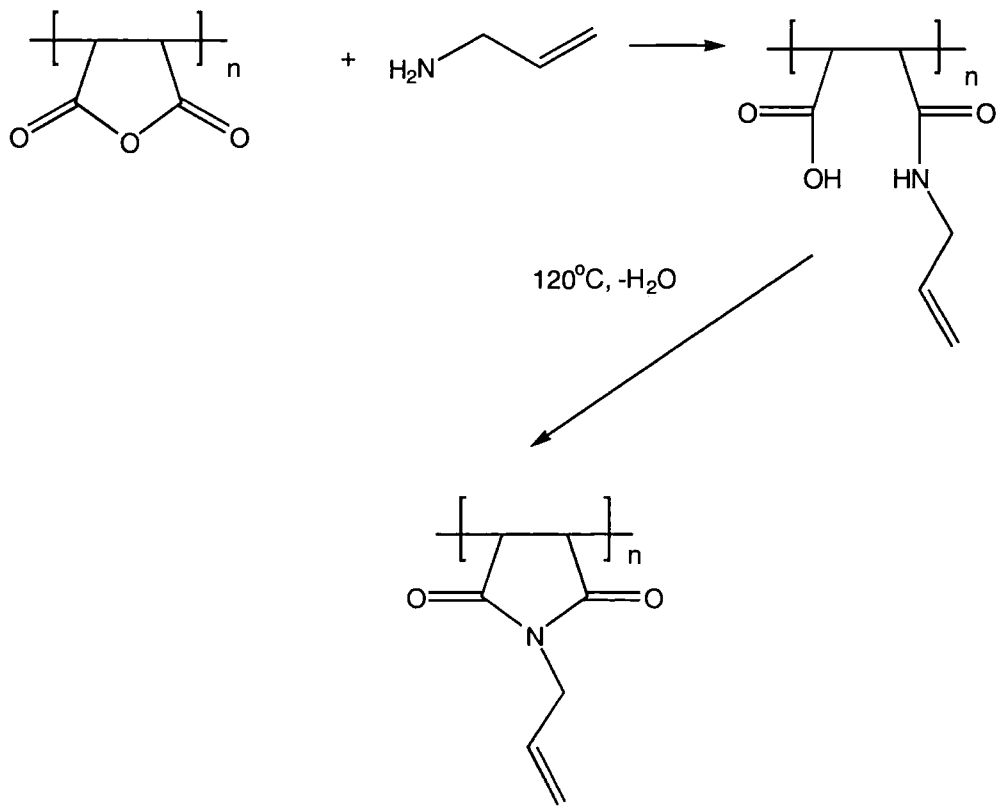

Figure 5.1 C(1s) XPS spectra of (a) MAPP; (b) MAPP exposed to allylamine vapour.

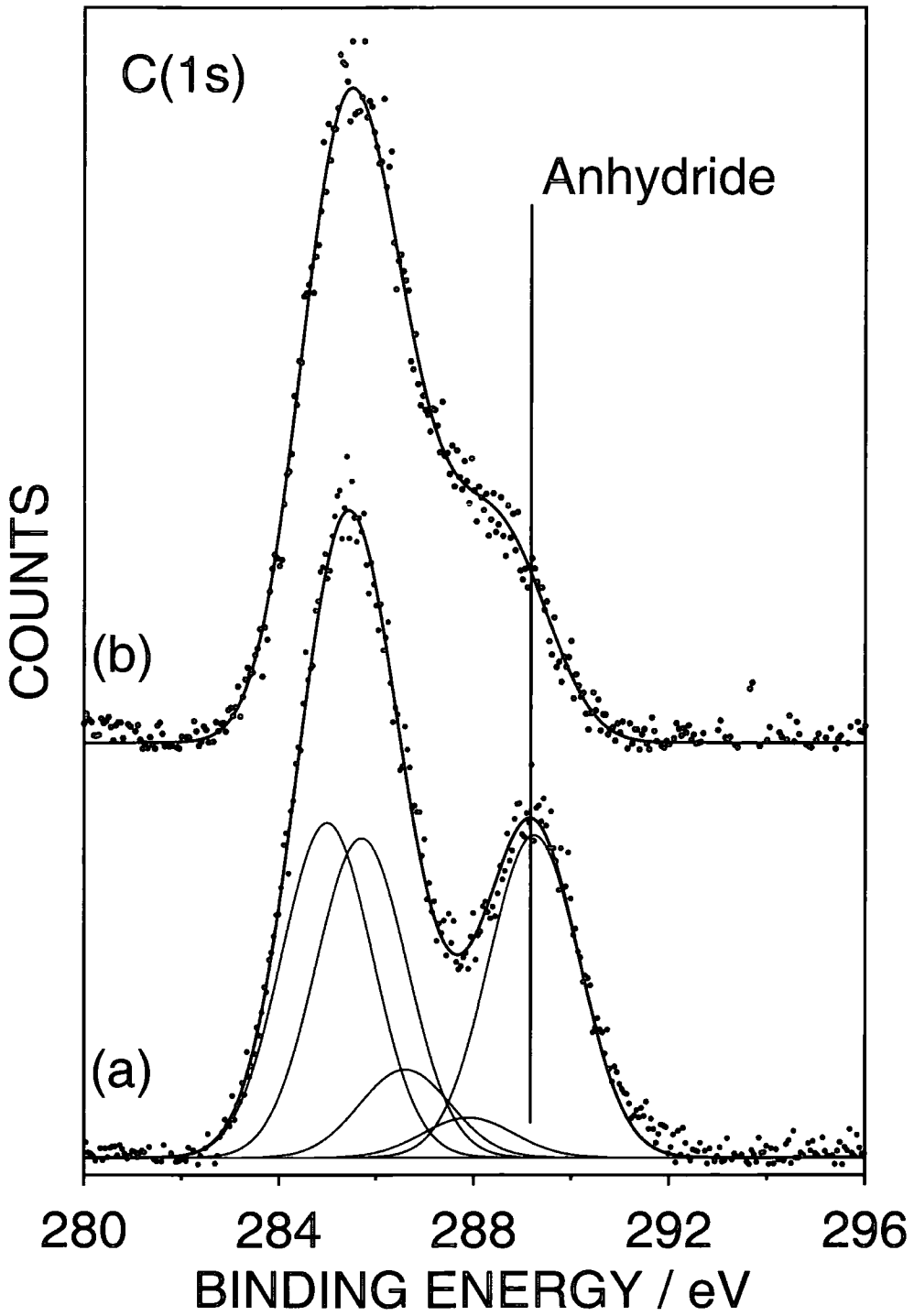

Figure 5.2 N(1s) XPS spectra of (a) MAPP; (b) MAPP exposed to allylamine vapour; and (c) following heating of (b) to 120°C.

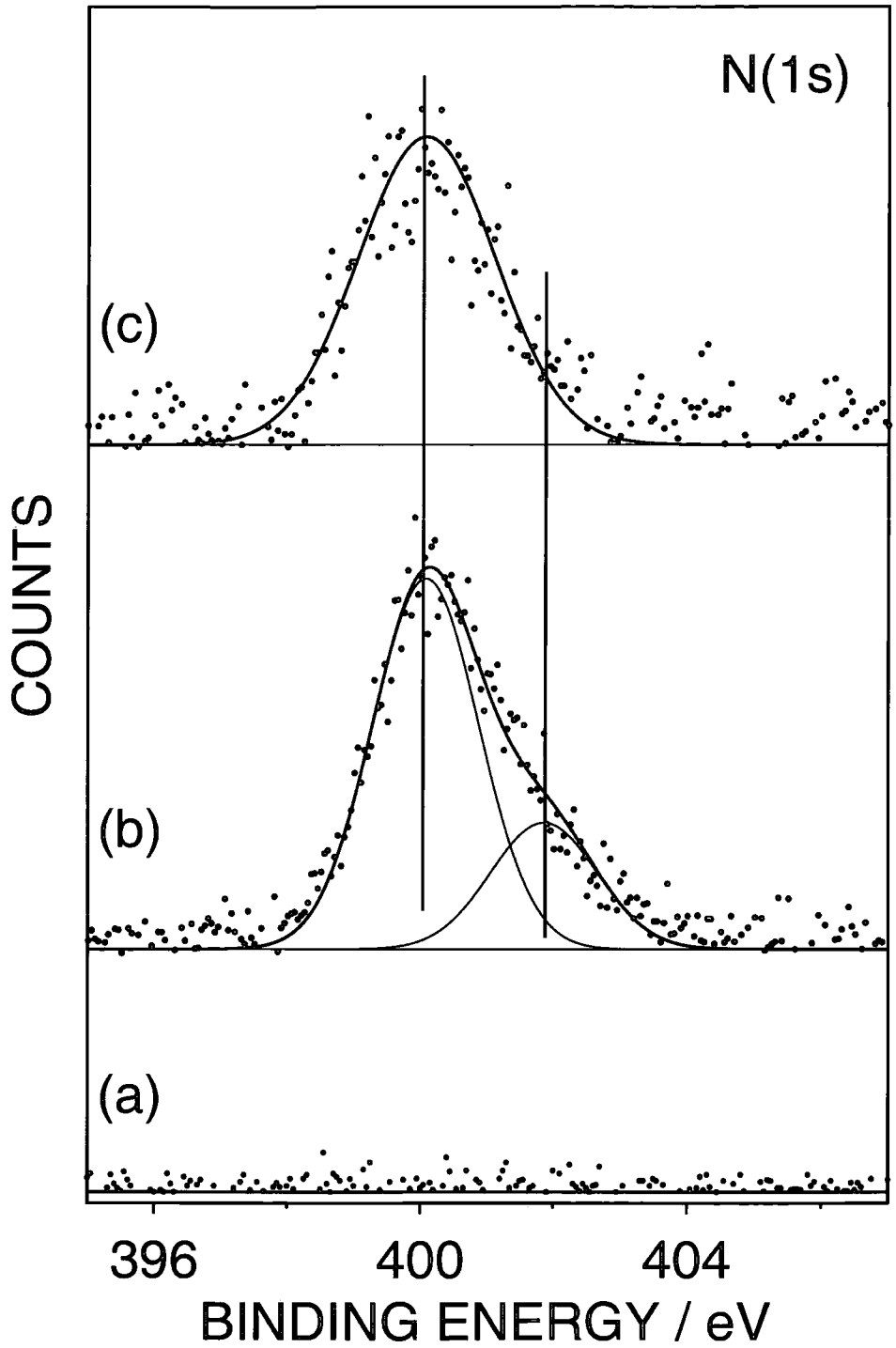

The maximum theoretical amount of nitrogen present after functionalization is 7.7 %, but the percentage of nitrogen detected by XPS is 11.2 % ± 0.5. It may be that some of the allyl amine is bonding to form the ammonium salt with the free acid that is formed in the ring opening reaction. This is confirmed by the N(1s) spectra which shows a peak at 402 eV, which is attributable to the ammonium salt. It is possible to calculate the maximum possible nitrogen incorporation at the surface by using the method given below. After heating of the sample to 120°C overnight, 6% nitrogen was detected by XPS, as the imide group is formed, so it is likely that any allyl amine that was attached via the ammonium salt to the acid is removed by heating, thereby halving the amount of nitrogen detected.

Assuming that there is a homogenous distribution of the elements throughout the XPS sampling depth, we can calculate the amount of functionalization occurring.[11,12] If we neglect the number of hydrogen atoms in the original polymer, since they are not detected by XPS, experimentally determined elemental composition, of the maleic anhydride is [C] = 67% and [O] = 33%. For each molecule of allylamine that is reacted, four more atoms are introduced, three carbon atoms and one nitrogen atom. If we then introduce a conversion factor, called *x*, where, when $x = 0$, there is no functionalization of the surface, and when $x = 1$, there is complete functionalization of the surface, equations can be written to represent the amount of nitrogen, [N], present at the surface.

$$[N] = \frac{x\left(\frac{[O]_o}{3}\right)}{[C]_o + [O]_o + 2x\left(\frac{[O]_o}{3}\right)}, \qquad \textit{Equation 5.1}$$

where $[O]_o$ is the initial oxygen concentration and $[C]_o$ is the initial carbon concentration.

These equations can easily be rearranged, and by using theoretical values of *x*, a graph of [N] against the *x*, theoretical degree of surface functionalization can be plotted. This allows the actual degree of functionalization to be calculated,

knowing the elemental abundance, as calculated from XPS, and reading from the graph shown below, Figure 5.3.

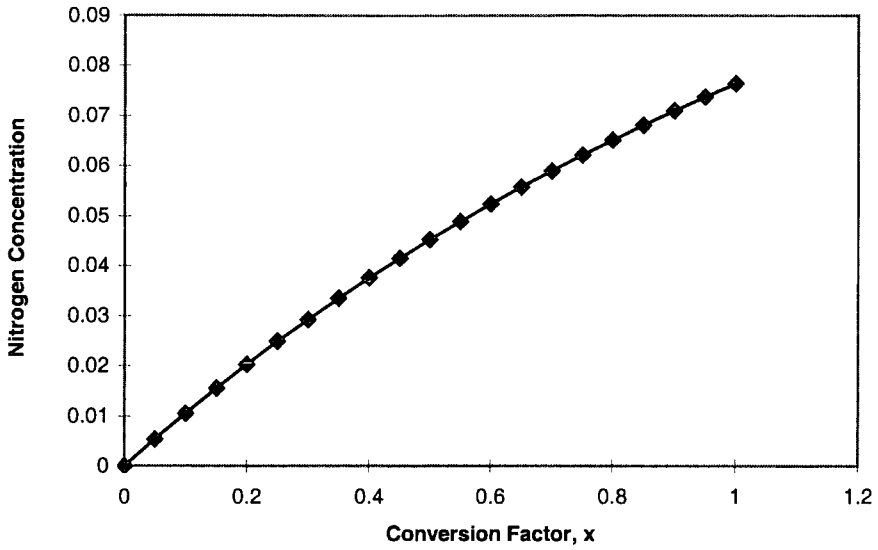

Figure 5.3 Theoretical amount of nitrogen incorporation with increasing conversion factor

Infrared spectroscopy provided further evidence for the reaction between allylamine and surface anhydride functionalities, as signified by Amide I (C=O stretching) and Amide II (NH bending) features at approximately 1680 cm^{-1} and 1650 cm^{-1}, Figure 5.4, page 104.[13] The peaks at approximately 1440cm^{-1} and 1400cm^{-1} are attributable to the presence of the alkene double bond, arising from the *cis* CH asymmetric rock. In all of the functionalized spectra, there is evidence of a peak in this region. The peak at 1250 cm^{-1} is attributable to the *cis* CH symmetric rock.

Figure 5.4 IR spectra of (a) MAPP, (b) MAPP exposed to ozone, (c) MAPP reacted with allylamine in the vapour phase and (d) MAPP reacted with allylamine in the vapour phase, and then exposed to ozone. (i) marks the ketone band and (ii) marks the NO band.

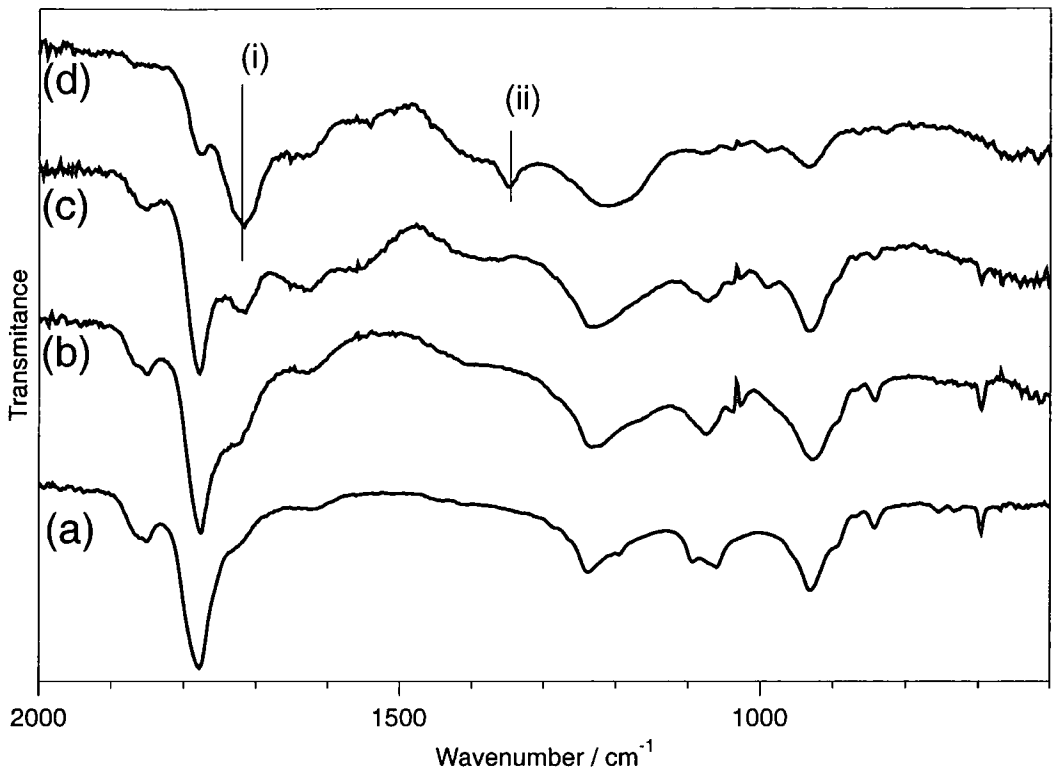

5.3.3 Ozonolysis Of Surface Alkene Groups

The reactivity of the terminal carbon-carbon double bonds immobilized on the surface was probed by exposing the surface to ozone in order to yield ketone groups. XPS analysis showed a strong increase in the C(1s) component at 287.9 eV corresponding to C=O groups, Figure 5.5(d), page 105. Infrared spectroscopy provided supporting evidence in terms of a strong ketone band at 1720 cm^{-1} (marked (i) on spectra) , Figure 5.4(d), page 104. Potentially, there may also have been some nitro-containing species produced via the oxidation of NH bonds to NO (marked (ii) on spectra) by ozone.[14-16]

A control experiment comprising ozone exposure to just the MAPP layer did not yield the observed ketone XPS and IR spectral features, thereby confirming ozonolysis must be taking place at the anchored alkene bonds.

Figure 5.5 C(1s) XPS of (a) maleic anhydride, (b) maleic anhydride exposed to ozone, (c) maleic anhydride reacted with allylamine in the vapour phase and (d) maleic anhydride reacted with allylamine in the vapour phase, and then exposed to ozone.

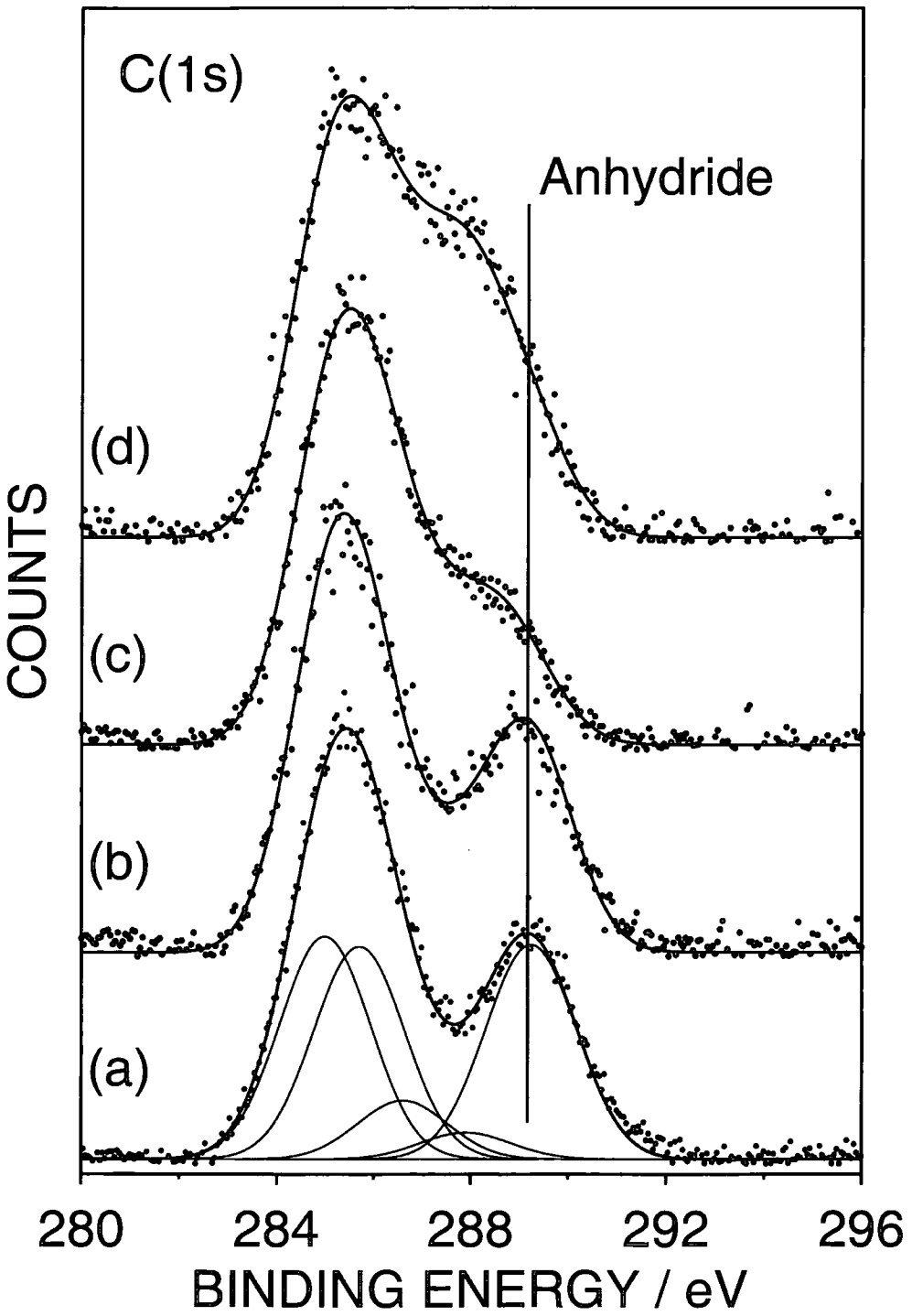

Ozone is a commonly used double bond cleavage reagent.[1] The ozone used is generated by passing a stream of oxygen through a high-voltage electrical discharge. It then adds to the alkene to produce the molozonide, which in turn rapidly rearrange to form ozonides. The ozonide can be further reduced to give carbonyl compounds, Scheme 5.7.

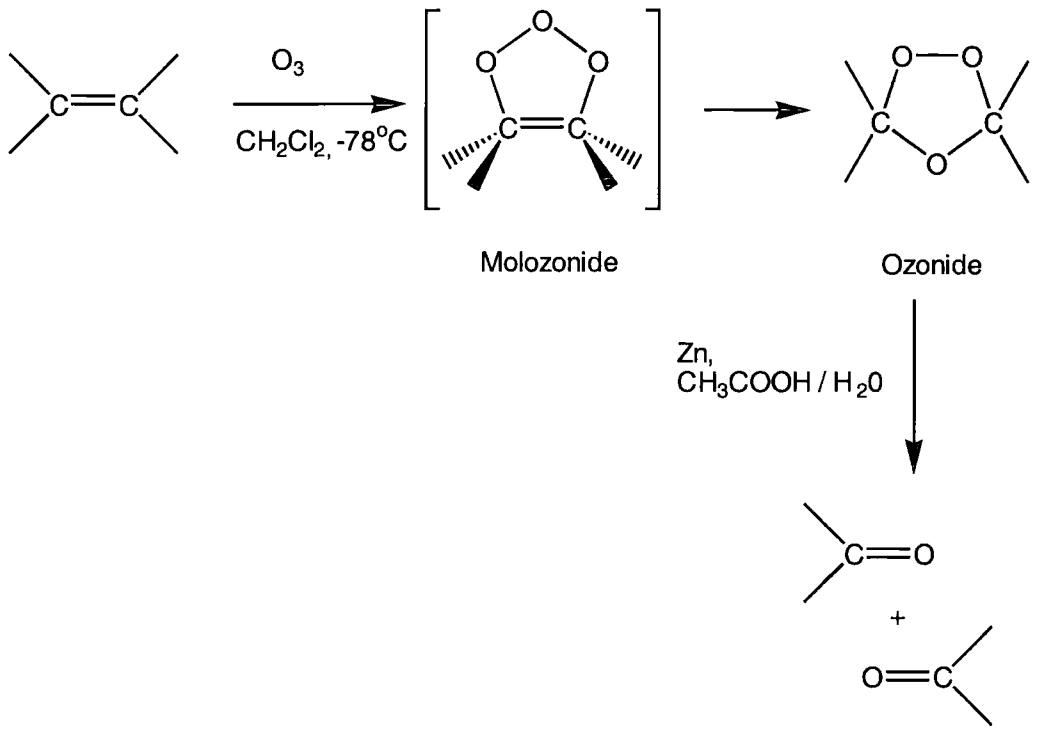

Scheme 5.7 The reaction of ozone with hydrocarbon double bonds

This reaction is of interest from a surface chemistry perspective, because it gives a method by which surface groups can be converted to functionalities that offer more scope for subsequent reactions that the starting material. The selective ozonlysis of a surface can also be useful for lithography.[17] In a polystyrene / poly(butadiene) blend, ozone will selectively react with the poly(butadiene), reacting with the double bonds in the backbone. Washing removes the degradation products, and a highly ordered polystyrene template remains.

5.3.4 Surface Diels-Alder Chemistry

Diels-Alder reactions were investigated using two different dienes, cyclohexadiene, Scheme 5.8, page 107, and butadiene. Scheme 5.9, page 107. In this case, the carbon-carbon double bond at the surface belonging to

the immobilized allylamine molecule acted as the dienophile. The results can be seen on Figure 5.6, page 108.

Scheme 5.8 Butadiene reacting with allylamine functionalized MAPP

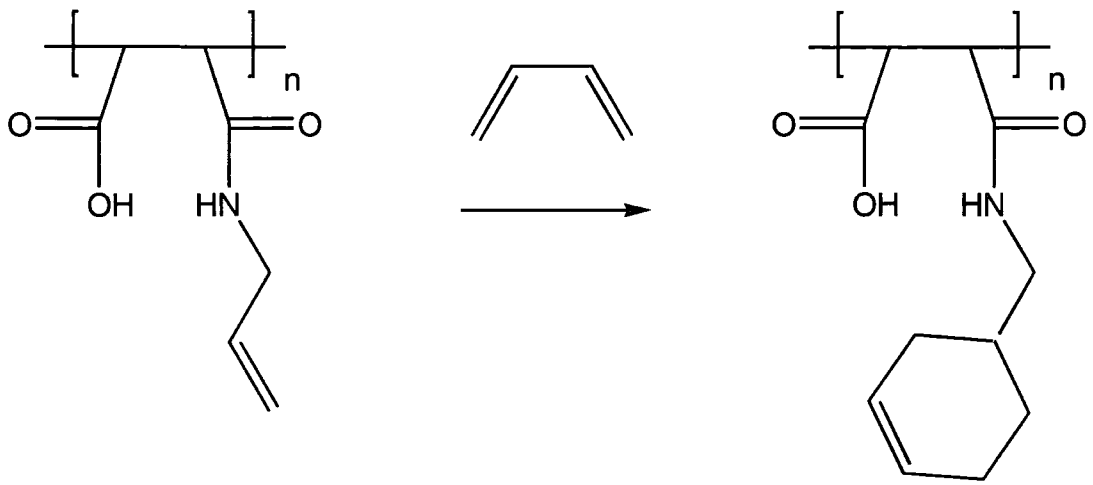

Scheme 5.9 Cyclohexadiene reacting with allylamine functionalized MAPP

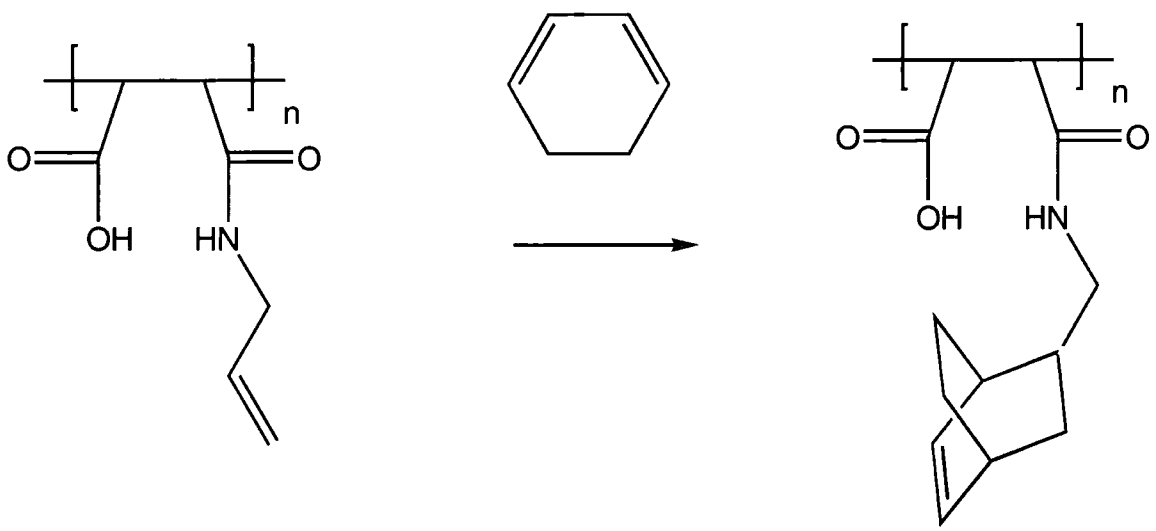

Figure 5.6 IR spectra of (a) MAPP, (b) MAPP functionalized with allylamine, (c) cyclohexadiene liquid, (d) shows (b) functionalized with butadiene and (e) shows (b) functionalized with cyclohexadiene.

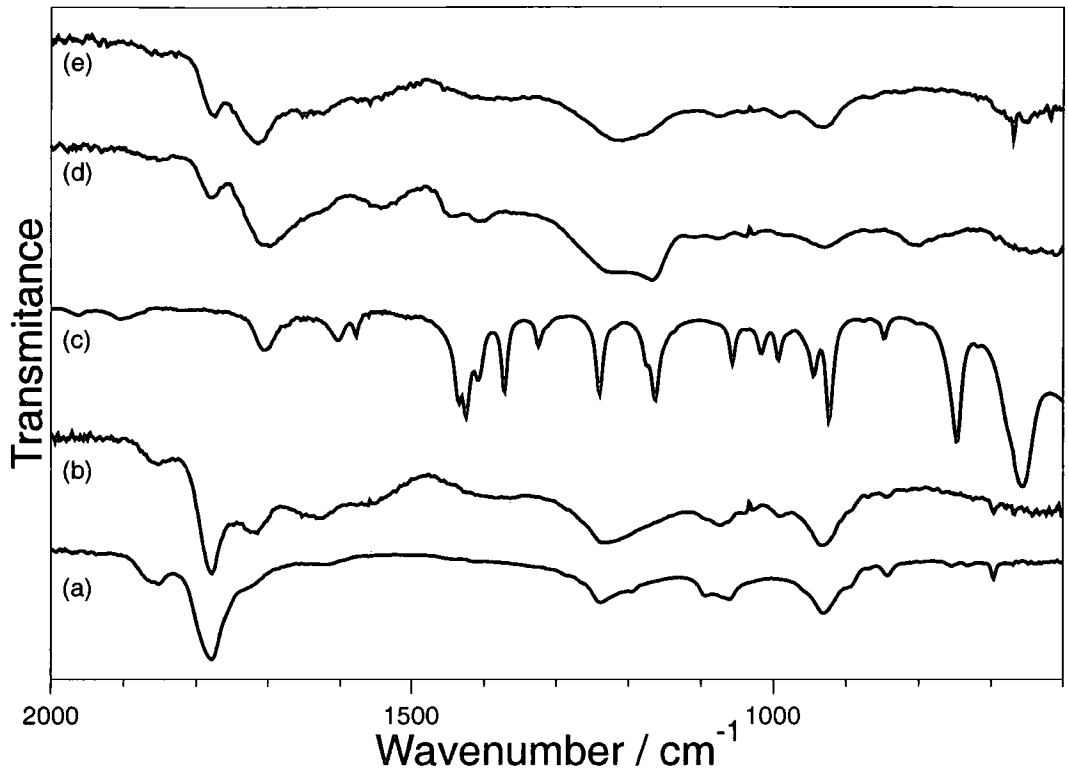

The IR spectra shown in Figure 5.6 show clear evidence of the reaction between the allylamine double bond and the dienes. Figure 5.6(a) shows the IR spectrum of the MAPP. The features which confirm that the layers is maleic anhydride are the peaks at 1849 cm^{-1} and 1780 cm^{-1} due to C=O anhydride stretches, and at 1249 cm^{-1} and 958 cm^{-1} attributable to cyclic anhydride features. A further discussion of the IR spectra of MAPP can be found in Chapter 2, section 2.3.1, page 39.

After reaction of MAPP with allylamine vapour, Figure 5.6(b), it is apparent that there has been a reaction between the two species, as the IR spectrum shows evidence of C=O acid stretches between 1725 and 1700 cm^{-1}. There is also evidence of the amide I & II features at 1660 cm^{-1} and 1560cm^{-1} respectively, arising from C=O stretches and N-H bending. There is also a slight feature between 1490 and 1400 cm^{-1} attributable to C-NH stretches.

Figure 5.6(c), page 108, shows the spectra of cyclohexadiene liquid. The peak at approximately 1700cm^{-1} arises from C=C stretches, and the peaks between 1400 and 1450 cm^{-1} are due to C-C stretches within the ring structure the peaks between 950 and 1000 cm^{-1} are also due to these. Finally, CH / CH_2 deformations account for features in the spectra between approximately 1150 and 1250cm^{-1}. It is the presence of these features is particular which can be used to show that the Diels-Alder reaction between the allylamine and butadiene or cyclohexadiene has occurred.

Figure 5.6(d) shows the IR spectra obtained after MAPP reacted with allylamine has been exposed to butadiene vapour. There are features present similar to those observed for the cyclohexadiene (Figure 5.6(c)), page 108. There is evidence of some C-C ring stretching between 1400 and 1450 cm^{-1} and again between 950 and 1000 cm^{-1}. There are still features attributable to the amide I & II, as discussed earlier for Figure 5.6(b), page 108. The CH / CH_2 deformations seen in the cyclohexadiene liquid spectra are also still apparent between approximately 1150 and 1250cm^{-1}. Scheme 5.9, page 107, shows us that we can expect all the features of a cyclohexene-like structure after reaction of the butadiene with the allylamine, and the evidence in the IR spectra supports this.

Finally, Figure 5.6(e), page 108, shows the IR spectra after reaction of MAPP reacted with allylamine has been exposed to cyclohexadiene vapour. This spectra is extremely similar to that seen in Figure 5.6(d), after reaction with butadiene. Figure 5.8 shows us the structure we would expect to have produced at the surface after this functionalization, and again the IR evidence supports this. As in Figure 5.6(d), there is still evidence of the underlying amide linkages, and all the ring features described for 5.6(d) apply here.

Table 5.1 shows the different peaks present, and on which spectra in Figure 5.6 they can be found.

Peak Position/ cm^{-1}	*Assignment*	*(a)*	*(b)*	*(c)*	*(d)*	*(e)*
1849	C=O anhydride stretch	*	*			
1780	C=O anhydride stretch	*	*			
1725-1700	Carboxylic acid stretch		*			
1772, 1710	Imide bands					
1700	C=C stretch			*	*	*
1660 – 1563 (Broad band)	Amide I (C=O stretching)and Amide II (N-H bending)		*			
1627-1590	NH_2 bands					
1625 – 1560, and 1550 - 1505	NH_3^+, antisymmetric and symmetric deformations					
1490-1400	C-NH stretch of monosubstituted amide		*			
1450	C-C ring stretches			*	*	*
1288-1240	Cyclic anhydride stretch	*				
1180-1000	C-N stretch		*			
1250-1150	CH/CH_2 overlapping CH deformation			*	*	*
1150-1060	C-O-C stretch					
1050	H-C= stretching			*	*	*
950	Ring stretching			*	*	*
958-935	Cyclic unconjugated anhydride	*				
950-780	C-C skeletal bands					
850	NH_2 wag		*			

5.4 CONCLUSION

In this chapter, the possibilty of performing Diels–Alder reactions at functionalized surfaces has been investigated. It has been shown that allyl amine can react with the MAPP to form amide linkages, whilst also presenting free double bonds at the surface which have the potential for further reaction.

The first reaction studied for these double bonds was ozonlysis. Free alkene groups were functionalized with ozone, and the presence of ketones, the products of the reaction were seen in the XPS and IR spectra.

The functionalization of the MAPP has been observed by XPS and IR analysis, and the presence of the double bonds was confirmed by IR spectroscopy. These double bonds can under go Diels – Alder type reactions with butadiene and cyclohexadiene. Functionalization was demonstrated by IR spectroscopy, which showed that double bonds are still present after the reaction.

In conclusion, it has been shown that it is possible to present free, unreacted double bonds at a solid surface, and to carry out conventional double bond chemistry with these groups.

5.5 REFERENCES

1 McMurry, J., Organic Chemistry, 3rd Edition, Brooks / Cole, Belmont, California, 1992.

2 Konecný, R., Doren, D.J. *J. Am. Chem. Soc.*, **1997** *119*, 11098.

3 Barriocanal, J.A., Doren, D.J. *J. Vac. Sci. Technol. A.*, **2000**, *18*, 1959.

4 Wang, G.T., Bent, S.F., Russel , J.N., Butler, J.E., D'Evelyn, M.P. *J. Am. Chem. Soc.*, **2000**, *122*, 744.

5 Hovis, J.S., Coulter, S.K., Hamers, R.J., D'Evelyn, M.P., Russell, J.N., Butler, J.E. *J. Am. Chem. Soc.*, **2000**, *122*, 732.

6 Konecný, R., Doren, D.J. *Surf. Sci.*, **1998**, *417*, 169.

7 Lee S.W., Nelen, L.N., Ihm, H., Scoggins, T., Greenlief, C.M. *Surf. Sci.*, **1998,** *410*, 773.

8 Lee, S.W., Hovis, J.S., Coulter, S.K., Hamers, R.J., Greenlief, C.M. *Surf. Sci.*, **2000,** *462*, 6.

9 Yousaf, M.N., Mrksich, M. *J. Am. Chem. Soc.*, **1999**, *121*, 4286.

10 Evenson, S.A., Fail, C.A., Badyal, J.P.S. *Chem. Mater.*, **2000**, *12*, 3038,.

11 Sutherland, I., Sheng, E., Brewis, D.M., Heath, R.J. *J. Mater. Chem.*, **1994**, *4*, 683.

12 Popat, R.P., Sutherland, I., Sheng, E. *J. Mater. Chem.*, **1995**, *5*, 713.

13 Silverstein, R. M.; Bassler, G. C.; Morril, T. C. Spectrometric Identification of Organic Compounds; Wiley: Singapore, 1991.

14 Munoz, F.; von Sonntag, C. *J. Chem. Soc.*, **2000**, *Part T2*, 2029.

15 Pietsch, J.; Schmidt, W.; Branch, H. J.; Worch, E. *Ozone Sci. Eng.*, **1999**, *21*, 23.

16 Liu, Y. L.; Bruening, M. L.; Bergbreiter, D. E.; Crooks, R. M. *Angew. Chem. Int. Ed. Engl.*, **1997**, *36*, 2114.

17 Mansky, P., Harrison, C.K., Chaikin, P.M., Register, R.A., Yao, N. *Appl. Phys. Lett*, **1996**, *68*, 2586.

CHAPTER SIX

Deposition and Functionalization of Allylamine plasma polymers (AAPP)

6.1 INTRODUCTION

Amine containing coatings are of particular interest for biomaterial applications, and recently work has been carried out to look at the deposition of AAPP's and their suitability for use in such conditions.[1] The AAPP's are of interest in this area because it is a solventless process that modifies the surface without altering the bulk properties of the material. Such films have recently been used to improve attachment of human cells, as the substrates produced in the plasma are superior to conventional surfaces.[2]

Polymers of allylamine have also been used in the formation of electrostatic multilayers.[3] The poly(allylamine) acts as a polycation and various other polymers have been used as the polyanion, including poly(styrenesulfonate) and DNA. Alternate layering of polyanion and poycation builds up layers that are of the order of several hundreds of Angstroms. DNA attachment or adsorption at surfaces is desirable for many purposes such as the detection of human pathogens in molecular recognition tests, and to purify and extract nucleic acids.[4,5] The poly(styrenesulfonate) acts as a polyanion through it's ability to interact with the

NH_2 groups of the amine[6], and the DNA is also considered to be a polyanion because of the negative charge on the sugar-phosphate backbone. DNA adsorption from solutions to positively charged lipid monolayers has also been carried out.[7] Kinetic studies of the adsorption of DNA onto aminated surfaces indicate that the deposition process occurs rapidly[8], but that pH can affect the rate of the deposition, as can the ionic strength of the system under investigation.

Polycation layers have also been used to stabilize metal colloids onto surfaces. In a similar way to the electrostatic layers described above, metal colloids have been encapsulated into polycation layers and subsequently overlaid by polyanion layers.[9] This technique allows conducting layers to be built up, and resisitivity measurements obtained for these polycationic / anion layers are similar to that of the bulk metal.[10] Amine and carboxylic acid functionalized poly(styrene) spheres have been used to stabilize platinum, palladium and gold colloids. It was found that if the surface of the sphere had a net positive charge (i.e. the amine surface), that excellent adhesion of gold colloids were achieved.[11,12]

In this chapter the plasma polymerization of allylamine has been carried out. This plasma polymer layer has then been used to attach functionalized poly(styrene) spheres, stabilize gold colloids, immobilse dye molecules and adhere DNA.

6.2 EXPERIMENTAL

6.2.1 Deposition of AAPP

The experimental method for depositing the AAPP layers was the same as outlined in Chapter 2, section 2.2, page 36. The only exception to this is that the pulse regime used in this case the on-time was 100μs and the off-time was 4000μ s and the peak power was 10 Watts. Using the equation given in Chapter 2, equation 2.1, page 37, this gives an average power of 0.25 Watts.

6.2.2 Functionalization of AAPP with heptafluorobutryl chloride

The AAPP layers were placed in a vacuum chamber and pumped down to base

pressure. This was done without exposure to air in order to avoid reaction of amine groups with atmospheric CO_2 and H_2O.[13,14] The vacuum pump was isolated and heptafluorobutryl chloride vapour was allowed to fill and equilibrate into the empty chamber at ambient temperature (~25° C). At this stage, timing of the surface functionalization reaction commenced. Upon termination of exposure, the acid chloride reservoir was isolated, and the whole apparatus was pumped back down to its initial base pressure.

6.2.3 Functionalization of AAPP with Polymeric Dye

Polyvinylamine with a sulphonate backbone (Sigma, R-478) was used to functionalize the AAPP. A 10% w/v solution of the polymeric dye was made, using water as the solvent. Glass slides with the plasma polymer coating had drops of the solution placed on them, and then left for 10 minutes. The samples were then rinsed with water and left to dry in air, prior to analysis.

Figure 6.1 Polymeric dye molecule

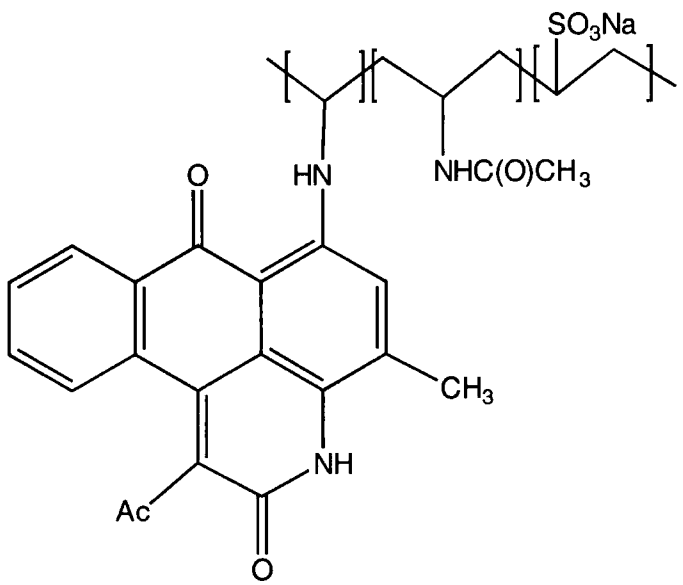

6.2.4 Functionalization of AAPP with DNA

DNA was purchased from Sigma (sodium salt from salmon testes). A solution of the DNA was made up in a 0.02M NaCl solution in water, maintained at pH 5. 0.1mg/mL of DNA was used.[3] Samples of the AAPP were treated overnight with

the DNA solution, and then rinsed repeatedly in high purity water. The samples were then air dried, and studied by XPS.

Figure 6.2 Schematic diagram of DNA

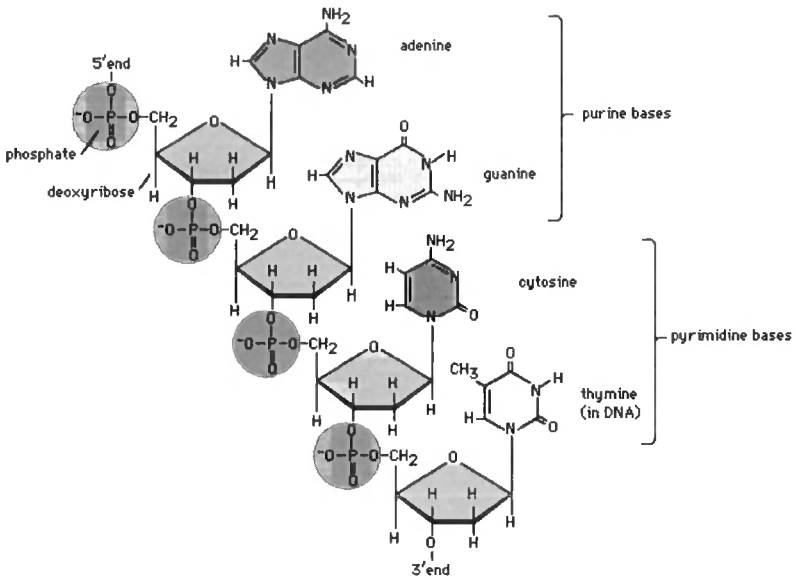

6.2.5 Functionalization of AAPP with COOH functionalized polystyrene and NH_2 functionalized polystyrene.

Functionalized polystyrene beads are supplied a solution in water (Bangs Labs. Inc. (PS-NH_2 beads are 0.66 μm mean diameter, PS-COOH beads are approximately 0.6μm mean diameter). These beads are diluted by ten times to give a bead concentration of 6.327 x 10^{10} beads per ml. The bead solution was applied to the plasma polymer surface as a solution. After the functionalization reaction had been allowed to occur, excess of beads was removed by rinsing in high purity water.

6.2.6 Functionalization of AAPP with Gold Colloids

The gold colloids are supplied as a solution in water (average diameter = 250 nm, concentration = 1.2×10^8 n /ml, Agar Ltd.). They are visible under the optical microscope. They were applied to the AAPP surface directly from the supplied solution, and excess was removed by rinsing in high purity water after the functionalization had occurred.

6.2.7 Surface Characterization

XPS and optical microscopy were used to characterize the functionalized surfaces. Details can be found in Chapter 1, section 1.4.2.4, page 21 and 1.6.3, page 26 respectively.

6.3 RESULTS AND DISCUSSION

6.3.1. Allylamine Plasma Polymer (AAPP)

Poly(allylamine) layers are of interest for biological purposes, and as polycation layers for electrostatic interactions. They provide a amine rich surface which is capable of undergoing further reaction with many different species, from human cells to DNA to metal colloids to dye molecules. Plasma polymerization of the allylamine monomer is often desirable as it provides a simple, dry, one step method, rather than multi-step wet chemistry methods.[1,15-17] It is also a useful process because any material can be used as the substrate for plasma polymer deposition, whereas other techniques which use aminpropyltriethoxysilane or similar to present amine groups at the surface require silica as a substrate.[18-20] Ammonia plasmas have been used to introduce amine groups at surfaces, but these have been shown to break down rapidly, resulting in the loss of the functionalized surface.[21,22]

In this work the AAPP was deposited onto glass slides, as in earlier work using maleic anhydride (see Chapter 2). XPS analysis of the surface showed that there was good retention of the amine functionality at the surface, as seen in the C(1s) spectra, Figure 6.3 (a), page 119, and the N(1s) spectra, Figure 6.4, page 120, revealed one peak at ~400 eV, which is indicative of the amine group. There was no evidence of ammonium salt formation, which would have been seen by a peak in the N(1s) at ~402 eV. The ratio of carbon to nitrogen in the monomer is 3:1, and in the plasma polymer it is 2.2:1, suggesting that there is some monomer break down during the plasma deposition.

Figure 6.3 C(1s) XPS spectra of a) AAPP, b) AAPP functionalized with heptafluorobutryl chloride, c) AAPP functionalized with polymeric dye, d) AAPP functionalized with DNA.

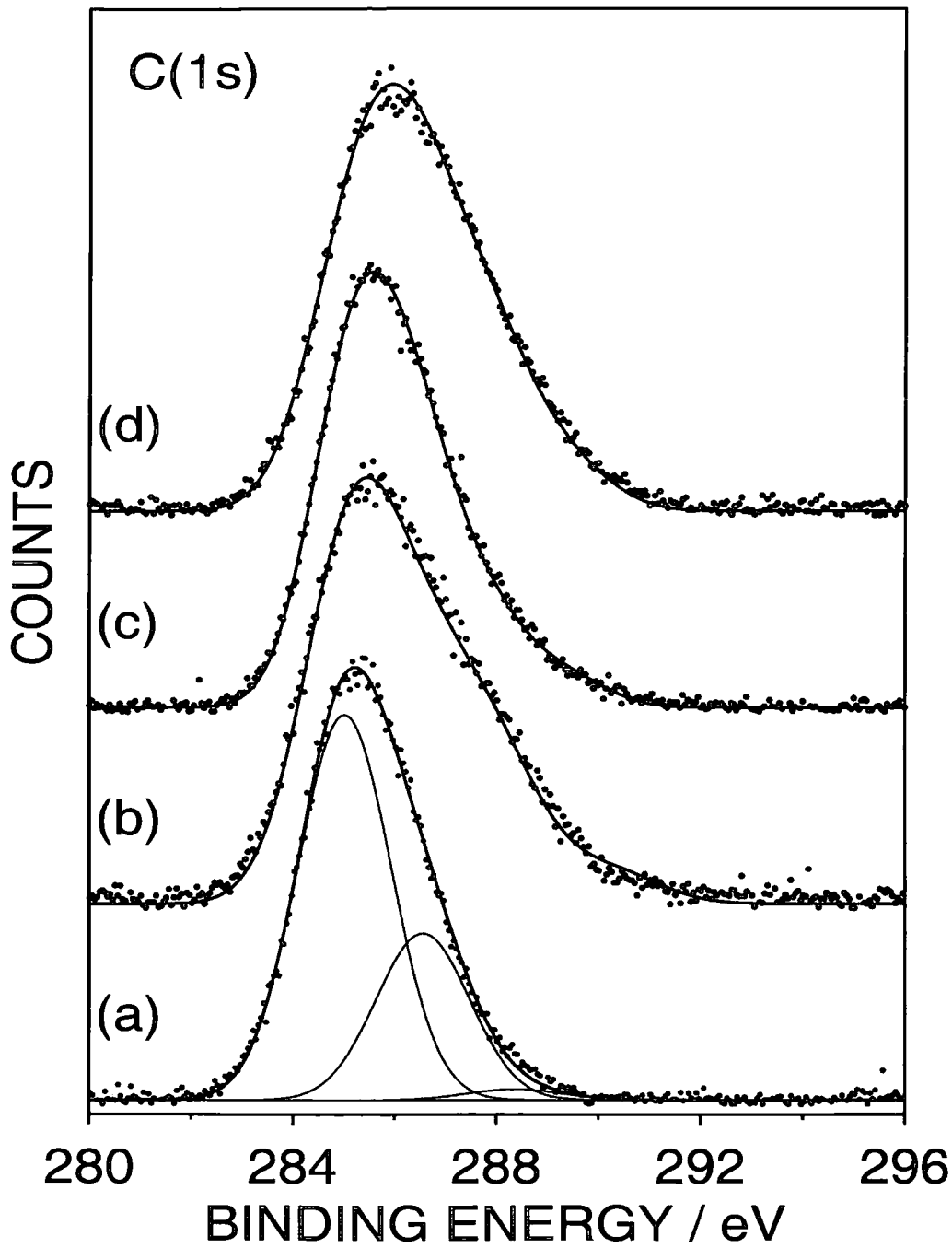

Figure 6.4 N(1s) XPS spectra of a) untreated substrate and b) AAPP.

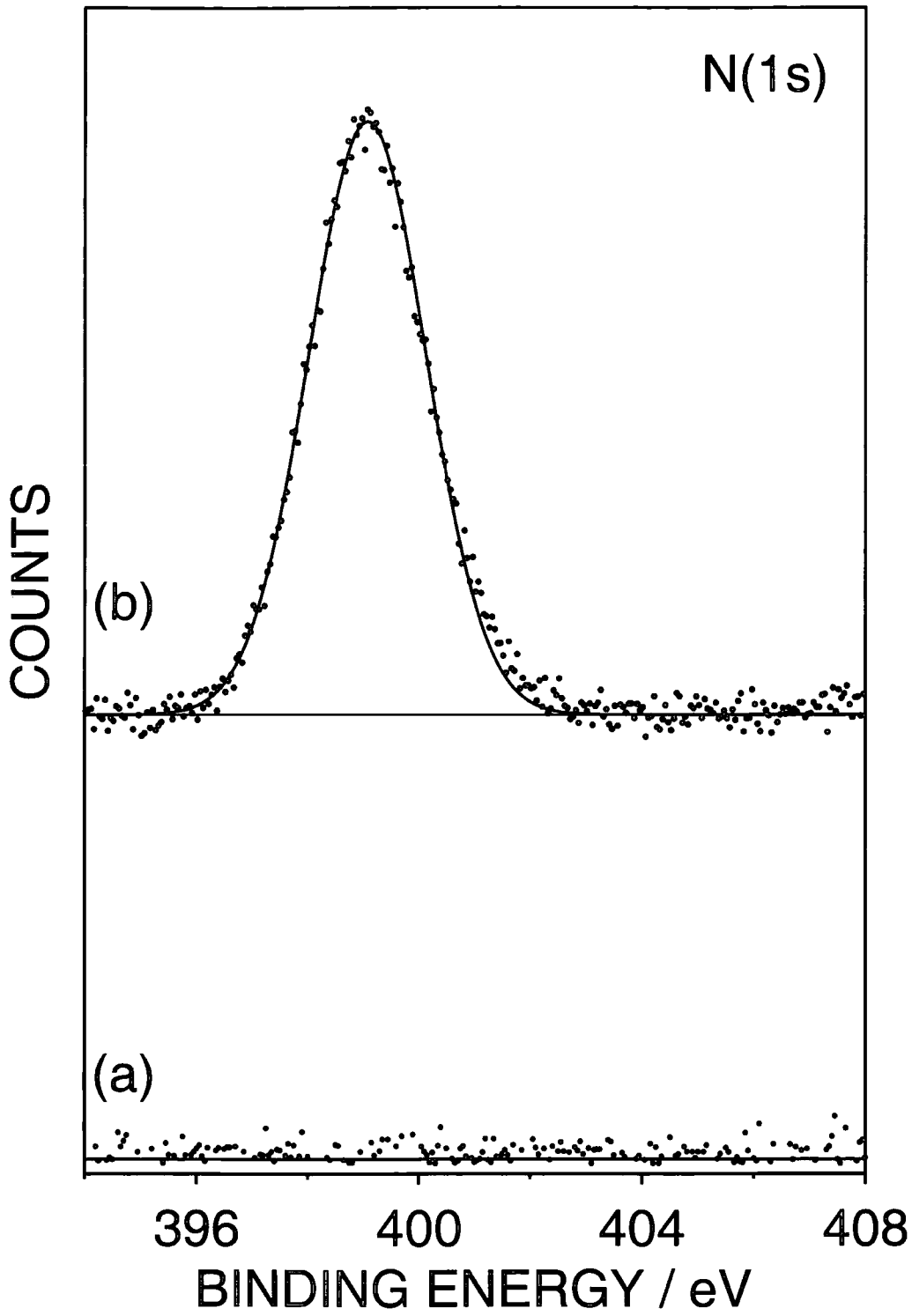

6.3.2 Reaction of AAPP with heptafluorobutryl chloride.

Amine groups react rapidly with acid halides to produce amides.[23] Hepatfluorobutrylchloride was used to functionalize the plasma polymer layers and to demonstrate that there were reactive. XPS analysis showed that functionalization of the AAPP layers with heptafluorobutryl chloride had occurred. The functionalized layers contained 4.3% ± 0.4 fluorine, and oxygen was also incorporated into the plasma polymer layer. The C(1s) spectrum shows evidence of a small amount of CF_3 and CF_2 in the layers.

In this chapter the deposition of the AAPP has been with the aim of producing a surface which is capable of acting as a polycation. The ability of poly(allylamine) to behave in this manner has been discussed previously, and has been further demonstrated in this chapter. The subsequent reactions use the polycationic nature of the AAPP layers to introduce new functional groups at the surface.

6.3.3 Reaction of the AAPP with the polymeric dye.

The polymeric dye was used because, like DNA, it can act as a poly(anion), through the sulphonate groups on the polymer backbone.[3,5] This was attempted to try and introduce chromophores at the surface. The XPS results and the UV spectra do seem to indicate that this is possible. By using XPS it was possible to detect the sulphur present in the backbone, and 1.5% sulphur was detected in the overall elemental abundance. The reduction in nitrogen content of the surface is due to the introduction of other atomic species at the substrate surface. The samples were also slightly tinged purple, even after thorough washing. Since this is the colour of the dye solution it does seem that it is possible to attach this molecule to the AAPP surface.

Table 6.1 Elemental abundances for the AAPP, and allylamine plasma polymer functionalized with polymeric dye.

Element	*Allyl amine plasma polymer*	*Allyl amine plasma polymer functionalized with polymeric dye*
C	68.7 ± 1	69.7 ± 0.7
N	31.1 ± 0.9	15.1 ± 0.2
O	0	13.7 ± 0.8
S	0	1.5 ± 0.2

Figure 6.5 UV-visible spectra of a) AAPP b), polymeric dye, c) AAPP reacted with polymeric dye, d) the difference between spectra c) and a), after subtraction of a) from c).

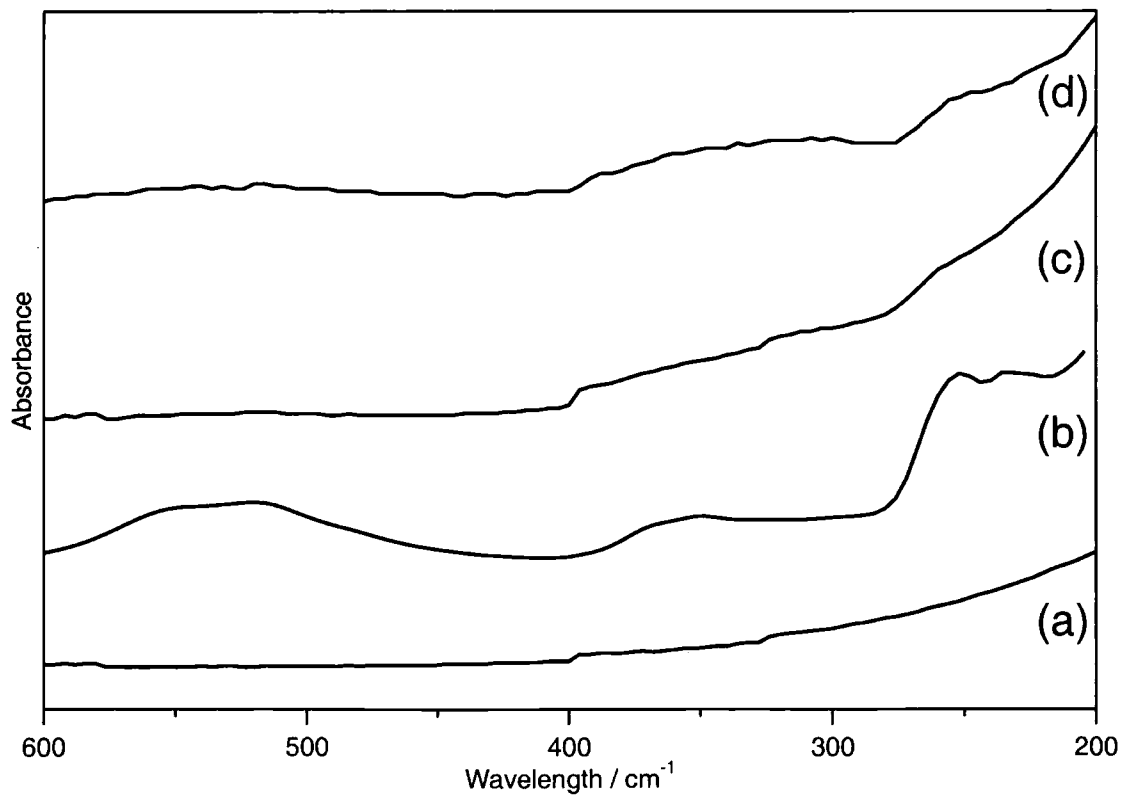

6.3.4 Reaction of the AAPP with deoxyribose nucleic acid (DNA).

The AAPP has been functionalized successfully with a solution of DNA. XPS analysis revealed peaks in the C(1s) spectra corresponding to carboxylic acid groups at 289.4 eV. There is also approximately 2% phosphorous present, which is indicative of the deposition of DNA, which is approximately 4-5% phosphorous, Table 6.2. Like the AAPP, the DNA has the potential to stabilize gold colloids. AFM analysis of the samples did show that DNA was being attached to the surface.

Table 6.2 Elemental abundances for AAPP, theoretical XPS values for DNA, and the practically obtained values after surface functionalization of the AAPP

Element	*Allyl amine plasma polymer*	*DNA theoretical values*	*Allyl amine plasma polymer functionalized with DNA*
C	68. 7 ± 1	47.6 ± 1.8	61 ± 0.7
N	31.1 ± 0.9	18 ± 6.4	19.8 ± 0.6
O	0	29.4 ± 4.9	17.2 ± 0.6
P	0	4.9 ± 0.3	2 ± 0.1

Figure 6.6 (a) AFM image of AAPP

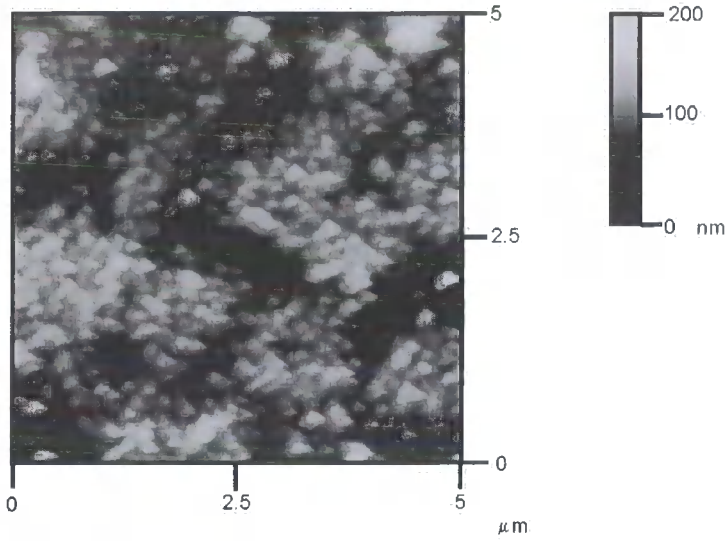

Figure 6.6 (b) AFM image of AAPP functionalized with DNA.

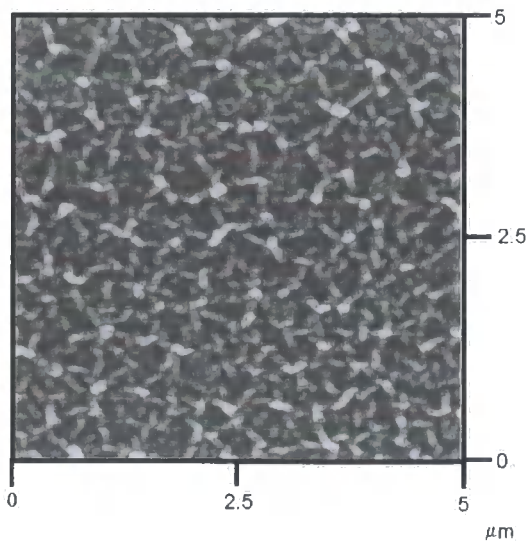

6.3.5 Reaction of the AAPP with carboxylic acid (COOH) and amine (NH_2) functionalized polystyrene beads.

The carboxylic acid functionalized and amine functionalized polystyrene beads were used to contrast with the work in Chapter 4, with MAPP, showed that amine functionalized PS beads will attach to an anhydride containing surface whereas carboxylic acid functionalized beads do not attach. In this case the AAPP should react with the COOH functionalized beads in preference to the NH_2 functionalized beads. Optical microscopy has shown this to be the case.

Figure 6.7 (a) Optical microscope image of COOH functionalized beads on AAPP. (Each image measures 100μm by 80μm).

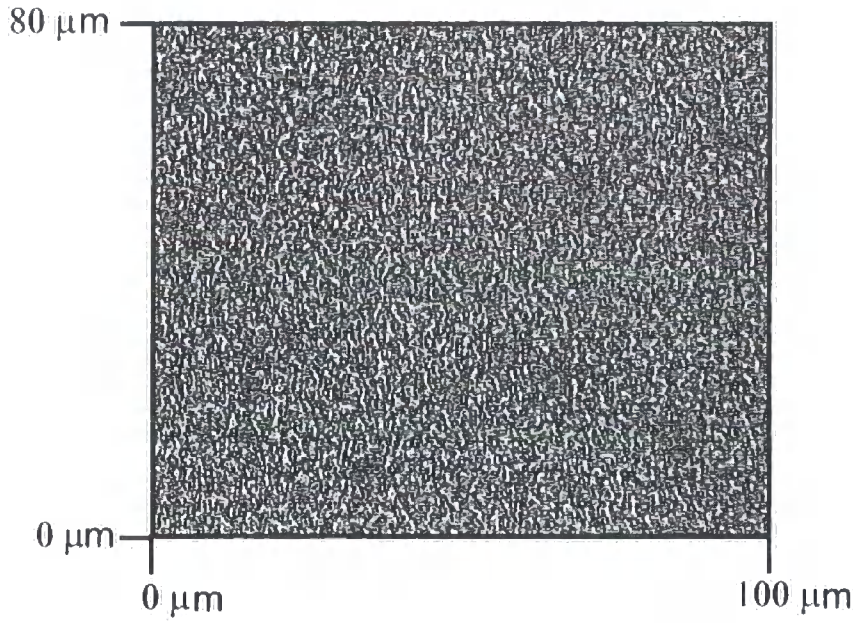

Figure 6.7 (b) Optical microscope image of NH_2 functionalized beads on AAPP

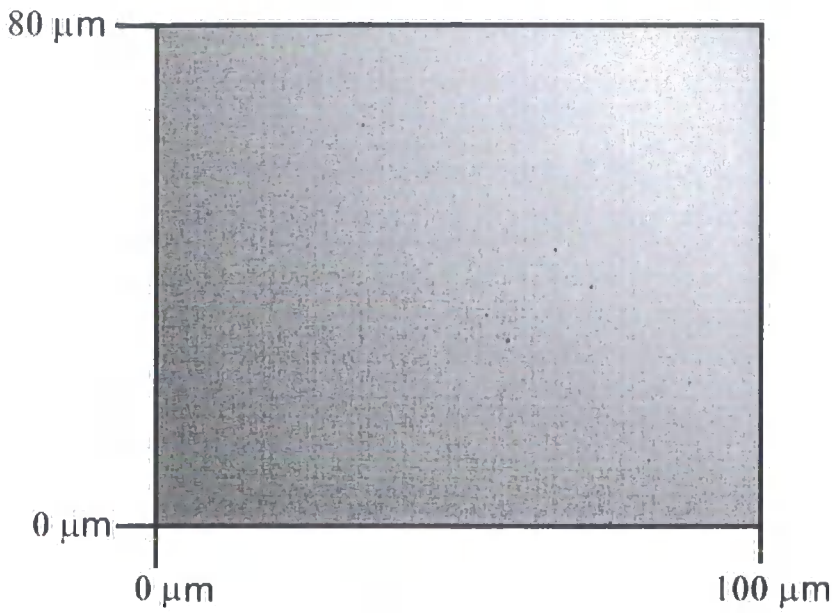

6.3.6 Reaction of the AAPP with gold colloid particles.

The gold colloids were used in order to demonstrate that the AAPP layer was capable of stabilising this type of particle in a similar manner to other amine containing layers.[9,10] Evidence for the presence of gold on these surfaces was obtained by optical and transmission electron microscopy. Gold colloid particles have been successfully deposited onto the AAPP surface. These were most readily seen by optical microscopy as small reflective beads at the plasma polymer surface. XPS analysis of the samples revealed no more than 0.2% gold present, which was consistent with the observation that the gold particles do not completely cover the surface. If there were complete coverage we would expect to see a completely gold surface in the XPS analysis, as the bead diameter is 250nm, which is much greater than the XPS sampling depth.

Figure 6.8 TEM image of Gold Colloid Particles on AAPP

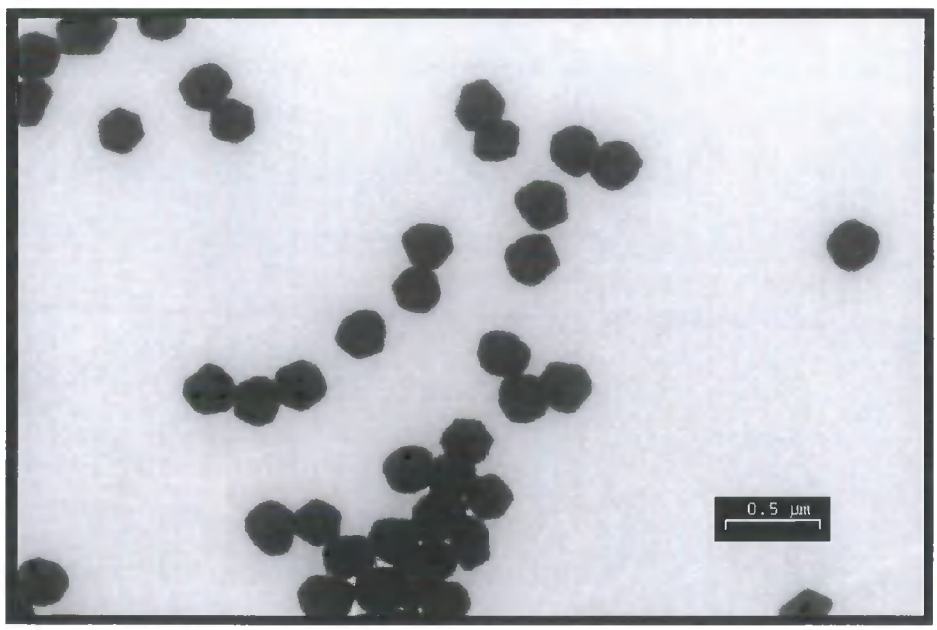

The extent of coverage obtained can be better seen using optical microscopy.

Figure 6.9 Optical image of gold colloids on the AAPP.

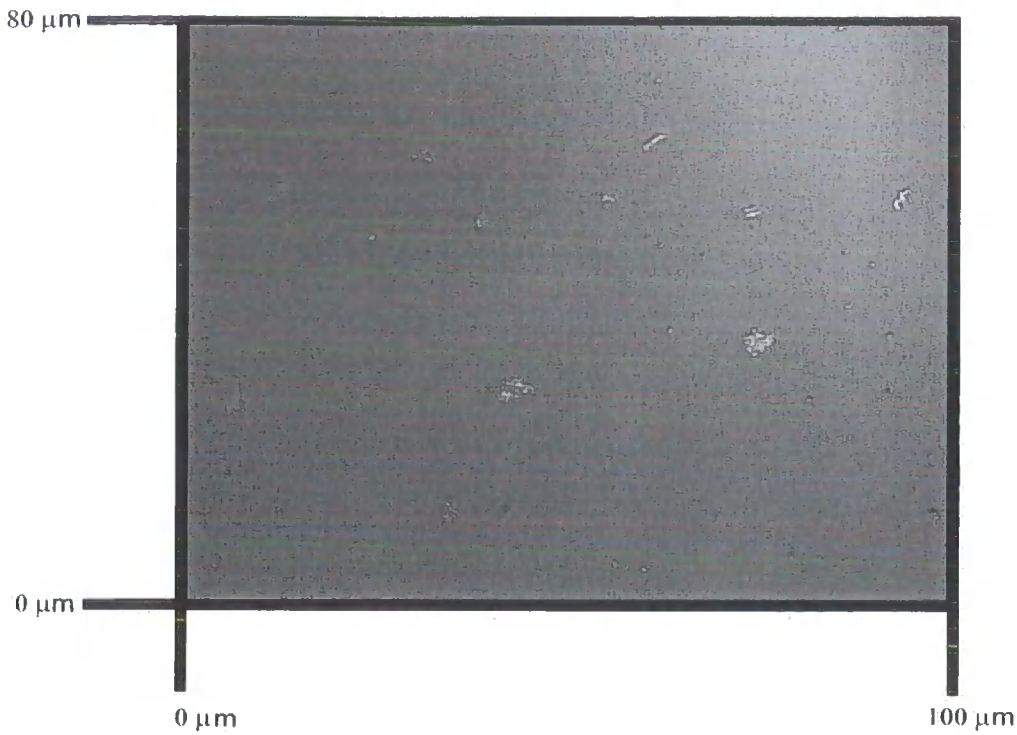

6.4 CONCLUSIONS

The plasma polymerization of allylamine has been successfully demonstrated here. It has also been shown that this layer is capable of forming polycation type layers that are of use for the attachment of polymeric dyes containing and ionic backbone, and DNA which can also be considered as a polyanion. Gold colloids can be stabilsed on the surface through the interaction of the NH_2 groups with the gold particles. The plasma polymer also reacts with carboxylic acid functionalized polystyrene spheres in preference to amine functionalized polystyrene spheres.

6.6 REFERENCES

1 Calderon, J.G., Harsch, A., Gross, G.W., Timmons, R.B. *J. Biomed. Materials Res.*, **1998**, *42*, 597.

2 France, R.M., Short, R.D., Dawson, R.A., MacNeil, S. *J. Mater. Chem.*, **1998**, *8*, 37.

3 Lvov, Y., Decher, G., Sukhorukov, G. *Macromolecules*, **1993**, *26*, 5396.

4 Yamada, O., Matsumoto, T., Nakashima, M. , Hagari, S., Kamahora, T., Ueyama, H., Kishi, Y., Uemura, H., Kurimura, T. *J. Virol. Methods*, **1990**, *27*, 203.

5 Boom, R., Sol, C.J.A., Salimans, M.M.M., Jansen, C.L., Wertheim van Dillen, P.M.E., Van der Noordaa, J. *J. Clin. Microbiol.*, **1990**, *28*, 495.

6 Lin, J.-C., Ko, T.-M., Cooper, S.L. *J. Colloid Interface Sci.*, **1994**, *164*, 99.

7 Erokhin, V., Popov, B., Samori, B., Yakovlev, A. *Mol. Cryst. Liq. Cryst.*, **1992**, *215*, 213.

8 Balladur, V., Theretz, A., Mandrand, B. *J. Colloid Interface Sci.*, **1997**, *194*, 408.

9 Yonezawa, T., Onoue, S.-Y., Kunitake, T. *Adv. Mater.*, **1998**, *10*, 414.

10 Liu, Y., Wang, Y., Claus, R.O. *Chem. Phys. Lett.*, **1998**, *298*, 315.

11 Dokoutchaev, A., James, J.T., Koene, S.C., Pathak, S., Prakash, G.K.S., Thompson, M.E. *Chem. Mater.*, **1999**, *11*, 2389.

12 Seizawa, T., Takeshita, H., Akashi, M. *Langmuir*, **1998**, *14*, 4088.

13 Chakraborty, A.K., Bischoff, K.B., Astarita, G., Damewood Jr., J.R. *J. Am. Chem. Soc.*, **1988**, *110*, 6947.

14 Penny, D.E., Ritter, T.J. *J. Chem. Soc., Faraday Trans. 1.*, **1983**, *79*, 2103.

15 Hoffman, A.S. *J. Appl. Polym. Sci. Appl. Polym. Symp.*, **1992**, *14*, 341.

16 Gombotz, W.R., Hoffman, A.S. *J. Appl. Polym. Sci. Appl. Polym. Symp.*, **1988**, *42*, 285.

17 Greisser, H.J., Chatelier, R.C., Gegenbach, T.R., Johnson, G., Steele, J.G. *J. Biomater. Sci. Polym. Ed.*, **1994**, *5*, 432.

18 Shlyakhento, L.S., Gall, A.A., Weimer, J.J., Hawn, D.D., Lyubchenko, Y.L. *Biophys. J.*, **1999**, *77*, 568.

19 Balladur, V., Theretz, A., Mandrand, B. *J. Colloid Interface Sci., 1997*, **194**, 408.

20 Lyubchenko, Y.L., Shlyakhtenko L.S. *Proc. Natl. Acad. Sci. USA.*, **1997**, *94*, 496.

21 Nakayama, Y., Takahagi, T., Soeda, F., Hatada, K., Nagaoka, S., Suzuki, J., Ishitani, A. *J. Polym. Sci. Polym. Chem.*, **1988**, *26*, 559.

22 Sipehia, R. *Cells Artif. Org.*, **1990**, *18*, 437.

23 McMurry, J. Organic Chemistry 3rd Ed.; Brooks/Cole: Pacific Grove, CA, 1992; 809.

CHAPTER SEVEN

Conclusions

This thesis has concentrated on the deposition of functionalized plasma polymer films, and the scope of these films to undergo subsequent functionalization reactions.

Much of the published work studying reactions at these functional group containing surfaces has been restricted to surfaces upon which self assembled monolayers (SAMs) can be formed, such as gold or silicon. The use of pulsed plasma polymerization to deposit functionalized layers as a starting point for further surface reactions means that the choice of substrate is broadened considerably, since plasma polymer layers can be deposited on a wide variety of surfaces.

Initially it was demonstrated the plasma polymer layers of maleic anhydride could be successfully functionalized in the vapour phase and characterized. It was also shown that through the choice of a suitably functionalized reactant, adhesion between the plasma polymer layers could be achieved.

The next two chapters showed further applications of the maleic anhydride plasma polymer, in the first case with poly(amidoamine) dendrimers. A high degree of control over the surface composition was demonstrated with these dendrimers, and this effect was in turn used to control the amount of gold that could be encapsulated at the surface. The second case utilized a wide variety of amine

containing moieties to introduce a variety of surface groups to the plasma polymer layer. These included fluorescent molecules, amine functionalized beads and polymeric amines. All of these surfaces were characterized and shown to be successfully attached.

Surface reactions of double bonds were investigated, by using allylamine to react with the anhydride groups, presenting free double bonds at the surface. Ozone, was used to show the presence of the double bonds at the surface, and then Diels-Alder reactions were carried out using cyclohexadiene and butadiene. IR analysis of these samples showed that the reactions had been successful.

Finally allylamine plasma polymer layers were deposited to study a different functionalized surface, and to look at complimentary reactions to those observed for the maleic anhydride plasma polymer layers. This was demonstrated well with the use of carboxylic acid functionalized polystyrene beads, which did not react with the maleic anhydride plasma polymer layers, but did react with the allylamine plasma polymer layers. The reverse effect was seen for amine functionalized polystyrene spheres. The allylamine plasma polymer layers were also shown to act as a polycationic layer, stabilising polymeric dyes and DNA. The fact that DNA can be stabilized on these surfaces could be of interest for biological applications.

In conclusion, the use of functionalized polymer surfaces, as deposited by the low power RF plasmas discussed here have been shown to be able to undergo subsequent reactions, with the possibility to introduce a wide range of species to the polymer surface.

In terms of future work, there are several areas in this thesis that would benefit from further investigation. It would be interesting to study the plasma polymerisation process itself, using a mass spectrometer to confirm the reactions that we believe are occurring inside the reactor. Further work could also be carried out to better characterise the MAPP, chemically by secondary ion mass spectrometry and physically by mechanical abrasion studies.

With reference to the surface chemistry carried out, there is plenty of scope for further work to be carried out. Further investigation of the PAMAM dendrimers bound to the MAPP surface could yield applications in the pharmaceutical industry for targeted drug delivery, heterogeneous catalysis and novel gas barrier layers, and I believe they should continue to be studied.

Allyl amine plasma polymer layers should be examined in future work as they provide amine rich surfaces, and have already been shown to be of interest in medical applications. The fact they can also be used as polycation layers has the potential to stabilize and attach many molecules of biological and chemical interest.

I think that the next stage of this work should be to investigate the wide variety of applications the attachment of PAMAM dendrimers to any solid surface, via the MAPP layer, could have.

APPENDIX

Seminars, Colloquia, Presentations and Lecture Courses

University of Durham

Board of Studies in Chemistry

POSTGRADUATE COLLOQUIA, LECTURES AND SEMINARS FROM INVITED SPEAKERS

1997 - 1998

October 15	Dr R M Ormerod, Department of Chemistry, Keele University Studying catalysts in action
October 22	Professor R J Puddephatt (RSC Endowed Lecture), University of Western Ontario Organoplatinum chemistry and catalysis
October 23	Professor M R Bryce, University of Durham, Inaugural Lecture New Tetrathiafulvalene Derivatives in Molecular, Supramolecular and Macromolecular Chemistry: controlling the electronic properties of organic solids
November 12	Dr J Frey, Department of Chemistry, Southampton University

	Spectroscopy of liquid interfaces: from bio-organic chemistry to atmospheric chemistry
November 26	Professor R W Richards, University of Durham, Inaugural Lecture A random walk in polymer science
December 2	Dr C J Ludman, University of Durham Explosions
January 14	Professor D Andrews, University of East Anglia Energy transfer and optical harmonics in molecular systems
February 18	Professor G Hancock, Oxford University Surprises in the photochemistry of tropospheric ozone
March 11	Professor M J Cook, Dept of Chemistry, UEA How to make phthalocyanine films and what to do with them.

1998 – 1999

October 21	Professor P Unwin, Department of Chemistry, Warwick University Dynamic Electrochemistry: Small is Beautiful
October 23	Professor J C Scaiano, Department of Chemistry, University of Ottawa, Canada In Search of Hypervalent Free Radicals, RSC Endowed Lecture
October 28	Professor J P S Badyal, Department of Chemistry, University of Durham Tailoring Solid Surfaces, Inaugural Lecture

November 3	Dr C J Ludman, Chemistry Department, University of Durham Bonfire night Lecture
November 18	Dr R Cameron, Department of Materials Science & Metallurgy, Cambridge University Biodegradable Polymers
January 20	Dr A Jones, Department of Chemistry, University of Edinburgh Luminescence of Large Molecules: from Conducting Polymers to Coral Reefs
January 27	Professor K Wade, Department of Chemistry, University of Durham Foresight or Hindsight? Some Borane Lessons and Loose Ends
February 10	Dr C Bain, University of Oxford Surfactant Adsorption and Marangoni Flow at Expanding Liquid Surfaces
February 17	Dr B Horrocks, Department of Chemistry, Newcastle University Microelectrode techniques for the Study of Enzymes and Nucleic Acids at Interfaces

1999 - 2000

October 27	Dr. C. Braddock, Imperial College Novel catalysts for Atom Economic Transformations
November 3	Professor D.W. Smith, University of Waikato, NZ The Strengths of C-C and C-H Bonds in Organic and Organometallic Molecules: Empirical, Semi-empirical and Ab Initio Calculations

November 10 Dr. I. Samuel, Department of Physics, University of Durham

Improving Organic Light Emitting Diodes by Molecular, Optical and Device Design

November 24 Professor T. Jones, Imperial College

Atomic and Molecular Control of Inorganic and Organic Semiconductor Thin Films

November 30 Rev. R. Lancaster

Principles and Practice

January 19 Dr. P.R. Fielden, UMIST

Miniaturised Chemical Analysis (Lab-on-a-Chip): Functional or Merely Fashionable?

February 23 Dr. N. Clarke, UMIST

The Flow of Polymer Blends

March 1 Professor D. Tildsley, Unilever (Head of Research)

Computer Simulation of Interfaces: Fact and Friction

CONFERENCES ATTENDED

13^{th} – 18^{th} August 2000

The Gordon Research Conference on Plasma Processing Science, Tilton School, New Hampshire.

EXAMINED LECTURE COURSES

Electron Microscopy (Dr. K. Durose)

Mass Spectroscopy (Dr. M. Jones and Dr. C. Woodward)

Experimental Design (Prof. J.P.S Badyal)